Role of SIRT1 and SIRT6 for the preservation of genetic stability

Dissertation
submitted to attain the academic degree
Doctor of Natural Sciences
at the Department of
Chemistry, Pharmacy and Geosciences
of the Johannes Gutenberg University Mainz

Submitted by
Elena Robeska
Born in Prilep (Macedonia)

Mainz, 2018

Dean:

1. Reviewer:

2. Reviewer:

Day of the oral examination:

Acknowledgment

"I can't change the direction of the wind, but I can adjust my sails to always reach my destination"

Jimmy Dean

Table of contents

I. Abbreviations

8-oxoG	7, 8-dihydro-8-oxoguanine
AcOGG1	Acetylated OGG1
AP	Apurinic/apyrimidinic
APE1	Apurinic/apyrimidinic endonuclease 1
APTX	Aprataxin
BER	Base excision repair
BRCA1	Breast cancer 1
BSA	Bovine serum albumin
CSK	Cytoskeleton buffer
DDR	DNA damage response
DANN	Deoxyribonucleic acid
DNA-PKc	DNA-dependent protein kinase
DSB	Double strand break
Endo IV	Endonuclease IV
FEN1	Flap endonuclease 1
Fpg	Formamidopyrimidine DNA glycosylase
GDH	Glutamatdehydrogenase
GG-NER	global genome nucleotide excision repair
GSH	Glutathione
GSH-Px	Glutathione peroxidases
H1	Histone 1
H_2O_2	Hydrogen peroxide
H_3K_{56}	Histone H_3 lysine 9
H_3mk_9	Trimethylation of lysine 9 on histone H3
HDAC	Histondeacetylase
HIF1α	Hypoxia-inducible factor 1-alpha
HR	Homologous recombination
IGF-1	Insulin-like growth factor 1
Lig I	Ligase I
Lig III	Ligase III
MEFs	Mouse embryonic fibroblasts
MMS	Methyl methanesulfonate
MPG	Methylpurine DNA glycosylase
NAM	Nicotinamide
nCaRE	Negative Ca^{2+} response element
NER	Nucleotide excision repair
NF-κB	Nuclear factor kappa B
NJEJ	Non-homologous end joining
O_2	Singlet oxygen
$O_2^{\cdot-}$	Superoxide
OGG1	8-Oxoguanine glycosylase
$OH^{\cdot}$	Hydroxyl radicals

p53	Tumor protein p53
PARG	Poly(ADP-ribose) glycohydrolase
PARP1	Poly(ADP-ribose)-polymerase 1
PBS	Phosphate buffered saline
PBSCMF	Phosphate buffered saline (calcium magnesium free)
PCR	Polymerase chain reaction
PNKP	Polynucleotide kinase 3′-phosphate
Pol-β	DNA polymerase β
PTM	Posttranslational modifications
Ref 1	Redox factor 1
RNA	Ribonucleic acid
ROS	Reactive oxygen species
SDS	Sodium dodecyl sulfate
Sir2p	Silent information regulator 2 protein
SOD	Superoxiddismutase
SSB	Single strand breaks
TDG	Thymine DNA glycosylase
Trx	Thioredoxin
XPA	Xeroderma pigmentosum, complementation group A
XPC	Xeroderma pigmentosum, complementation group C
XRCC1	X-Ray Repair Cross- Complementing Group 1

II. List of Figures

III.   List of tables

1   Introduction

1.1   Genomic instability as a major driving force of carcinogenesis

Cell division is a continuous process by which a cell has the capacity to divide into two cells, ensuring the reproduction of specific cell types. This involves the accurate duplication of the genome and distribution of the duplicated genome into the two daughter cells. Failure to achieve this purpose will result in various forms of genome alterations (mutations) in the daughter cells. Genomic instability is a situation characterized by an increased rate of spontaneous mutations throughout each replicative cell cycle (Shen, 2011). There are different types of genomic instability. Microsatellite instability is characterized by random insertions or deletions of several base pairs in microsatellite sequences. Nucleotide instability causes subtle sequence changes as a result of DNA polymerase infidelity, aberrant base excision repair (BER) or nucleotide excision repair (NER). Chromosomal instability is the most frequently observed type of genome instability that has the greatest potential to lead to oncogenic transformation (Pikor, Thu, Vucic, & Lam, 2013).

There are several major mechanisms that have evolved to maintain genomic integrity during cell division. Such mechanisms include high-fidelity of DNA replication during S-phase; accurate distribution of chromosomes among daughter cells during mitosis; error-free repair of sporadic DNA damage throughout the cell cycle and cell cycle progression and checkpoint control. The mechanisms are accompanied with multiple and complex molecular process which ensures accurate maintenance of genomic integrity (Shen, 2011).

There are several tools / techniques to investigate genomic instability at the chromosome level. The micronucleus assay is one of most widely used, providing a comprehensive indicator for chromosome breakage, chromosome rearrangement, chromosome loss, non-disjunction. Micronuclei mainly originate from acentric chromosome fragments, acentric chromatid fragments or whole chromosomes that failed to be incorporated in the daughter nuclei at the completion of telophase during mitosis, due to their failure to attach with the spindle during anaphase. These displaced chromosomes or chromosome fragments are eventually enclosed by a nuclear membrane and, except for their smaller size, are morphological similar to nuclei (Fenech, 2002).

Micronuclei from acentric chromosome or chromatid fragments are formed as products of double strand breaks (DSBs). DSBs are formed directly as a result of exposure to ionizing radiation or through endogenous processes, such as DNA replication and DNA repair mechanisms (Cannan & Pederson, 2016). Ionizing radiation generates not only single strand breaks (SSBs), but also oxidised bases and sites of base loss which are subject to base excision repair. For instance, simultaneous excision repair of damaged

(e.g. 8-oxoguanine (8-oxoG)) or inappropriate bases incorporated in DNA (e.g. uracil) that are in proximity and on opposite complementary DNA strands, particularly if the gap-filling step is not completed, leads to DNA DSBs and micronuclei formation (Figure 1.1. A) (Fenech et al., 2011). Furthermore, collapse of the replication fork and subsequent DSB formation could result from the stalling of the polymerase during replication (Figure 1.1. B) due SSBs, unusual DNA secondary structures, bulky lesions, polymerase blocking oxidative lesions, abasic sites and etc (Cannan & Pederson, 2016).
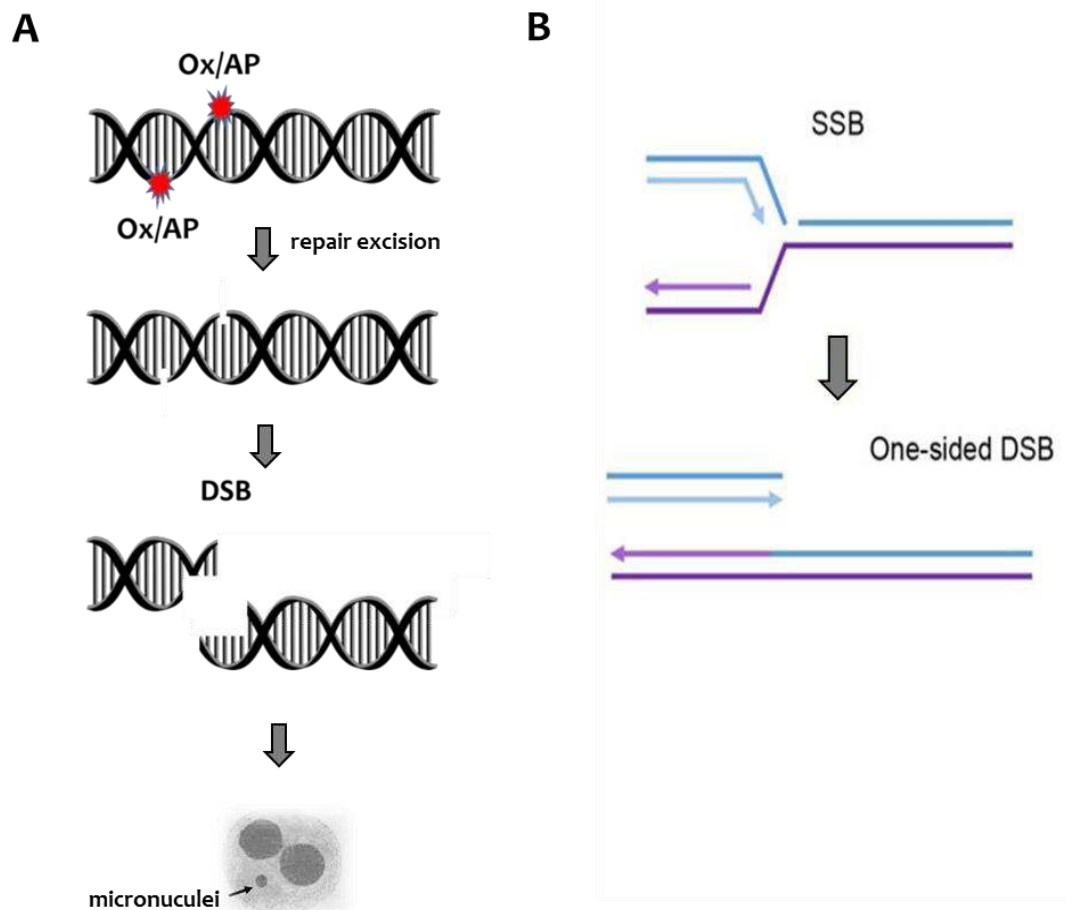
Figure 1.1 Micronuclei formation as result of DSB formation via: (A) attempted base excision repair of closely opposed oxidative lesions; (B) via replication fork collapse (Cannan & Pederson, 2016)

Induction of a genomic instability phenotype is a crucial early event in carcinogenesis. It enables cells to accumulate mutations that disrupt the normal regulation of cell proliferation and thus cause the uncontrolled cell division that is characteristic for cancer. Cancer is a complex multifactorial disease in which cells abnormally grow as a result of altered gene expression, division and cell cycle regulation. At more advanced stages, cancerous cells invade other tissues and disrupt their normal function leading to cellular death (Shen, 2011).

Maintaining genome stability in mammalian cells is accomplished by the activity of DNA repair mechanisms. These mechanisms depend on transcriptional or posttranslational regulation of the proteins directly involved in the repair as well as the accessibility of the repair enzymes to the chromatin. Many studies have shown that posttranslational modifications are key mechanisms to maintain genome integrity (Bhakat, Mokkapati, Boldogh, Hazra, & Mitra, 2006; Wei & Yu, 2016).

1.2   Sirtuins

Sirtuins are an evolutionary conserved family of proteins. Historically, their roles as histone modifiers, provided one of the first links between chromatin regulation and aging (ascribed to the accumulation of unrepaired damage to cellular and organismal components over time) (Lombard, 2009). The founding member of the sirtuin protein family is the silent information regulator 2 protein (Sir2p) of *Saccharomyces cervisiae*. Overexpression of this protein leads to extension of the yeast replicative lifespan by prevention of rDNA recombination and synthesis of extrachromosomal rDNA circles (Lombard, 2009; Mei et al., 2016; Mostoslavsky et al., 2006).
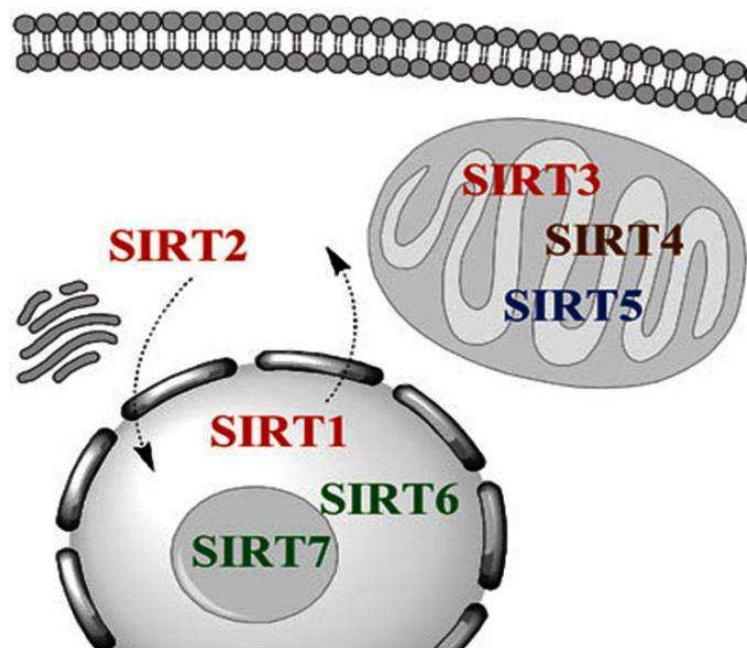
Figure 1.2 Localization of mammalian sirtuins (Herskovits & Guarente, 2013)

The mammalian genome encodes seven Sir2 homologues, (SIRT1–7), with a highly conserved NAD^+- binding catalytic domain but variable C- and N-terminus. Diversity in subcellular localization, enzymatic activity and binding targets are the result of the divergent terminal extension (Mei et al., 2016). SIRT1, SIRT6 and SIRT7 are mainly located in the nucleus. SIRT2 is generally localized in the cytoplasm. SIRT3, SIRT4 and SIRT5 are

present in the mitochondria (Figure 1.2). It was shown that in particular circumstances sirtuins are translocated from their typical compartments. SIRT1 is detected in the nuclei, but is excluded from the nucleoli, whereas SIRT6 and SIRT7 are associated with heterochromatic regions and nucleoli, respectively. During the G2/M phase, SIRT2 binds chromatin in the nucleus. SIRT3 might also be a nuclear protein that transfers to the mitochondria during cellular stress (Yamamoto, Schoonjans, & Auwerx, 2007).
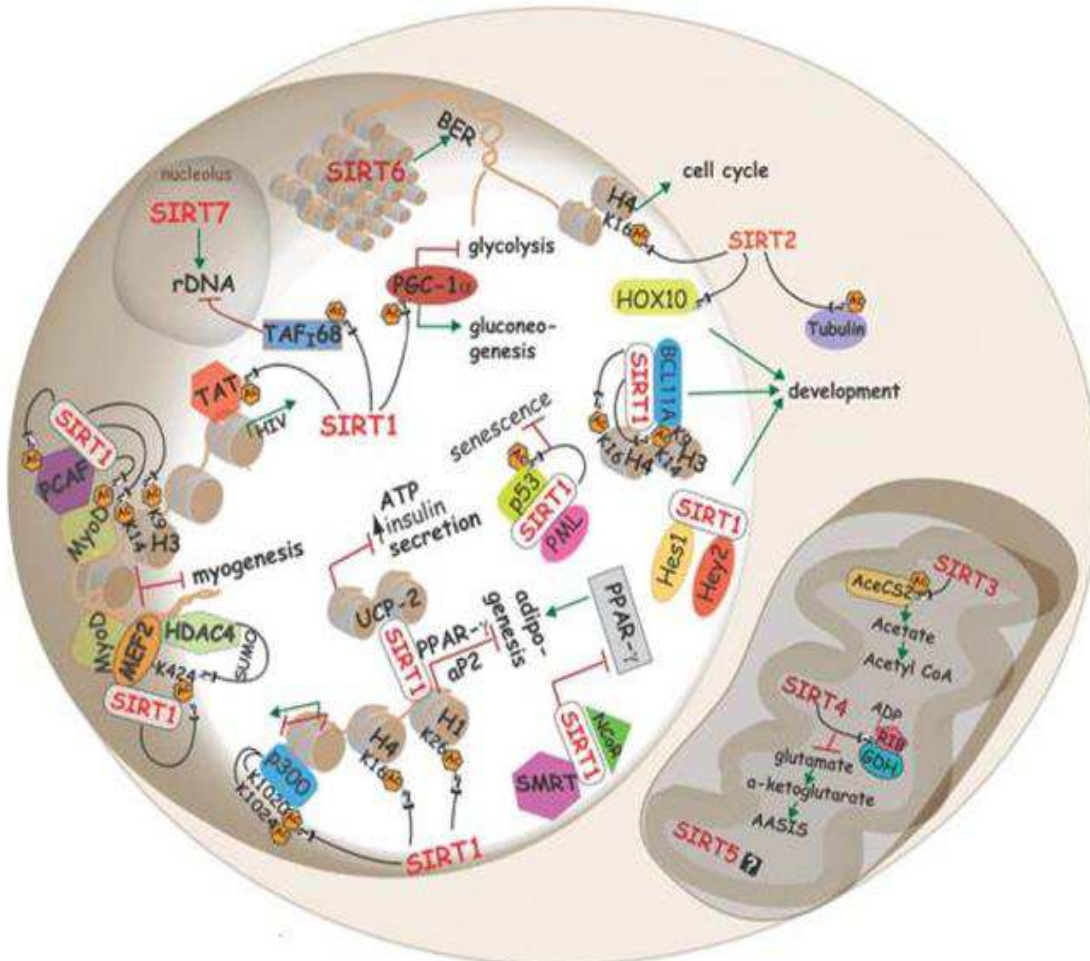
Figure 1.3 Overview for the function of sirtuins in metabolism and DNA repair and further influence on their roles in cancer mainly by affecting genome integrity and cancer-associated metabolism (Michan & Sinclair, 2007)

Biochemically, sirtuins are NAD^+-dependent deacetylases, mono-ADP-ribosyl transferases, lipoamidases (SIRT4), demalonylases and desuccinylases (SIRT5). All seven sirtuins with, NAD^+-dependent deacetylation as major function are class III histone deacetylases (Dai & Faller, 2008; Martínez-Redondo & Vaquero, 2013). In particular capability to deacetylate great number of targets, (from histones to transcriptional factors and metabolic enzymes) make sirtuins involved in diverse cellular processes, such as stress response, DNA repair, energy metabolism, tumorigenesis and genome stability (Mei et al., 2016; Rodriguez, Fernandez, & Fraga, 2013).

1.2.1 SIRT2, SIRT3, SIRT4, SIRT5 and SIRT7

In human breast and liver cancers SIRT2 expression is reduced. *Sirt2*-knockout mice develop breast, liver, and other cancers (Kim et al., 2011). SIRT2 was implicated in DNA damage response (DDR) by deacetylating multiple key components within the DNA damage signalling pathway (Zhang, Head, & Yu, 2016). Moreover, SIRT2 was also involved in regulating development by interacting with the homeobox transcription factor HOXA 10 (Michan & Sinclair, 2007).

Among the mitochondrial sirtuins, SIRT3 functions as a primary mitochondrial stress-responsive protein deacetylase (Arumugham, Hsieh, Tanzer, & Laine, 1986). One study showed that mice deficient in *Sirt3* exhibited globally increased acetylation of the mitochondrial proteins (Masumi, Suzuki, Iijima, & Tsukada, 1990). A physical interaction between SIRT3 and the repair glycosylase OGG1 (see chapter 1.3.8.1) was demonstrated. Mitochondrial OGG1 acetylation is modulated by SIRT3. Moreover, deacetylation by SIRT3 stabilized OGG1 protein. After irradiation of the cells with and without depletion of SIRT3, 8-oxoG induction in the mitochondria was higher in the SIRT3 deficiency cells. Dysfunction of SIRT3 led to deregulation of mtDNA repair. Deacetylation of OGG1 catalysed by SIRT3 therefore seems to be important for protecting mtDNA from oxidative damage and preventing apoptotic cell death (Cheng et al., 2013).

SIRT4 regulates amino-acid-stimulated insulin secretion in pancreatic β-cells, by mono-ribosylation, inhibiting activity of glutamatdehydrogenase (GDH) (Haigis et al., 2006). Knockdown of SIRT4 expression enhances fatty acid oxidation in hepatocytes, which is accompanied by a change in gene expression of mitochondrial and fatty acid metabolism enzymes (Chailley, Bork, Gounon, & Sandoz, 1986). It was reported that SIRT4 functions as a tumour suppressor *in vitro* and *in vivo* (Csibi et al., 2013; Jeong et al., 2013). In contrary, there are indications for an oncogenic function of SIRT4, via a protection of cancer cells against stress (Jeong, Hwang, & Seong, 2016).

The mitochondrial sirtuin, SIRT5 has been implicated in the regulation of ammonia production and ammonia-induced autophagy by regulating glutamine (Szabó, Hoffmann, & Bogáts, 1972) and heart metabolism (Bialostozky, 1974). SIRT5 protects cells from oxidative stress through IDH2 desuccinylation and G6PD deglutarylation (Zhou et al., 2016).

Sirt7$^{-/-}$ mice show a premature aging phenotype: premature kyphosis, reduced weight and fat content, compromised haematopoietic stem cell function and leukopenia, reduced levels of circulating insulin-like-growth factor-1 (IGF-1) protein, and increased p16INK4 expression (Vazquez, Thackray, & Serrano, 2017). Most of the SIRT7$^{-/-}$ embryos die at late stages of embryonic development or during the first month after birth. Those that survive to adulthood suffer from a shortened lifespan. SIRT7 activates RNA Pol I-

mediated transcription and expression of ribosomal RNA genes. (Vazquez et al., 2016). SIRT7 as one of the three nuclear mammalian sirtuins, has been shown to promote DNA repair (non-homologous end joining) (Scalabrino & Grimaldi, 1967) by inducing chromatin changes at DSBs and regulating the activity of DNA repair factors (Crade & Taylor, 1979; Vazquez et al., 2016).

1.2.2   SIRT1

SIRT1 is a histone modifier that deacetylates lysine residues at positions 9 and 26 of histone H1, 9 and 14 of H3 and 16 of H4 (Michan & Sinclair, 2007). SIRT1-mediated deacetylation of H4K16Ac and H3K9Ac is directly associated with the function of SIRT1 to coordinate the formation of constitutive and facultative heterochromatin (Vaquero et al., 2004; Vaquero et al., 2007). Deacetylation of H3K9 is a requirement for subsequent methylation of the same residue H3K9me2/3 a hallmark of higher orders of chromatin compaction (Martínez-Redondo & Vaquero, 2013).

Few studies described the phenotype of SIRT1 deficient mice. A role of SIRT1 in several developmental processes in 129SVEV/B6C57 mice strain was demonstrated. SIRT1 deficient mice and embryos were significantly smaller, embryos had cardiac defects and eye abnormalities. Mice carrying mutations of SIRT1 died at perinatal stages or up to several months in adulthood. In Table 1.1 it can be seen that crossing $Sirt1^{+/-}$ mice, $Sirt1^{-/-}$ embryos are present at approximately Mendelian ratios, even at late stages of gestation (E18.5). However, after birth there is poor representation of SIRT1 deficient mice, which comprised 10% of total pups, 67% of which died within the first week after birth (Cheng et al., 2003).

Table 1.1 Genotypes of litters from SIRT1$^{+/-}$ intercross (Cheng et al., 2003)

Age	+/+	+/-	-/-	Total
E12.5	7	10	10	27
E13.5	3	3	2	8
E15.5	1	6	2	9
E16.5	5	8	4	17
E18.5	11	17	11	39
P > 0	45	96	16	157
P >1 week	45	96	5	146

In contrast to the study by Cheng et al. (2003), which showed that SIRT1 deficient mice died at perinatal (around the time of birth) stages up to several months in adulthood, another study indicated that the majority of $Sirt1^{-/-}$ mice died at E9.5-E14.5. From 442 offspring analysed, only 1 % in a 129SVEV/FVB and 8.5 % in a 129SVEV/FVB/Black Swiss background Sirt1 homozygous mutant survived. Thus these $Sirt1^{-/-}$ mice exhibited an even more severe phenotype than those reported in the previous study (Wang et al., 2008).

In a third study, similar to the previous strains of SIRT1 deficient mice, nearly two thirds of $Sirt1^{-/-}$ newborns (129/CD1 strain) died shortly after birth and the majority of surviving $Sirt1^{-/-}$ manifest growth retardation. Despite growth retardation both male and female $Sirt1^{-/-}$ mice were fertile and had reduced levels of serum IGF-1. It turned out that SIRT1 modulates the estrogen-IGF-1 signalling for postnatal development of mammary gland in mice (Li et al., 2007).

Taken together, observations in independent studies indicate that the genetic background has a profound effect on the phenotypes of different SIRT1 mutant strains. (Cheng et al., 2003; Li et al., 2007; McBurney et al., 2003; Wang et al., 2008).

Wang et al. (2008) observed that the absence of SIRT1 causes genomic instability. SIRT1 deficiency in E10.5-E12.5 showed reduced level of trimethylation of lysine 9 on histone H3 (H3mK9) and increased acetylation of H3K9 that lead to chromosome condensation. Consequently, this altered histone modification lead to the formation of chromosome bridges, chromosome breaks, unequal chromosome segregation and aneuploidy. Trimethylation of lysine 9 on histone H3 is necessary for proper chromosome segregation. They suggested that a primary reason for the death of mutant embryos could be this profound genetic instability (Wang et al., 2008).

Besides histones, SIRT1 deacetylates numerous substrates affecting plenty of cellular processes. Different mechanisms were described by which SIRT1 activity regulates cell survival and cell cycle (via deacetylation of Ku70, E2F1, p53, p73), stress resistance (via deacetylation of FOXO transcription factors), kidney diseases (via deacetylation of the Smad7), cardiac hypertrophy, cellular senescence, inflammation (by deacetylation of the RelA / p65 subunit of NF-kB), development (by deacetylation of Hes1, Hey2), breast, liver, prostate and brain cancer (Michan & Sinclair, 2007). By deacetylating the p53 tumor suppressor gene, initiation of transcriptional apoptosis can be inhibited, giving the cell more time to repair damage and promote cell survival. Recent results, however, indicate that SIRT1 also simultaneously prevents the translocation of p53 into the nucleus and directs it from the cytosol into the mitochondria, where initiates transcriptional-independent apoptosis in response to an increased level of reactive oxygen species (Gonfloni et al., 2014; Houtkooper, Pirinen, & Auwerx, 2012; Kruszewski & Szumiel, 2005).

The role of SIRT1 in cancer is under debate. It is not clear if its overexpression in several types of human cancers is just a marker for tumorigenesis or indeed affects tumor growth (Bradbury et al., 2005; Hida, Kubo, Murao, & Arase, 2007). In another study it was found that SIRT1 levels are lower in many cancers than normal tissues, such as glioblastoma, bladder carcinoma, prostate carcinoma and ovarian cancers. It was shown that the absence of p53 did not rescue embryonic lethality associated with SIRT1 deficiency although SIRT1 inhibition causes p53 hyperacetylation and increases p53-dependent transcription activity (Lain et al., 2008; Wang et al., 2008). Wang et al. (2008) demonstrated that tumors developed in $Sirt1^{+/-}p53^{+/-}$ mice, still maintained one wild type allele of SIRT1. Treatment with resveratrol that activates SIRT1 could partially inhibit tumor formation. They suggested that proper dose of SIRT1 is critical for inhibiting tumorigenesis and SIRT1 serves as haploid tumor suppressor gene (Wang et al., 2008).

SIRT1 is involved in the regulation of the cellular response to DNA double strand break, and / or DNA damage repair by deacetylating Ku70 (Jeong et al., 2007) and NSB1 (Yuan, Zhang, Sengupta, Lane, & Seto, 2007). Primary $Sirt1^{-/-}$ MEFs are more sensitive to γ-irradiation and UV (Wang et al., 2008). Some of the non-histone target proteins that could make SIRT1 important for the BER pathway are apurinic/apyrimidinic endonuclease (APE1) (Yamamori et al., 2010) and glycosylase OGG1 (Sarga et al., 2013). In the bioinformatic analysis by Antoniali et al. (2013) it was found that SIRT1 gene expression is modulated by APE1. Another finding suggesting that SIRT1 is important modulator of BER was reported by Madabushi et al. (2013). They showed that SIRT1 enhances TDG glycosylase activity, deacetylates TDG and suppresses TDG gene expression. Ming et al. (2010) were investigating the role of SIRT1 in global genome nucleotide excision repair (GG-NER). They showed that SIRT1 KO cells have slower repair of UVB induced lesions and lower levels of XPC protein, one of the key players in GG-NER. It was also demonstrated that deacetylation of XPA by SIRT1 plays a positive role for repair of UV-induced DNA damage (Fan & Luo, 2010).

1.2.3   SIRT6

SIRT6 is a NAD$^+$-dependent deacetylase of histone H3 lysine 9 (H3K9) and H3 lysine 56 (H3K56) (Beauharnois, Bolívar, & Welch, 2013; Kugel & Mostoslavsky, 2014). SIRT6 is excluded from the nucleoli and is generally associated with the heterochromatic regions of the cell (Michishita, Park, Burneskis, Barrett, & Horikawa, 2005). Since histone deacetylation is associated with a closed chromatin conformation, SIRT6 has been postulated to be associated with decreased chromatin accessibility (Kugel & Mostoslavsky, 2014). In this manner SIRT6 influences telomeric chromatin. As telomere structure is necessary for genomic stability and telomere length decreases with age, SIRT6 is involved in the biology of aging (Mostoslavsky et al., 2006).

The highest concentrations of SIRT6 have been found in the muscles, heart, brain, liver and thymus (Mostoslavsky et al., 2006; Pereira, Lebiedzinska, Wieckowski, & Oliveira, 2012). In mice, SIRT6 deficiency or inactivation of SIRT6 results in shortened life span and degenerative phenotype. $Sirt6^{-/-}$-knockout mice appear normal at birth but lower in weight than *wild-type* mice. After two weeks, mice begin to exhibit metabolic/degenerative effects such as severe hypoglycemia, lymphocytic apoptosis, low levels of serum IGF-1 receptor, loss of subcutaneous fat, a curved spine, resembling a progeroid-like syndrome. Mice die at around 1 month of age (Beauharnois et al., 2013; Lombard, Schwer, Alt, & Mostoslavsky, 2008; Mostoslavsky et al., 2006; van Meter, Mao, Gorbunova, & Seluanov, 2011a).

Reduction in insulin sensitivity or insulin secretion produces diabetes and shortens lifespan. Mechanistically, SIRT6-mediated down regulation of AKT phosphorylation allows nuclear relocalization of FOXO proteins and thus influences glucose metabolism. This contributes to the degenerative phenotype and early death of $Sirt6^{-/-}$ mice. It was shown that SIRT6 might regulate the response to a caloric restriction. Caloric restriction is associated with lower levels of reactive oxygen species that influence DNA damage (Lombard et al., 2008). In addition, SIRT6 also influences transcriptional repression. By attenuating NF-κB signalling SIRT6 plays a role in aging, proliferation, inflammation and immunity. It modulates glucose homeostasis through a Hif1α-dependent pathway via H3K9 deacetylation of the gene promoters (Beauharnois et al., 2013). In one study it was demonstrated that SIRT6 overexpression is activating p53 and p73 apoptotic signalling cascades in multiple cancer cells, probably by mono-ADP ribosylation in particular of p53 and p73 (van Meter, Mao, Gorbunova, & Seluanov, 2011b).

Mounting evidence has shed light on the fact that SIRT6 plays diverse roles in DNA repair, in particular in DSB repair under conditions of oxidative stress. It was found that SIRT6 interacts with and ADP-ribosylates poly (ADP-ribose)-polymerase 1 (PARP1) and stimulates its activity (Beneke & Bürkle, 2007; Mao et al., 2011). Another evidence that SIRT6 promotes DSB repair result from analyses which show its interaction with DNA-dependent protein kinase (DNA-PKc) and the crosstalk with the chromatin remodeler SNF2H (McCord et al., 2009; Toiber et al., 2013).

Mostoslavsky et al. (2006), showed that the hypersensitivity of SIRT6-deficient MEFs against DNA damaging agents such as the alkylating agent methyl methanesulfonate (MMS), hydrogen peroxide (H_2O_2), and ionizing radiation, but not UV, was rescued by expression of the dRP-lyase domain of DNA polymerase β (Pol β), the major polymerase involved in short patch BER.

Further research into sirtuins, described as regulators of lifespan - maintaining telomere integrity and metabolic homeostasis, preventing genomic instability, enhancing aging-associated gene expression, aid in the development of treatments for diseases of

premature aging, metabolic disorders and cancer (Lombard et al., 2008).

1.3   Reactive oxygen species and oxidative stress

1.3.1   ROS

In living cells, reactive oxygen species (ROS) (see Table 1.2) are formed continuously as a consequence of metabolic and other biochemical reactions as well as external factors. Sequential reduction of oxygen through the addition of electrons leads to the formation of various types of ROS, namely superoxide ($O_2^{\cdot-}$), hydrogen peroxide (H_2O_2) and hydroxyl radicals ($OH^{\cdot}$) (Sies, 1993).

$$O_2 \xrightarrow{e^-} O_2^{\cdot-} \xrightarrow{e^-+2H^+} H_2O_2 \xrightarrow{e^-+H^+} OH\cdot \xrightarrow{e^-+H^+} H_2O$$
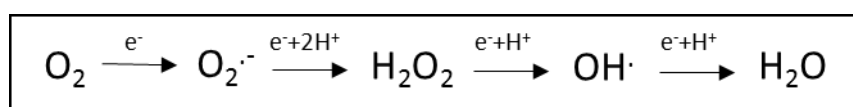
Figure 1.4 Sequential reduction of molecular oxygen.

Another important ROS is singlet oxygen ($^1O_2$) which is mostly generated by photosensitization, following the excitation of endogenous or exogenous chromophores by UV or visible light. Several ROS (Table 1.2) can directly oxidize DNA, which lead to several types of DNA damage, such as oxidized bases and single - and double-strand breaks (see chapter 1.3.3).

Table 1.2 Reactive oxygen species

Reactive oxygen species	
$HO^{\cdot}$	Hydroxyl radical
$^1O_2$	Singlet oxygen
$O_2^{\cdot-}$	Superoxide anion radical
$RO^{\cdot}$	Alkoxyl radical
H_2O_2	Hydrogen peroxide
$ROO^{\cdot}$	Peroxyl radical
$NO^{\cdot}$	Nitric oxide radical

The most frequently endogenously produced ROS is the superoxide anion radical. During mitochondrial respiration, a small fraction of oxygen undergoes single electron transfer, generating the superoxide anion radical. However, the superoxide anion radical cannot

pass through biological membranes due to its charge. This molecule shows limited reactivity but is converted to hydrogen peroxide by superoxide dismutase (Figure 1.5) (Fridovich, 1995).

$$2\,O_2^{\cdot-} + 2\,H^+ \longrightarrow H_2O_2 + O_2$$

Figure 1.5 Spontaneous or enzymatic dismutation of the superoxide anion radical.

Besides from endogenous sources (mitochondria, cytochrome P450 metabolism, peroxisomes and inflammatory cell activation (Valko, Rhodes, Moncol, Izakovic, & Mazur, 2006), ROS can be generated by exogenous agents such as ionizing radiation, tobacco, toxins, drugs, chemicals, environmental pollutions, other xenobiotics such as potassium bromate (Ballmaier & Epe, 1995; Epe, Pflaum, & Boiteux, 1993) Ro 19-8022 (Will et al., 1999). However, ROS, in addition to their negative properties, also have an important redox signal function in the cell. They interact directly with signal molecules or indirectly trigger gene expression in the context of an adaptive response. Thus, ROS are not only toxic agents, but appear as important intra- and intercellular messengers (Valko et al., 2006).

1.3.2   Antioxidative mechanisms for the defense of ROS

Because aerobic organisms constantly produce small amount of ROS, including O_2^- and H_2O_2 that potentially lead to oxidative damage, they have evolved antioxidant strategies to protect themselves from ROS. Besides prevention of their formation, there is deactivation of already formed damaging species by different various non-enzymatic antioxidants. Among the non-enzymatic antioxidants are glutathione (GSH), thioredoxin (Trx), the vitamins C and E, carotenoids and secondary plant constituents such as flavonoids and polyphenols, which are absorbed with food. Additionally, there are antioxidant enzymes, such as superoxide dismutases (SOD), catalase and glutathione peroxidases (GSH-Px) (Figure 1.6) (Sies, 1993).
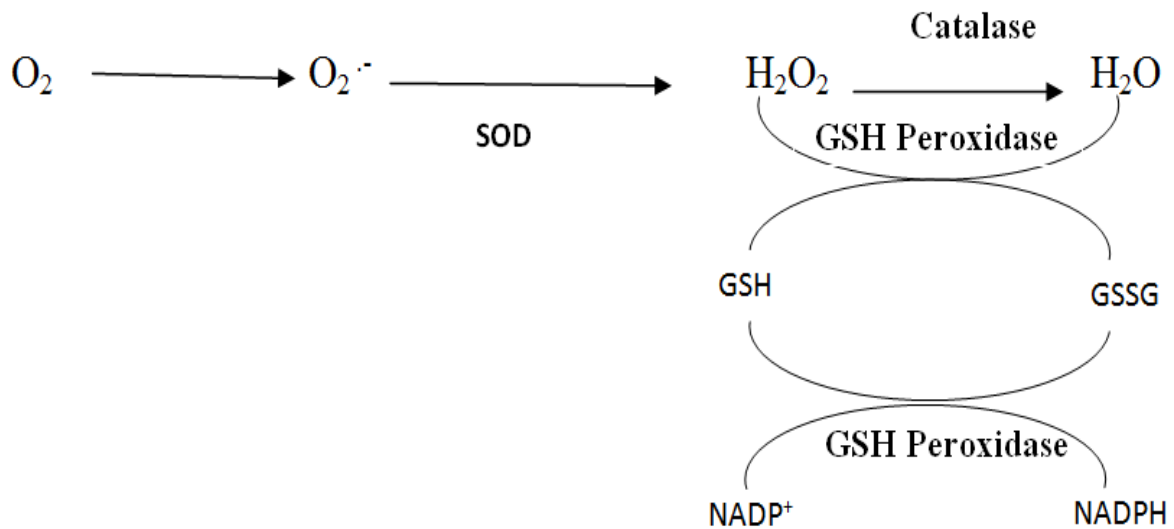
Figure 1.6 Mechanism of antioxidant and oxidants (Sies, 1993)

1.3.3 DNA damage by oxidative stress

Imbalance between ROS and anti-oxidative processes in favour of the prooxidative side is referred to as **oxidative stress** that leads to damage of all types of biological molecules including DNA, lipids, proteins and carbohydrates. Oxidative stress is often associated with mutagenesis and carcinogenesis (Sies, 1991; Valko et al., 2006).

DNA damage is induced by oxidative stress although neither O_2^- nor H_2O_2 react directly with DNA. Two indirect mechanisms are important.

The first mechanism is $\cdot$OH radical formation in a reaction of H_2O_2 with reduced transition metal ions (Fenton reaction). Although $\cdot$OH does not diffuse significant distances within the cell, H_2O_2 easily crosses the cell membrane and penetrates into the nucleus where it reacts with ions of iron or cooper that are bound to or very close to the DNA. As a result of oxidative stress, metal ions could also be released within the cell and then bind to the DNA (Halliwell & Aruoma, 1991).

The second mechanism of DNA damage is by activation of Ca^{2+} dependent endonucleases due to oxidative stress provoked changes of metabolic reactions. The two mechanisms are not mutually independent, and their effects could be additive. Taken together, O_2^- and H_2O_2 do not react with any of the nucleotides efficiently but can produce highly reactive $OH^{\cdot}$ radicals and an OH^- anion through the Fenton and Haber-Weiss mechanisms that involve metal cations (Halliwell & Aruoma, 1991).

$$O_2^{-\bullet} + Fe^{3+} \longrightarrow O_2 + Fe^{2+}$$

$$Fe^{2+} + H_2O_2 \longrightarrow HO^{\bullet} + OH^- + Fe^{3+}$$
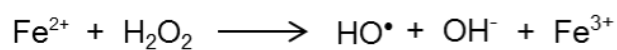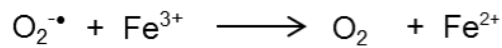
Fenton-Reaction
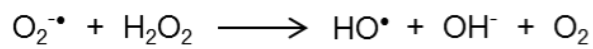
Haber-Weiss-Reaction

$$O_2^{-\bullet} + H_2O_2 \longrightarrow HO^{\bullet} + OH^- + O_2$$

Figure 1.7 Metal-catalysed formation of hydroxyl radicals.

1.3.4   Oxidative DNA modifications

Reactive oxygen species generated as by-products of the normal aerobic metabolism can damage the nuclear genome. Oxidation affects either the base or the sugar-phosphate backbone, giving rise to oxidized bases, apurinic/apyrimidinic (AP) sites, and strand breaks (Dizdaroglu, 1992). Many different types of oxidative DNA modifications are known. Some of the most important are shown in Figure 1.8.

1.3.4.1   8-Oxoguanine

The most easily oxidised of the bases in DNA is guanine, due to its lowest ionization (oxidation) potential. The major mutagenic base modification 7, 8-dihydro-8-oxoguanine (8-oxoG), is formed by oxidation of the C8 position of guanine. 8-oxoG is strongly mutagenic because it is able to base pair with adenine and thus cause G:C → T:A transversion mutations during replication (Bjelland & Seeberg, 2003).
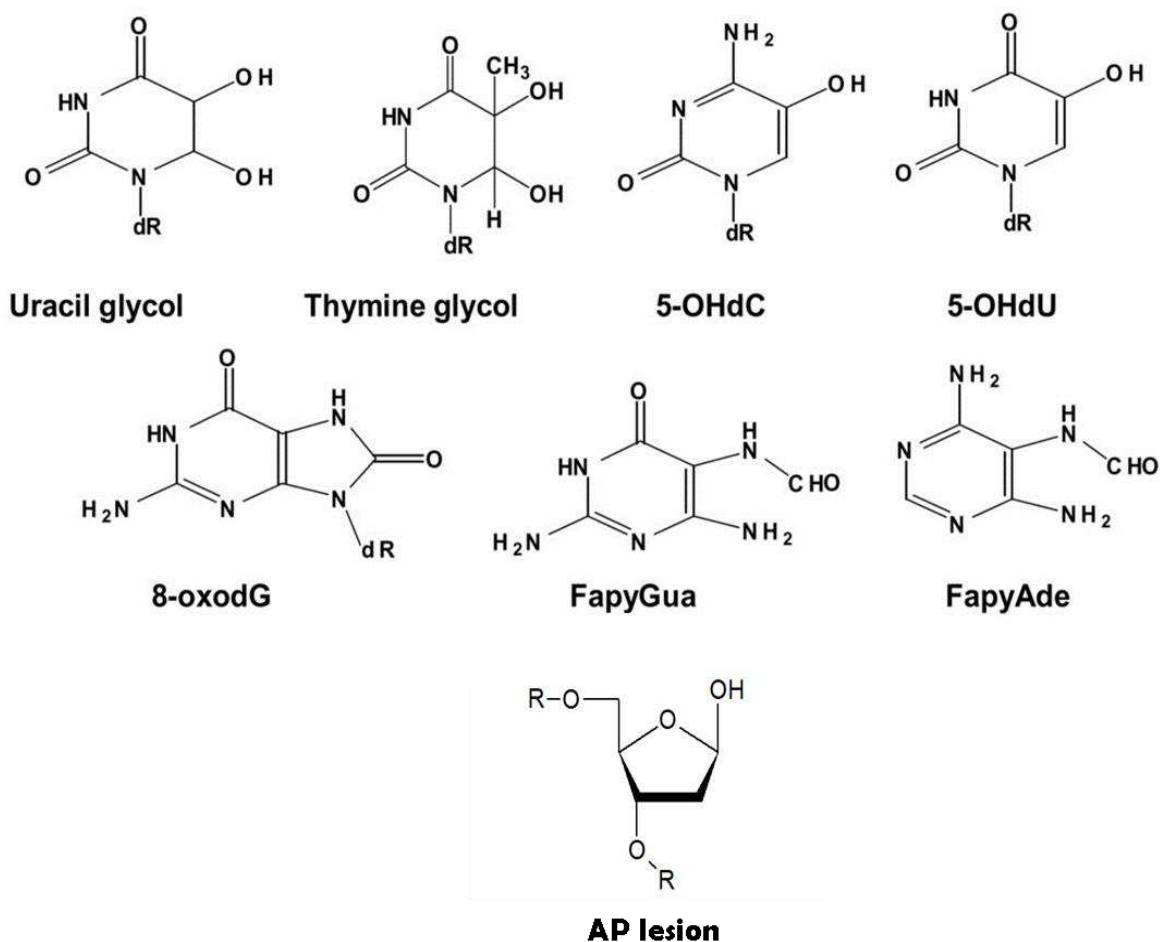
Figure 1.8 Oxidatively generated DNA lesions.

When paired with cytosine, 8-oxoG adopts the normal *anti* conformation at the *N*-glycosylic bond, forming a stable Watson–Crick base pair with three hydrogen bonds. When paired with adenine, 8-oxoG adopts the *syn* conformation at the *N*-glycosylic bond, forming a stable Hoogsteen mispair which consists of two hydrogen bonds (Figure 1.9). This is the structural basis for the 8-oxoG mutagenicity (Damsma & Cramer, 2009; Kunz, Saito, & Schär, 2009).
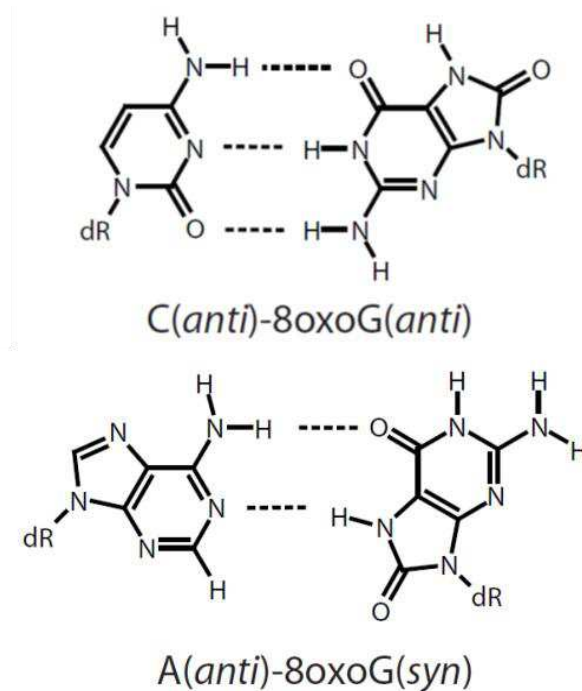
Figure 1.9 Base paring properties of 8-oxoG, according to Damsma et al. 2009. A stable Hoogsteen base pair of 8-oxoG with adenine in DNA escapes the proofreading activity of the replicative DNA polymerase leading to incorporation of wrong bases. The same type of base pairing occurs in the active site of RNA polymerases during transcription of damaged DNA, leading to transcription errors.

1.3.4.2 AP sites

DNA AP sites occur as a consequence of non-enzymatic hydrolysis of base-sugar bonds in DNA. They are also generated by DNA glycosylases as reaction intermediates in the BER pathway (Dyrkheeva, Lebedeva, & Lavrik, 2016; Lindahl & Barnes, 2000; Sengupta et al., 2016). The total generation rate of AP sites in a mammalian cell from these sources is over 10,000 per day. They are potentially mutagenic and lethal lesions that can block DNA replication and transcription (Boiteux & Guillet, 2004; Kitsera et al., 2011).

1.3.4.3 SSB

One of the main sources for SSBs is oxidative attack by endogenous ROS. SSBs can occur directly through the attack of the ROS at the sugar-phosphate backbone or indirectly as an intermediate during the DNA base-excision repair of oxidized bases, AP sites, or bases that are damaged or altered in other ways. SSBs can also arise as a result of incorrect or abortive activity of cellular enzymes such as DNA topoisomerase 1 (Caldecott, 2008; Chatterjee & Walker, 2017). A mutagenic potential of SSB cannot be excluded. Unrepaired SSB, especially at the replication fork, could lead to DSBs (see chapter 1.1) which have high cytotoxic and mutagenic potential (Chatterjee & Walker, 2017). As it was described in chapter 1.1 DSBs are the main source for micronuclei generation and genomic instability.

In this work the mechanism of micronuclei formation from SSBs produced with different damaging agents ($KBrO_3$, H_2O_2 and MMS) was investigated.

1.3.5   DNA damaging agents

KBrO$_3$ - Mechanism of bromate-induced DNA damage differs from general types of oxidative stress. Potassium bromate ($KBrO_3$) can cause DNA damage through oxidative stress. It was proposed that $KBrO_3$ together with GSH form reactive metabolites, which in turn can directly oxidize the guanine residues of the DNA and thus lead to 8-oxoG lesions. The exact mechanism has not yet been clarified, but it is assumed that GSH is subject to a rapid redox reaction, in which bromate is reduced to BrO_2^- and further reduced to BrO^- and Br. These reactive metabolites, in turn, abstract an electron from the guanine, making it a radical cation. This radical may also react with water molecule, followed by the oxidation leading to the 8-oxoG formation (see Figure 1.10). GSH is a tripeptide and as it was mentioned in chapter 1.3.2 is one of the most important antioxidant substances in cells. It reduces ROS and thus normally protects the cell from damage by radicals (Kawanishi & Murata, 2006).
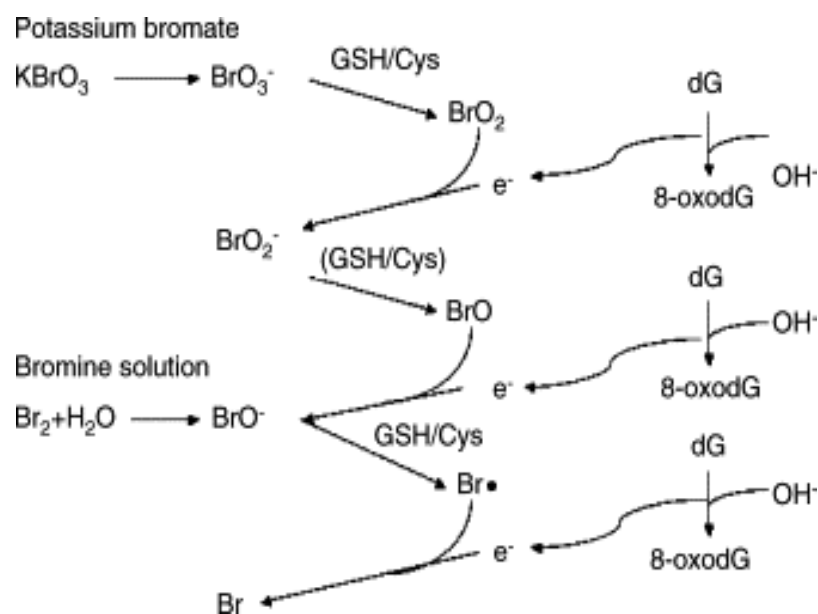
Figure 1.10 A possible mechanism of guanine oxidation induced by KBrO$_3$ in the presence of GSH / Cys (Kawanishi & Murata, 2006)

H$_2$O$_2$ - Possible mechanisms of DNA damage induction by H_2O_2 are described in chapter 1.3.3.

MMS - Methyl methanesulfonate (MMS) is a DNA alkylating agent that modifies both guanine to 7-methylguanine and adenine to 3-methyladenine. DNA damage caused by alkylating agents is predominantly repaired by the BER pathway. Methylpurine glycosylase (MPG) initiates BER of alkylated bases such as 7-methylguanine and 3-methyladenine and leads to the formation of AP sites (Jacobs & Schär, 2012).

Ro 19-8022 - Ro 19-8022 is a potent type II photosensitizer with an absorption maximum at 427 nm that in the presence of light gives rise to DNA damage via singlet oxygen. High numbers of 8-oxoG modifications (60% of all modifications) are generated via irradiation of the cells with visible light after incubation with Ro 19-8022 (Will et al., 1999).
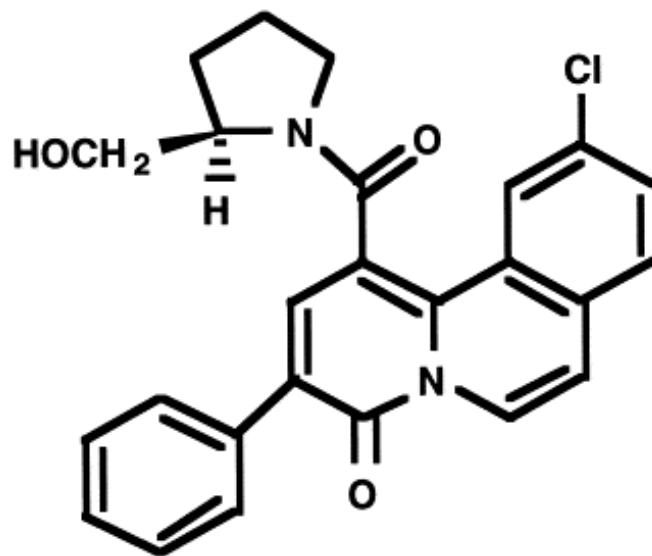
Figure 1.11 Chemical structure of Ro 19-802.

Oxidatively modified DNA is, despite extensive DNA repair, abundant in many tissues. Therefore, many defence mechanisms within the organism have evolved to limit the levels of reactive oxidants and repair the DNA damage they induce.

1.3.6   Base excsision repair (BER)

The most important pathway for the repair of endogenously generated base damage resulting from alkylation, deamination, depurination/depyrimidation and oxidation is the base excision repair pathway (BER) (Sancar, Lindsey-Boltz, Unsal-Kaçmaz, & Linn, 2004).

For the repair of a specific lesion by BER, four proteins are required: a DNA glycosylase, an apurinic/apyrimidinic endonuclease (APE) or AP DNA lyase, a DNA polymerase, and a DNA ligase.

The first step in BER is catalysed by DNA glycosylases, which recognise and excise damaged base. Glycosylases hydrolyze N-glycosidic bonds, removing the damaged base and generating abasic site, apurinic or apyrimidinic site (AP site). After base excision, the second step in the BER process is strand cleavage at the AP site. This can involve three different mechanisms: hydrolysis catalyzed by apurinic/apyrimidinic endonuclease 1 (APE1) or β or β, δ elimination by bifunctional DNA glycosylases. APE1 generates a nick at the 5'-side of the AP site formed after the removal of the damaged base. Some DNA glycosylases are simple glycosylases, catalyzing only the hydrolytic removal of the base (monofunctional), whereas others contain AP lyase activity and cleave off the base (bifunctional) (Table 1.3). In the AP lyase reaction by DNA glycosylases, DNA strand is cleaved at the AP site by β-elimination, generating a 3'-phosphor-α, β-unsaturated aldehyde (3'-dRP) at the strand break or by β, δ elimination at the AP site removes the deoxyribose residue to produce a 3'-phosphate terminus. After the lyase reaction, the 3'-sugar residue is generally removed by an AP endonuclease incising 5' to the abasic sugar to form a gap that is filled by DNA polymerase, and the resulting product is ligated. In cases where the glycosylase lacks lyase activity, the 5' incision is first made by APE1 in mammalian cells, and the abasic sugar can be removed by the dRP lyase activity of DNA Pol β, which concurrently fills in the 1-nucleotide gap. Ligation by XRCC1-Lig3 complex is completing the repair pathway. The 1-nucleotide replacement pathway is called the short-patch base excision repair.

Alternatively, long –patch BER pathway is available, with gap-filling of several nucleotides (Robertson, Klungland, Rognes, & Leiros, 2009; Sancar et al., 2004).In this mechanism the DNA polymerase β or δ are recruited to proceed with the re-synthesis of a DNA strand of 2 to 8 nucleotides, displacing the old one. The resulting flap is removed from flap endonuclease 1 (FEN1) and the DNA strand is finally closed by ligase I (Lig I) (Klungland & Lindahl, 1997). When a base modification is repaired by short patch and when by long patch is not known. For the switch between short-patch and long-patch there are few potential factors hypothesised: the ATP concentration, 5'-dRP intermediate produced by AP endonuclease activity (Robertson et al., 2009) as well the type of lesion and the cell cycle (Frosina et al., 1996).
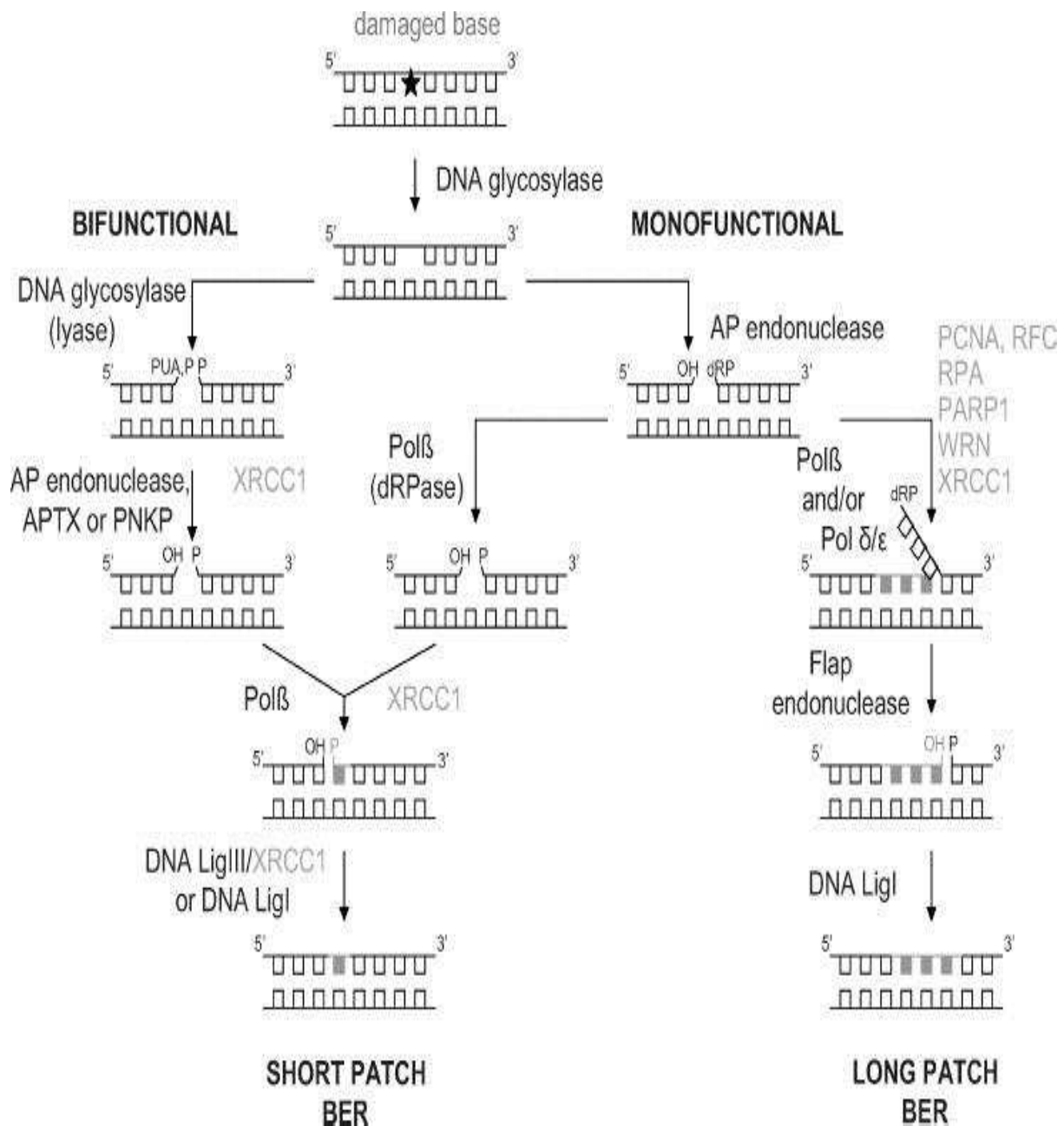
Figure 1.12 Base excision repair mechanism: short- and long patch (Baute & Depicker, 2008)

There are at least 11 different mammalian glycosylases that can detect more or less specifically different types of damaged bases, making BER a widely usable repair pathway that can deal with a wide variety of modified bases (Table 1.3). (Jacobs & Schär, 2012; Robertson et al., 2009).

Table 1.3 DNA Glycosylases and their substrates (Jacobs & Schär, 2012)

Glycosylase	Substrate	Monofunctional(M) Bifunctional (B)
OGG1	8-oxoG, FaPy,8-oxoA,dsDNA	B
UNG	U, 5-FU,ssDNA, dsDNA	M
SMUG1	U, 5-hm, 5-FU, ssDNA, dsDNA	M
TDG	T, U,5-FU, εC, 5hmU, 5-fc, 5-caC opposite G, ds DNA,	M
MBD4	T, U,5-FU, εC opposite G dsDNA	M
MUTYH	A opposite 8-oxoG	M
NTHL1	Tg, FapyG, 5-hC, 5-hU, dsDNA	B
NEIL1	Tg, FapyG, 5-hC,5-hU FapyA, 8-oxoG, ssDNA, dsDNA	B
NEIL2	as NTHL1/NEIL1	B
NEIL3	FapyG, FapyA, prefers ssDNA	B
MPG	3-meA, 7-meG, 3-meG, hypoxanthine, εA, ssDNA, dsDNA	M

1.3.7   Single strand break repair (SSBR)

Single strand break repair (SSBR) is considered a specialized, sub-pathway of BER, since it includes proteins dedicated to BER. The initiation of SSB repair starts with the binding of poly (ADP-ribose) polymerase 1 (PARP1) to the SSB. The binding activates auto-poly (ADP) ribosylation of PARP1 and recruits the XRCC1/Ligase III complex (Caldecott, 2008; Chatterjee & Walker, 2017). The polyADP-ribose chains are degraded by the poly (ADP-ribose) glycohydrolase (PARG), thereby restoring PARP1 to its de-ribosylated state for subsequent dissociation to detect the next SSB (Davidovic, Vodenicharov, Affar, & Poirier, 2001). Downstream processing of SSBs depends of the nature of 3′ and 5′ ends that are processed by the large number of enzymes that are available for this process that lead to

3′-hydroxyl (3′-OH) and 5′-phosphate moieties formation. If this is not the case, the ends undergo end processing by the APE1, polynucleotide kinase 3′-phosphate (PNKP) and aprataxin (APTX) (Caldecott, 2008). Subsequently, repair is completed via short or long BER pathway (Chatterjee & Walker, 2017).
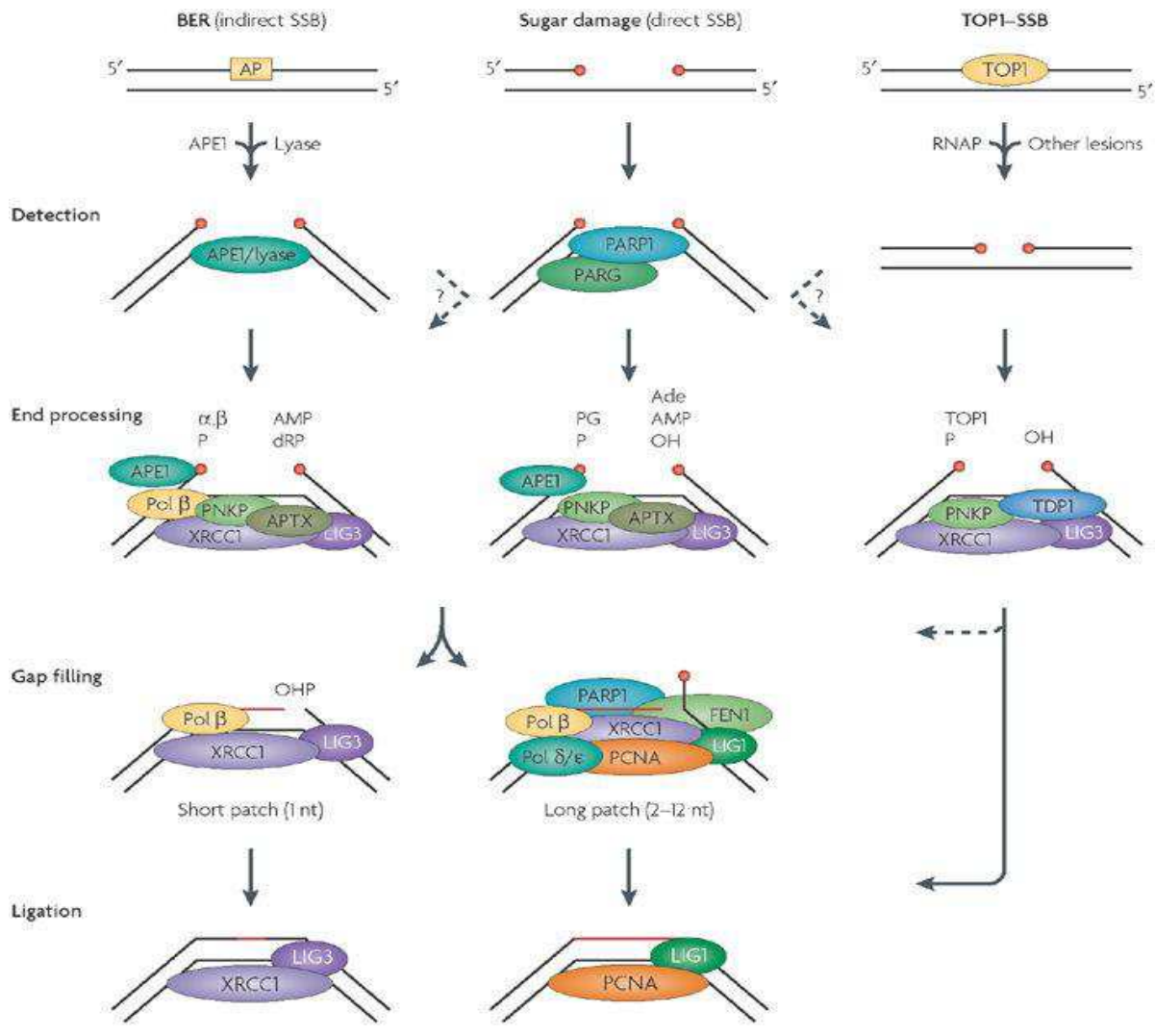
Figure 1.13 Single strand break repair (Caldecott, 2008)

1.3.8 Posttranslational modifications of BER proteins

1.3.8.1 OGG1

As a major initiator of BER OGG1, is evolutionary highly conserved, from yeast to mammals and humans. The human *OGG1* is located on the chromosome 3 (Radicella, Dherin, Desmaze, Fox, & Boiteux, 1997). Originally, seven different splice variants were found, resulting from alternative splicing of mRNA at the C-terminus (Nishioka et al., 1999). Based on their last exon they have been classified in two groups: OGG1-α (mainly

found in the nucleus) and OGG1-β (found only in the mitochondria). Glycosylase activity has been detected only for OGG1-α (Hashiguchi, Stuart, de Souza-Pinto, N C, & Bohr, 2004). As described in chapter 1.3.6 OGG1 belongs to bifunctional group of glycosylases. *In vitro* analyses showed that in addition to the glycosylase activity, excision of 8-oxoG by attacking N-glycosidic bond and creating an AP site, OGG1 possess a lyase activity by which cleaves the sugar phosphate backbone at AP site and leaves 3'-α,β-unsaturated aldehyde residue as a final product (Vidal, Hickson, Boiteux, & Radicella, 2001). However, it was recently demonstrated by Allgayer et al. (2016) that OGG1 does not manifest β-lyase activity *in vivo* and the strand cleavage is catalysed by APE1 (Allgayer, Kitsera, Bartelt, Epe, & Khobta, 2016). OGG1 is ubiquitously expressed in all tissues (Radicella et al., 1997) as a house-keeping gene (Dherin, Radicella, Dizdaroglu, & Boiteux, 1999). The bacterial structurally-unrelated, functional-homologue of OGG1 is formamidopyrimidine DNA glycosylase (Fpg) (Boiteux, O'Connor, & Laval, 1987). Fpg recognises besides 8-oxoG, FapyA, FapyG and AP lesions (Dherin et al., 1999). In bacteria, a lack of Fpg could be functionally corrected by transfection of OGG1. Mice lacking the *Ogg1* gene are viable and show no overt pathology. However, there is an age-dependent accumulation of 8-oxoG in various organs (Klungland et al., 1999; Osterod et al., 2001). An increased frequency of spontaneous mutations was also observed in liver and testes but no increased tumor incidence had been detected (Klungland et al., 1999).

DNA is packed within nucleosomes, an additional barrier for DNA repair enzymes to access damaged DNA. Radicela et al. (2010) have demonstrated that OGG1 is recruited to specific chromatin domains. In their experiments they showed that higher order chromatin organization (that was achieved by sucrose that lead to chromatin condensation) creates a first barrier for the access of the BER machinery to the lesion and slower repair. OGG1 was excluded from heterochromatin and colocolizes with euchromatin-associated proteins (Amouroux, Campalans, Epe, & Radicella, 2010). Bhakat et al. (2006) suggested that repair is enhanced due to better accessibility of DNA glycosylase to DNA. Treatment of the cells with the deacetylase inhibitor trichostatin A, which induces chromatin condensation, resulted in better repair of 8-oxoG by OGG1 (Bhakat et al., 2006).

However, Radicela et al. (2010) demonstrated that recognition or affinity of OGG1 for the lesion is not the driving force for the re-localisation of OGG1, but for the release from euchromatin compartments OGG1 requires completion of the repair.

Repair efficiency of OGG1 is modulated by posttranslational modifications such as phosphorylation and acetylation (Bhakat et al., 2006; Dantzer, Luna, Bjørås, & Seeberg, 2002; Hu, Imam, Hashiguchi, de Souza-Pinto, Nadja C, & Bohr, 2005). It has been demonstrated by Dantzer et al. (2002) that PKC is responsible for phosphorylation of OGG1. However, further analyses are required for more conclusive information about this role of the phosphorylation event. On the other hand OGG1 is acetylated by p300, both *in*

vivo and *in vitro,* at Lys 338 and Lys 341 as the major acetyl acceptor sites. Under normal conditions one fifth of the OGG1 is present in the acetylated form in HeLa cells (Bhakat et al., 2006). A model was proposed in which acetylation of OGG1, and not the change of the level of OGG1 protein, has a regulatory role in the repair of genomic 8-oxoG in response to exogenous oxidative stress. Oxidative stress enhances p300 activity which in turns acetylates OGG1. A moderate enhancement of 8-oxoG excision by AcOGG1 was demonstrated in the absence of APE1, whereas in the presence of APE1 a four fold higher activity was observed for AcOGG1 than for the unmodified OGG1. Strong stimulation by APE1 of OGG1 activity without their physical interaction was also demonstrated by (Hill, Hazra, Izumi, & Mitra, 2001). Acetylation of OGG1 reduces its affinity for the product AP site, thus enhancing its turnover. At the end balance is achieved when histone deacetylases restore OGG1 (Bhakat et al., 2006).

Besides HDACs class I (Bhakat et al., 2006) SIRT1 was shown to play a role in the regulating the acetylation status of OGG1 (Sarga et al., 2013). In the conditions of oxidative stress, AcOGG1 levels, that are lower in the hippocampus of high-running (aerobic) capacity rats (HCR) when compared to hippocampus from low-running (aerobic) capacity (LCR) rats, were accompanied with inverse correlation of SIRT1 levels. This observation suggested that SIRT1 could be a modulator of acetylation status of OGG1 in hippocampal cells.

It is interesting to note that SIRT1 was observed to modulate AcOGG1 level in neural cells, while histone deacetylases (TSA) are the primary modulators in non-neural cells (Sarga et al., 2013).

1.3.8.2   APE1

Another BER enzyme important for maintaining genome stability is apurinic / apyrimidinic endonuclease (APE1) (Lirussi et al., 2012). APE1, also known as redox factor 1 (Ref1), is a ubiquitously expressed multifunctional protein. One of its principal functions is the reduction of nuclear transcription factors, maintaining them in the DNA-binding form. The N-terminal portion of the protein is responsible for the transcriptional activity as regulatory redox activator, while the C-terminal domain exerts the endonuclease activity at AP sites. It also plays role in RNA metabolism by interacting with different proteins involved in ribosome biogenesis, pre-mRNA maturation/splicing, ribonucleotide catabolism and has the ability to cleave abasic RNA. Human APE1 is located on chromosome 14 (Dai et al., 2014).

APE1 undergoes several posttranslational modifications such as acetylation, phosphorylation, nitrosylation, ubiquitination, proteolysis and sumoylation (Busso, Iwakuma, & Izumi, 2009; Larsson, 2003; Sengupta et al., 2016). What could make APE1 a

multifunctional protein is the modulation of its posttranslational modifications. Posttranslational modifications will lead to conformational changes of the APE1 structure and makes it adjustable or expands its activity/interaction through other substrates. APE1 is an abundant and relatively stable protein with mainly nuclear localisation (Entman, 1990).

Lirusi et al. (2012) have shown that positively charged lysine ($K^{27}/K^{31}/K^{32}/K^{35}$) residues in the non-structured N-terminal domain of APE1 are essential for APE1's nucleolar accumulation through stabilization of protein interaction with nucleophosmin (NPM1) and rRNA. APE1 acetylation is mediated by p300. Besides APE1's protective role against genotoxic agents (MMS) (Yamamori et al., 2010), it was observed that its nucleolar accumulation is important for cell proliferation (Lirussi et al., 2012). Modulation of APE1 functions through posttranslational modifications was demonstrated by Bhakat et al. (2003); Fantini et al. (2008). APE1 acetylation at lysine K^6/K^7 residues is increased after genotoxic stress (MMS treatment) and the acetylation status of APE1 is reduced by SIRT1. The authors postulate a model in which, under genotoxic stress, SIRT1 deacetylates APE1, enhances its binding to XRCC1 and stimulates AP endonuclease activity (Yamamori et al., 2010).

It was speculated that SIRT1 deacetylation of lysine K^6/K^7 residues of APE1 may be reduced by full acetylation of lysine K^{27-35} residues of APE1, suggesting that the acetylation status of lysine $K^{27}/K^{31}/K^{32}/K^{35}$ residues controls the stability of SIRT1/APE1 complex. A mechanism was proposed for the coordination the overall acetylation status of APE1 according to which SIRT1 first deacetylates lysine $K^{27-35Ac}$ before deacetylating lysine K^6/K^{7Ac}. Equilibrium between acetylated and not acetylated residues of APE1 has to be achieved to guarantee a maximum enzymatic activity at the abasic DNA. APE1 acetylation may provoke its exit from the nucleoli to nucleoplasm where can be deacetylated by SIRT1 (Lirussi et al., 2012). Although there is no known acetyltransferase that is able to acetylate APE1 within the nucleoli, Lirussi et al. (2012) have suggested that SIRT1 by modulating acetylation status could be responsible for APE1 trafficking within the cell (subnuclear localization of the protein).

APE1 has role as transcriptional repressor through binding to the negative Ca^{2+} response element (nCaRE) in the promoters of parathyroid hormone, renin, Bax and APE1 itself. Interstingly, APE1 also binds the nCaRE-B sequences present in the human SIRT1 promoter. In different studies it was demonstrated that SIRT1 expression and function are regulated by external stressors, including exposure to genotoxic agents (MMS) (Cohen et al., 2004; Kim & Um, 2008; Yamamori et al., 2010).

Antoniali et al. (2013) demonstrated a dose dependent increase of SIRT1 transcription after H_2O_2 treatment. A hypothesis for an auto-regulatory loop between APE1 and SIRT1 was proposed: APE1 binds to the nCaRE element present within the SIRT1 promoter

modulating SIRT1 expression, which in turn, regulates APE1 function through deacetylation of APE1's lysine residues K6/7 (Antoniali et al., 2014; Gallagher, Bianchi, & Gessman, 1989; Yamamori et al., 2010). In the proposed model, under oxidative stress 8-oxoG is generated in the nCaRE in the promoter of SIRT1 gene. Among BER proteins that are subsequently recruited to 8-oxoG, APE1 is also present and will introduce a nick in the nCaRE sequence. While removing 8-oxoG, chromatin loops will be formed that bring RNA polymerase II (RNPII) to the transcription start site, and initiate transcription.

In summary, the studies described above indicate that SIRT1 as a posttranslational modifier is targeting many proteins and modulates their enzymatic activity, their interactions with other proteins, or their nuclear trafficking. Posttranslational modifications of DNA repair proteins may serve as adaptive cell response to DNA damage.

2   Aim

Aim of this work was to investigate the influence of sirtuins, namely SIRT1 and SIRT6, on genome stability.

As outlined above, genome instability often arises from defective DNA repair. According to my hypotheses, sirtuins, which are NAD^+-dependent deacetylases of histones and other proteins, could influence genome stability in principle by three different mechanisms. Firstly, they could modify chromatin and therefore facilitate the access of repair proteins to the DNA. Secondly, they could modify the expression of repair proteins or they could influence DNA repair by posttranslational modifications of the proteins involved. Thirdly they could affect the cellular metabolism and ROS production in a way that causes an increase of the DNA damage load.

To test these hypotheses, I used the formation of micronuclei (MN) as an indicator of genome stability / instability in my studies. For SIRT1, I addressed the following questions:

1) Does SIRT1 overexpression or deficiency influence the frequency of MN, either in untreated cultured cells or in cells exposed to agents that generate different types of DNA damage such as 8-oxoG, SSB and AP sites?

2) Is the repair kinetic of 8-oxoG, SSB or AP sites affected by the overexpression or deficiency of SIRT1 and do the influences on repair correlate with those on MN formation?

3) Is the activity of major base excision repair enzymes, in particular APE1, influenced by SIRT1, either directly or in response to DNA damage?

For SIRT6, I used *Sirt6*$^{-/-}$ knock-out mice and *Sirt6*$^{-/-}$/*Ogg1*$^{-/-}$ double knock-out mice as models to answer the following questions:

1) Does SIRT6 influence the levels of endogenously generated oxidative base modifications in spleen cells?

2) Does SIRT6 influence the repair of SSB?

3) Does SIRT6 have influence on the generation of micronuclei in peripheral blood?

4) Does SIRT6 is involved in OGG1-independent back-up repair of endogenously generated oxidative base modifications and induced 8-oxoG?

3 Material and Methods

3.1 Material

3.1.1 Instruments and Software

Autoradiography cassette type G	Rego, Augsburg
Autoclave	Technoclav 50 6.0 bzw. 2.0 (Fedegari Autoclav SPA,Albuzzo, Italy)
Balance	PB 3002, Delta Range, max. 3100 g (Mettler Toledo, Switzerland) AG 245, max. 210 g (Mettler Toledo, Switzerland)
Centrifuge	Eppendorf Centrifuge 5415 (Eppendorf Hamburg) Tablecentrifuge Galaxy Mini (VWRTM International Darmstadt) Universal 320R Centrifuge (Hettich Tuttlingen) Preparative Ultracentrifuge (Beckmann Instruments, Palo Alto, CA, U.S.A.)
Coulter Counter	Z2 Coulter® Particle Count and Size (Beckman Coulter Fullerton, U.S.A.)
Distillation apparatus	(Destamat® Heraeus Instruments Hanau)
Fluorescence microscope	(Zeiss, Oberkochen) Filter 46 63 01-9901 Leica Micro Systems Bensheim
Fraction collector	Ultrac 2070 II (Pharmacia / LKB, Uppsala, Sweden) and MM 10, Neolab 4 with timer SM 999 (Neolab, Heidelberg)
Fluorometer	TKO 100, DNA Fluorometer (Hoefer Scientific Instruments, San Francisco, USA), SFM 25 Fluorimeter (Kontron Instruments, Zürich, Schweiz
Freezer (-20 °C)	KG 3666-23 (Liebherr)
Freezer (-80 °C)	Colora UF 85-300S (Colora, Lorch)

Gel documentation system	Gel Doc 1000 with Molecular Analyst® Bio-Rad (Hercules, U.S.A.) Software Molecular Imager® Gel Doc™ XR+ Bio-Rad Hercules, U.S.A.
Halogen lamp	Osram SLG 1000-Studio (Osram, Munich) with Flecta halogen mini-burner (Reflekta)
Image Lab™ Software Version 3 Gel Electrophoresis Chamber (SDS-PAGE) Agarose-gel SDS-PAGE	Bio-Rad, Hercules, U.S.A. MGV 202 C.B.S. Scientific Del Mar, U.S.A.
Incubator	CO_2 incubator BB16, BB6060 O2 Heraeus Instruments, Hanau and Hera-Cell 25D Incubator Shaker New Brunswic New Jersey, U.S.A.Scientific
Light microscope	Telaval 31 Zeiss Oberkochen
Microwave	Micromat 175 Z (AEG) and Dimension 4 (Panasonic Service, Wiesbaden)
Peristaltic pump	ISM 759 Ismatec Laboratoriumstechnik Switzerland
PH Meter	PHM 62 Radiometer Copenhagen, Den Mark
Pipette	Pipetman P 20, P 100, P 200, P 1000, P 5000 and P 10000 (Gilson, France)
Power Supply	Power Pac 300/Power Pac BasicTM Bio-Rad Hercules, U.S.A.
PCR-Cycler	TGradient Thermocycler Biometra®; (Biometra, Göttingen)
Shakers	Scaker Labnet Orbit™ LSLabnet International Inc. Edison, U.S.A Vortex Genie 2TM Vortex-Schüttler Bender & Hohbein AG Zurich, Switzerland
Sonicator	Bachofer GM 70 HD ultrasonic Bachofer GmbH Reutlingen processor

Spectrophotometer	Biowave S2100 Spectrophotometer WPA Cambridge, U.K. Nanodrop 2000 Spectrophotometer Thermo Scientfific Waltham, U.S.A.
Transferchamber	Mini Trans®-Blot Cell Bio-Rad Hercules, U.S.A
Ultrasonic processor	Bachofer GM 70 HD Bachofer GmbH, Reutlingen
UV-Lamp	UV-B Lampe TL20W/12RS Philips Licht Hamburg
Waterbath	Köttermann Type 3042 Köttermann Uetze-Hänigsen

3.1.2   Chemicals

30 % Acrylamid-, Bisacrylamid-Stock solution Rotiphorese® Gel 30 (37,5:1)	Carl Roth, Karlsruhe
Acetic acid,	Carl Roth, Karlsruhe
Agarose Ultra Pure	Invitrogen, Carlsbad, USA
Activated carbon	Merck, Darmstadt
Albumin Fraktion V, proteasefrei	Carl Roth, Karlsruhe
Ammoniumperoxodisulfat	Carl Roth, Karlsruhe
BIORAD Protein Assay Bio-Rad,	Hercules, USA
Bisbenzimid (Hoechst No. 33258)	Sigma Aldrich, Steinheim
Bromphenolblau	Sigma Aldrich, Steinheim
$CaCl_2$* $2H_2O$	Roth, Karlsruhe
Calibration solutions (pH 5, 7, 8, 10, 11)	Merck, Darmstadt
Chloroform Carl	Roth, Karlsruhe
cOmplete Mini Protease Inhibitor Cocktail Tablets	Roche Diagnostics, Mannheim
DEPC	Carl Roth, Karlsruhe
Developer	Ilford, England
DirectPCR® Lysis: Schwanzbiopsien	Peqlab Biotechnologie GmbH
DMSO	Sigma Aldrich, Steinheim
DMEM- Medium PAA	Cölbe
EDTA	Carl Roth, Karlsruhe
EDTA Dinatriumsalz Dihydrat	Carl Roth, Karlsruhe
Ethanol, absolute	Carl Roth, Karlsruhe
Ethanol, technisch	Merck, Darmstadt

Ethidiumbromid	Carl Roth, Karlsruhe
FCS PAA Laboratories,	Cölbe (GE Healthcare Europe GmbH)
Ficoll	Biochrom, Berlin
Fixier Rapid Fixer	Ilford, England
Formaldehyd, 36 %	Sigma Aldrich, Steinheim
Giemsa Solution	Sigma Aldrich, Steinheim
Glutamin PAA,	Cölbe
Glycin	Sigma Aldrich, Steinheim
Hydrogen peroxide solution, 8.8 M	Sigma Aldrich, Steinheim
Glycerol	Sigma Aldrich, Steinheim
Isopropanol	Carl Roth, Karlsruhe
Isoton II-Solution	Beckman Coulter, Krefeld
Kaliumchlorid	Merck, Darmstadt
Kaliumdihydrogenphosphat	Merck, Darmstadt
Natriumacetat	Merck, Darmstadt
Natriumchlorid	Carl Roth, Karlsruhe
Natriumdihydrogenphosphat Monohydrat	Merck, Darmstadt
Natrium-Deoxycholat	Sigma Aldrich, Steinheim
di-Natriumhydrogenphosphat	Merck, Darmstadt
di-Natriumhydrogenphosphat Dihydrat	Merck, Darmstadt
Natriumhydroxid	Merck, Darmstadt
Magnesiumchlorid, 50 mM	Life Technologies GmbH, Darmstadt
May-Grunwald eosine-methylene solution	Sigma Aldrich, Steinheim
Orange G	Carl Roth, Karlsruhe
Penicillin/Strepto mycin PAA Laboratories Cölbe (GE Healthcare Europe GmbH	
Phenylmethylsulfonylfluorid (PMSF)	Sigma Aldrich, Steinheim
Ponceau S	Sigma Aldrich, Steinheim
Proteinase K	Carl Roth, Karlsruhe
Hydrochloric acid, 37 %	Merck, Darmstadt
SDS-Pellets	Carl Roth, Karlsruhe
Nitrogen, liquid	Höllriegelskreuth
Sulfosalicylic acid	Sigma Aldrich, Steinheim
TEAH	Merck, Darmstadt
TEMED	Carl Roth, Karlsruhe
Trichloroacetic acid	Carl Roth, Karlsruhe
Tris	Carl Roth, Karlsruhe
Triton X-100	Sigma Aldrich, Steinheim
Tween 20	Carl Roth, Karlsruhe
Western Lightning®-ECL	PerkinElmer,Rodgau

3.1.3   Inhibitors

DPQ   Sigma Aldrich, Steinheim

Nicotinamide   Sigma Aldrich, Steinheim

3.1.4   Kits

LipoFectamine 2000   Qiagen, Hilden, Germany

Effectene   Qiagen, Hilden, Germany

siRNA-Lipofectamine RNAiMAX complex   Qiagen, Hilden, Germany

3.1.5   Enzyme

Endonuclease IV (EndoIV)   New England Biolabs, Frankfurt a. M

Fpg (Formamidopyrimidin-DNA-Glycosylase)   produced by D. Warken (crude extract)
from E.coli;   according to (BOITEUX et al. 1990)

Catalase   Serva Electrophoresis GmbH, Heidelberg

Proteinase K   Carl Roth, Karlsruhe

3.1.6   Primers and siSIRT1

All primers used were ordered from Eurofins MWG Operon (Ebersberg).

Primer	Sequence (5'-)
Ogg1 for	ATGAGGACCAAGCTAGGTGAC
Ogg1 rev (*wild type*)	GCCTCACAATCAACTTATCCC
Ogg1 rev (*knockout*)	ATCTGCGTGTTCGAATTCGCCAAT
Sirt6 for	CAGGACTGGGGAATCCACTA
Sirt6 rev (*wild type*)	GTTTCATGCTGTTCCCACAA
Sirt6 rev (*knockout*)	GCAGGACCACTGGATCATTT

Prior to the first application of the primers they were diluted to 25 μM with TE buffer and frozen at -20 °C until further use.

siRNA	Sequence 5' → 3'
siSIRT	GCG-GCU-UGA-UGG-UAA-UCA-GUA-55

3.1.7   DNA & Marker

Calfthymus-DNA	Sigma Aldrich, Steinheim
DNA Marker (Gene Ruler TM100 bp Plus)	Thermo Scientific, Waltham, MA, USA
GeneRuler 100 bp DNA Ladder Inclusive 6x DNA Loading Dye (SM0241)	Thermo Scientific, Dreieich DNA

PM2-Plasmid-DNA: 10000 bp; DNA from Bacteriophag PM2; prepared according (SALDITT et al. 1972) by Ina Schulz, Mainz

3.1.8   Antibody and Protein marker

Ac-OGG1 rabbit polyclonal Ab (K338+K341) (Ab-93670)	Abcam, Cambridge UK
β-Actin (C4) (sc-4778; Lot C3012)	Santa Cruz Biotechnology, Inc. Heidelberg
OGG1 (rabbit mAb) (EPR4664(2)	Abcam, Cambridge UK
Goat anti rabbit IgG-HRP (sc-2004, Lot F1212)	Santa Cruz Biotechnology, Inc. Heidelberg
Goat anti-Rabbit IgG (H+L), Alexa Fluor 594	Thermo Fisher Scientific
Goat anti mouse IgG-HRP (SC-2005, Lot A2312)	Santa Cruz Biotechnology, Inc. Heidelberg
Page RulerTM Prestained Protein Ladder (26616)	Thermo Scientific, Dreieich
SIRT1 (rabbit mAb) (E104:ab32441)	Abcam, Cambridge UK
Ref-1 (mouse mAb) C4:sc-17774	Santa Cruz Biotechnology, Inc. Heidelberg

3.1.9   Cell lines & Mice

3.1.9.1   Cell lines

U2OS-SIRT1-GFP

Humane osteosarcoma cell line, stably transfected with SIRT1-GFP plasmid (peGFP-1 SIRT1-wt)

U2OS-Ctrl-GFP

Humane osteosarcoma cell line, stably transfected with only GFP plasmid (peGFP-1 control eV)

U2OS-Flag-SIRT1

Humane osteosarcoma cell line, stably transfected with pCMV-3-Tag-1A-dXhoI-SIRT1

U2OS-pCMV-3-Tag-1A

Humane osteosarcoma cell line, stably transfected with pCMV-3-Tag-1A

The osteosarcoma (U2OS) cells were kindly provided by Elisa Conrad and Dr. T. Hofmann (DKFZ, Heidelberg). The functional activity of the overproduced SIRT1 was demonstrated by deacetylation of the K382 of p53 (Vaziri et al., 2001).

LN428

Lentiviral transduced glioblastoma cells with knock-down of the SIRT1 gene and isogenic control cell line (Trevigen Inc.; Gaithersburg, USA/AMS Biotechnology; Frankfurt).

HeLa - OGG1-GFP

Human epithelial cervical cancer HeLa cell line stably transfected with OGG1-GFP were kindly provided by Dr. J. P. Radicella (Amouroux et al., 2010) (CEA - Laboratory for Research in Genetic Instability, Fontenay-aux-Roses, Paris, France).

HeLa

Human epithelial cervical cancer HeLa cell line were kindly provided by Dr. J. P. Radicella (CEA - Laboratory for Research in Genetic Instability, Fontenay-aux-Roses, Paris, France).

3.1.9.2   Mice strain

Heterozygous mice of the strain **129-Sirt6$^{tm1Fwa/J}$** were bought from the Jackson Laboratory and interbred to obtain mice homozygous for the 129-Sirt6$^{tm1Fwa/J}$ allele and wild type mice. This mutant mouse strain contains a *lacZ* gene knock-in resulting in a loss of function of the targeted allele. A *LacZ* gene was inserted in frame after the first 21 bp of exon 1 via homologous recombination replacing exons 1 to 6.

BigBlue® - homozygous transgenic mice from Stratagene (Germantown, USA) have the parent background C57BL6. On chromosome 7 have the bacterial *lacI* gene as a transgene.

Double knock-out Sirt6$^{-/-}$/Ogg1$^{-/-}$ and **Sirt6$^{+/+}$/Ogg1$^{-/-}$** were generated by crossing heterozygous BigBlue® and heterozygous mice of the strain 129-Sirt6$^{tm1Fwa/J}$ (see chapter 3.2.1.2)

3.1.10 Buffers, Solutions & Medium

3.1.10.1 Cell culture

Culture medium for HeLa, U2OS, LN428	DMEM (Gibco)
	10 % FCS
	1 % pyruvat
	Penicillin (100 U/ml)
Culture medium for MEF	DMEM (Gibco)
	15 % FCS
	Penicillin (100 U/ml)
Culture medium for splenocytes	RPMI 1640 (Gibco)
	10 % FCS
	Penicillin (100 U/ml)
Trypsin-EDTA	Gibco by Life Technolgies Darmstadt
PBSCMF pH 7.5	137 mM NaCl
	2.7 mM KCl
	6.5 mM Na2HPO4
	1.5 mM KH2PO4
	adjusted to pH 7.5 in deionized water and autoclaved

3.1.10.2 MEFs preparation

PBS pH7,2	137 mM NaCl
	2.7 mM KCl
	6.5 mM Na2HPO4
	1.5 mM KH2PO4

sterilized by autoclaving

0.25% trypsin-EDTA solution   Gibco by Life Technologies
                                      Darmstadt

3.1.10.3 Isolation of the splenocytes

PBSCMF pH 7.5   137 mM NaCl
                                       2.7 mM KCl
                                       6.5 mM Na2HPO4
                                       1.5 mM KH2PO4
                                       adjusted to pH 7.5 in deionized
                                       water and autoclaved

PBS   1.4 M NaCl
                                       0.1 M NaH2PO4
                                       adjusted to pH 7.2 in deionized
                                       water and autoclaved

Erythrocyte-Lyses buffer   8.29 g/L NH4Cl
                                       1 g/L KHCO3
                                       0.037 g/L EDTA
                                       adjusted to pH 7.4 in deionized
                                       water and sterile filtered (0,2 μm)

Culture medium   RPMI 1640 (Gibco)
                                       10 % FCS
                                       Penicillin (100 U/ml)

3.1.10.4 Alkaline elution

BE1 Buffer, pH 7.5	20 mM	Tris
(autoclaved)	100 mM	NaCl
pH adjusted with conc. HCl	1 mM	Na_2H_2EDTA
BE1 pH 7.5 with BSA	15 mg	BSA
	30 ml	BE1 pH7.5

Lysis Buffer pH 10	2%	SDS
pH adjusted with conc. NaOH	100 mM	Glycin
	20 mM	Na_2H_2EDTA

Elution buffer pH 12.1-12.2 pH adjusted with TEAH	20 mM	H_4EDTA
Washing buffer pH 10 (autoclaved) pH adjusted with 10N NaOH	20 mM	H_2EDTA
Phosphate Buffer pH 6.0 (autoclaved)	87.8 mM 12,2 mM	NaH_2PO4 Na_2HPO4
Phosphate Buffer pH 7.2 (autoclaved)	28 mM 72 mM	NaH_2PO4 Na_2HPO4
Phosphate Buffer pH 7.2 with Bisbenzimide 1% (v/v) Add bisbenzimide shortly before use, protect from light	0.15 mM	Bisbenzimide

3.1.10.5 Microscopy

Cytoskeleton (CSK) buffer	100 mM	NaCl
	300 mM	sucrose
	10 mM	PIPEs pH 6.8
	3 mM	MgCl2

3.1.10.6 PM2-Relaxation assay

Lysis buffer	20 mM	Tris-HCl pH 8.0
	250 mM	NaCl
	1 mM	EDTA pH 8.0
	Protease inhibitor 10x (cocktail tablet)	
PMSF stock aliquots stored on -20	100 mM PMSF in Isopropanol	
Precipitation solution pH 7.2	2.5 mM	Natriumacetat in Ethanol
Reaction buffer	10 mM	Hepes pH7.5
	1 mM	$MgCl_2$

	200 mM	NaCl
Solution I pH 7.4	0.1 M	Natriumacetat
	0.1 M	NaCl
Solution II pH 8	0.2 M	Tris-HCl
	1 mM	EDTA
TAE-Buffer 10X pH 7.8	400 mM	Tris
pH adjusted with Acetic acid	500 mM	Natriumacetat
	100 mM	EDTA
Stop Buffer	1 ml	TAE 10X
	7 ml	Glycerol
	5 mg	Bromphenol blue
	2 ml	EDTA (50 mM pH 7)
	0.5 %	SDS

3.1.10.7 Western Blot

APS 10 %	100 µl	Ammoniumpersulfat
aliquots stored on -20	1 ml	dist.H_2O
Blocking solution	1.5 mg	BSA
	30 ml	0.1 % TBST
Electrophoresis buffer 5X	15.1 mg	Tris
	94 g	Glycin
	25 ml	SDS 20 %
	1 l	dist. H_2O
Loading Buffer 6X	8 ml	1M Tris-HCl pH 6.8
	2 g	SDS
	10 ml	Glycerol
	Small drop of spatula	Bromophenol blu
	1.4 ml	2-Mercaptoethanol
PMSF-Stock solution (100 mM)	175 mg	PMSF
aliquots stored on -20	10 ml	Isopropanol
Ponceau red 10X	2 g	Ponceau S

		30 g	Trichloroacetic acid
		30 g	Sulfosalicylic acid
		1l	dist. H_2O

| Protease Inhibitor Coctail 10X | 1 Tablet | cOmplete |
| aliquots stored on -20°C | 1 ml | dist.H_2O |

RIPA buffer	1 M	Tris-HCl pH 7.4
storage: light protected 4-8°C	1 M	NaCl
	250 µl	Triton-X100
	250 µl	Natrium-Deoxycholat
	20 %	SDS
	0.5 M	EDTA
	25 ml	dist.H_2O

add PMSF solution before use (final concentration 1 mM)

| SDS 20 % | 10 g | SDS |
| | 50 ml | dist. H_2O |

Separation gel SDS-PAGE (10%)	30% Acrylamid-Bisacrylamid Solution
	1.5 M	Tris pH 8.8
	20 %	SDS
	10 %	APS
	TEMED
	in dist. Water

Stacking gel SDS-PAGE	30% Acrylamid-Bisacrylamid Solution
	1 M	Tris pH 6.8
	20 %	SDS
	10 %	APS
	TEMED
	in dist. Water

TBS 10X pH 7.5	200 mM	Tris
(autoclaved)	1.5 M	NaCl
	700 ml	H_2O

Adjust pH with conc.HCl   ad. 1 l dist.H_2O

TBST 0.1 %	100 ml	10XTBS
	1 ml	Tween
	ad. 1 l H_2O

TBST 0.5 %	100 ml	10XTBS
	5 ml	Tween
	ad. 1 l H_2O	
Transfer buffer without SDS	5.8 g	Tris
storage :4-8 C	2.9 g	Glycin
	200 ml	Ethanol
	ad. 1 l H_2O	

3.2   Methods

3.2.1   Working with animals

3.2.1.1   Breeding and keeping

Animals were housed in the Central Animal Facility (ZVTE) at the University Hospital Mainz. Keepers of the institution were taking care for the animals. Animals were housed in optimal conditions: transparent plastic cage with metal grid including slot for diet and drinking water, in a temperature-controlled room, 12h light-dark cycle and constant humidity of 50-70%. The breeding, keeping and animal experiments were performed according to the provisions of the German Animal Protection act.
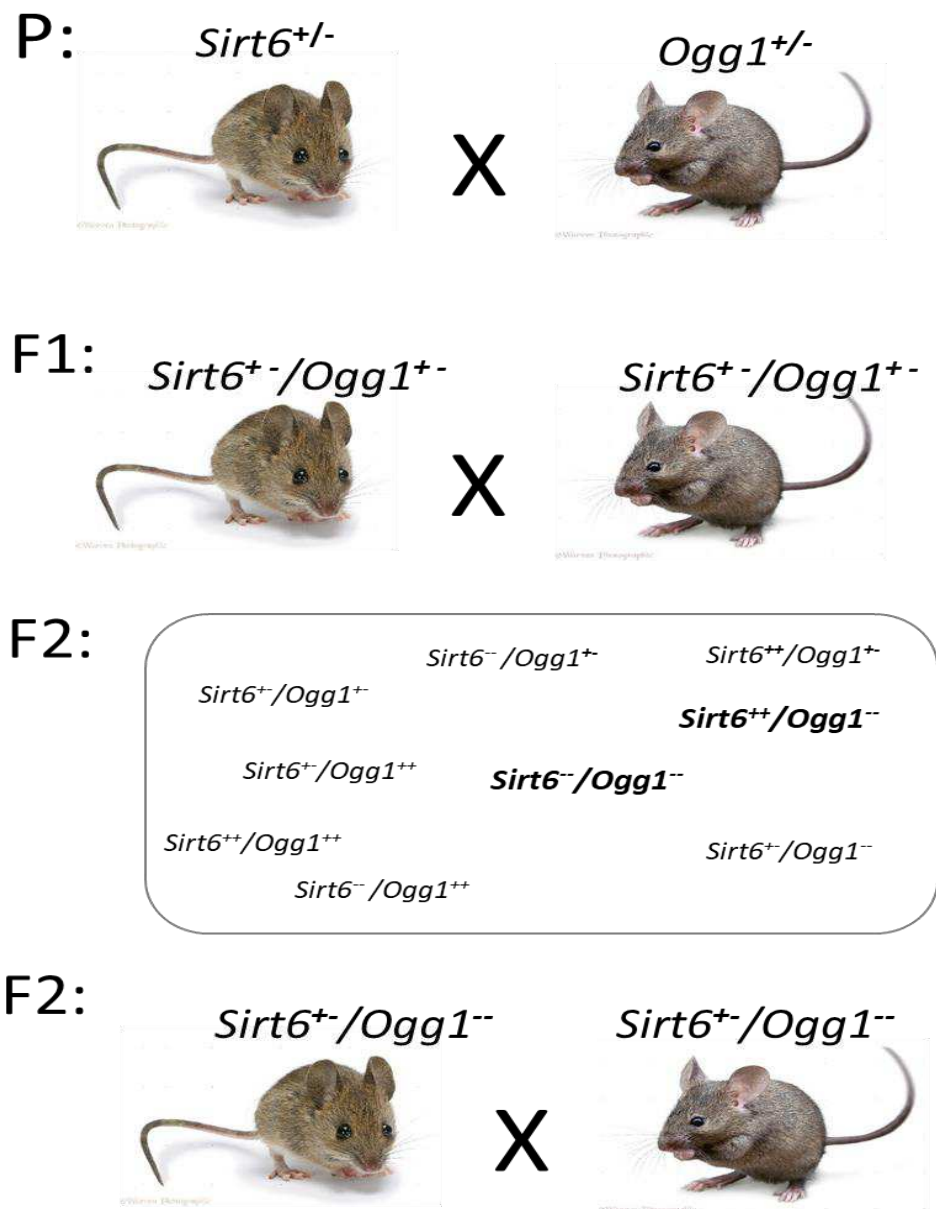
Figure 3.1 Generation of Sirt6$^{+/+}$Ogg1$^{-/-}$ and Sirt6$^{-/-}$Ogg1$^{-/-}$ double knockout mice.

3.2.1.2   Generation of different genotypes

In the first breading step, heterozygous 129-*Sirt6*^{tm1Fwa}/J mice were interbred. Mating was polygamous, in all breading steps one male was breed with two females. With this interbreeding, three genotypes were generated: *Sirt6*^{+/+} wild type, *Sirt6*^{+/-} heterozygous and *Sirt6*^{-/-} deficiency. Crossing heterozygous 129-*Sirt6*^{tm1Fwa}/J mice with heterozygous Ogg1^{+/-} Big Blue mice, Sirt6^{+/-}Ogg1^{+/-} mice were generated. In the second breading step, F1 generation, Sirt6^{+/-}Ogg1^{+/-} mice were crossed. In F2 generation, nine genotypes were generated (see Figure 3.1). Homozygous Sirt6^{-/-}Ogg1^{-/-} double knockout and Sirt6^{+/+}Ogg1^{-/-} mice as a control were used for further experiments.

3.2.1.3   Marking of the animals

To distinguish the animals, it was used ear punching that involves using a special punch to either produce a small (0.5-2 mm) notch near the edge or to punch a hole in the middle of the ear. The number and combination of the ear holes in each mouse was used to distinguish the animals.

3.2.1.4   Mouse genotyping

Genotype of the mice was determinate by polymerase chain reaction (PCR) using specific primers. Ear biopsy was used for the isolation of genomic DNA. 200 µl of lyses buffer Peqlab DirectPCR® Lyses Reagent Tail containing Proteinase K (0.4 mg/ml) were added to the ear biopsy and incubated for 3-16 h at 55°C. On the following day, samples were incubated for 1h at 90°C in order to inactivate Proteinase K and were ready for PCR use or stored on -20. The sizes of the PCR products were analysed by agarose gel electrophoresis. PCR was used to exponentially amplify defined DNA fragment *in vitro*. The length and position of the amplifying fragment was determined by the choice of the primers. Isolated DNA from the mouse tail biopsies served as DNA templates. By combination of forward and reverse primers specific for the *Sirt6*-wild type allele and *Sirt6*^{tm1Fwa} *knockout* allele, homozygous wild type, knockout and heterozygous animals can be distinguished. PCR for the determination of the *Sirt6* and *Ogg1* genotypes was made using the PeqlapGold Taq-DNA-Polymerase "all inclusive" kit according to the manufacturer. During the PCR, the reaction mixture containing the double-stranded DNA template, forward and reverse primers, dNTPs and DNA polymerase were subjected to different requiring temperature conditions.

Table 3.1 Mouse Genotyping OGG1.

			# Cycle	[C°]	[min]
Reaction buffer Y	5	µL	1	94	3
Enhancer P	10	µL	35	94	45 s
dNTP-Mix	1	µL		59	1
Upstream primer (25 pmol/µL)	2	µL		72	2
Downstream primer KO	2	µL	1	72	10
Downstream primer WT	2	µL			
Taq polymerase	0.25	µL			
H$_2$O sterile	26.75	µL			
	49				
+ template DNA	1	µL			
Sum	50	µL			

Table 3.2: Mouse Genotyping SIRT1

			# Cycle	[C°]	[min]
Reaction buffer Y	5	µL	1	94	3
Enhancer P	10	µL	35	94	45 s
dNTP-Mix	1	µL		55	45 s
Upstream primer (25pmol/µL)	2	µL		72	30 s
Downstream primer KO	2	µL	1	72	10
Downstream primer WT	2	µL			
Taq polymerase	0.25	µL			
H$_2$O sterile	25.75	µL			
	48	µL			
+ template DNA	2	µL			
Sum	50	µL			

3.2.1.5   Agarose gel electrophoresis

PCR products were separated in a 2% agarose gel electrophoresis. 2g of agarose gel was completely dissolved in 100 ml 1xTAE buffer by heating in the microwave. The solution was bubble-free poured in a gel chamber equipped with combs. Samples were mixed

with 5 µl 6X loading dye. GeneRuler-100bp-DNA ladder was used as molecular size. Total volume of 30 µl (25 µl sample +5 µl loading dye) was loaded into gel pockets. DNA electrophoresis was performed for 2h at 100 V. To visualize DNA under UV light, gels were stained with 0.5 mg/L ethidium bromide in TAE buffer for 30 minutes and rinsed briefly in deionised water. Images of the gels were taken with a BioRad Gel Doc 1000 and analyzed with Image Lab™ software. The size of the PCR product obtained from the DNA of the Sirt6 and Ogg1 knockout mice is 300 bp. However, the size of the PCR product from the Sirt6 wild type mice is 400 bp and that from Ogg1 wild type is 250 bp (see Figure 3.2).
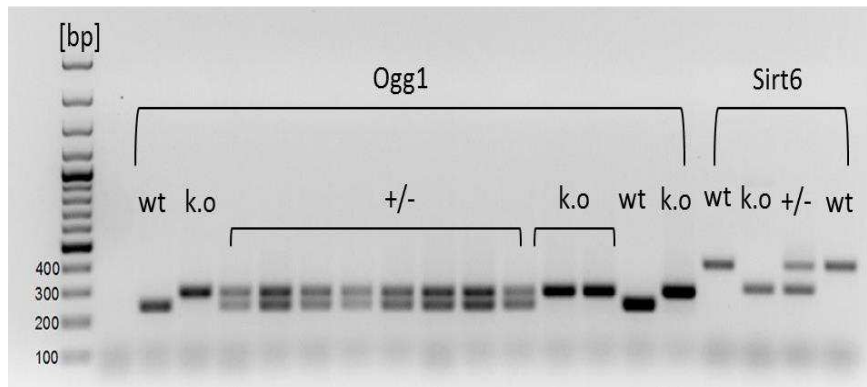
3.2 Agarose gel picture of genotyping.

3.2.1.6 Isolation of the cells from the spleen

Mice were placed in a chamber containing isoflurane. To assure death, cervical dislocation was performed. Mice were placed on their back and their extremities were fixed with tape. Abdomen was opened with Y-cut and spleen was taken out and placed in a petri dish. One ml of cold PBSCMF was injected into the spleen with 25 G cannula in several places. Cell suspension released in the petri dish was drowned back in the syringe and filtered through the cell strainer (100 µm pore size) into a 50 ml falcon. Cell suspension in the falcon was diluted up to 30 ml with PBSCMF and centrifuged for 10 minutes, 1500 rpm, 4°C. Pellet was re-suspended in 1 ml erythrocyte lysis buffer, incubated for 5 minutes on ice. Solution was diluted with RPMI medium (10% FBS, 1% P/C) to 30 ml and centrifuged for 10 minutes at 1500 rpm, 4°C. Pellet was re-suspended in 1 ml RPMI medium and cell number was determinate with Coulter counter. Cells were frozen in a FBS containing 10% DMSO (see chapter 3.2.2).

3.2.1.7 Preparation and culture of mouse embryonic fibroblasts (MEFs)

Mouse embryonic fibroblasts (MEFs) can be isolated from mouse embryos with any genetic background. However, it is recommended that wild-type-control and mutant MEFs be prepared from mice with identical strain backgrounds, to reduce the risk of

possible genetic background–dependent variations. If the transgenic or homozygous mutant mice are viable and fertile, wild-type and mutant embryos can be generated from wild-type and mutant mating pairs, respectively. If the homozygous mutant mice are infertile or lethal, heterozygous mating pairs should be used to produce wild-type, heterozygous, and homozygous embryos. The optimal ages of mouse embryos for MEF isolation are from embryonic day 13.5 (E13.5) to E15.5.

In order to prepare primary MEFs from 129-$Sirt6^{tm1Fwa}$/J mice, one adult $Sirt6^{+/-}$-heterozygous male was placed in same cage with two adult $Sirt6^{+/-}$-heterozygous females or one male $Sirt6^{+/-}Ogg1^{+/-}$-double heterozygous mouse was placed in same cage with two $Sirt6^{+/-}Ogg1^{+/-}$-double heterozygous female mice. After 48h females were transferred into new cages and that day was recorded as E0.5 day. On E13.5 day mice were placed in a chamber containing isoflurane. To assure death it was performed cervical dislocation. Mice were placed on their back and their extremities were fixed with tape. Abdomen was opened with Y-cut. The entire uterus containing all embryos was dissected. Uterus was transferred into a 50 ml falcon with 30 ml sterile PBSCMF. Tube was inverted several times to wash the uterus. In a laminar flow, uterus with embryos was transferred into a 10-cm tissue culture dish containing 10 ml sterile PBSCMF. Individual embryos were exposed by cutting one side of the uterine wall with dissection scissors. Yolk sac was opened to dissect out all fetuses intact. All fetuses were transferred into a new dish containing 10 ml sterile PBSCMF. Liver and heart were discarded and by removing the upper part of the head, brain was also removed. The remaining part of each fetus was washed in sterile PBSCMF to remove as much blood as possible and then fetus was transferred into a new dish.

For analyses of the genotype of individual embryos, one of the hind limbs (for E13.5 and older embryos) or the yolk sac (for 12.5 and younger embryo) were collected. DNA was extracted and PCR was performed (see chapter 3.1.4).

2-3 ml of ice-cold 0.25 % trypsin-EDTA was added to the dish. With two pairs of forceps all fetuses were teased into fine pieces. Using a pipet, all material was transferred into a 15 ml falcon, and ice-cold 0.25 % trypsin-EDTA was added to bring the total volume to 3 ml per embryo. Tubes were incubated overnight at 4°C, to allow trypsin to diffuse into the tissues (trypsin has no activity at 4°C).

Next morning, without disturbing the tissue at the bottom of the tube, most of the trypsin solution was aspirated, leaving an amount equivalent to approximately two volumes of the tissue. Tube was incubated 30 min in a 37°C water bath.

After the incubation, 8 ml MEF culture medium was added for a 15-ml tube and pipet vigorously and repeatedly up and down to break up the digested tissues into a cell suspension. One minute incubation allowed remaining clumps to fall to the bottom of the

tube. Supernatant cell suspension was transferred into a new tube. More MEF culture medium was added to the tube containing the remaining tissue clumps and vigorously pipet up and down for 1 min. Sedimentation of the cell suspension by gravity for 1 min to let remaining clumps to fall to the bottom of the tube was repeated and the supernatant cell suspension was combined with the cell suspension already collected.

Mixed cell suspension was plated in 75-cm^2 culture flask with 10 ml MEF culture medium and incubated overnight. Next day, medium was aspirated and cells were washed with 10 ml PBSCMF to remove all nonadherent cells. 10 ml fresh MEF culture medium was added to the flask and cells were cultured to the near confluency. Cells at this stage are designated as passage 1 MEFs. When cells reached confluency, they were splitted (see chapter 3.2.). Proliferation of MEFs in primary culture decreases by passage 6-7. All functional analyses were performed with MEFs no later than passage 6-7.

3.2.2   Cell culture

3.2.2.1   Culture of adherent cells – cell passaging, cell number determination

Work with cell culture was always performed under sterile conditions, under the laminar flow, using sterile or autoclaved materials. Cultivation of the cells was done in a cell incubator at 37°C, 5% CO2 and 99% humidity. Cells were cultured in DMEM (Dulbecco's Modified Eagle) medium, where additionally were added 2 mM pyruvate, 2 mM L-glutamine, 100 U / ml penicillin. In case of cells derived from human tissue 10% FCS was added to the medium, whereas 15% FCS was added to the medium for mouse embryonic fibroblasts. G418 µl/ml was used to maintain the selection pressure for culturing HeLa and U2OS cells transfected stably with the OGG1-GFP or SIRT1-GFP plasmid, respectivaly. For lentiviral transduced LN428 glioblastoma cells, 1 mg/ml puromycin was used.

When cells were reaching confluence (approximately 75% of the cultured surface covered with cells), they were washed with 1xPBSCMF and incubated with trypsin in the cell incubator at 37°C for maximum of 5 minutes, until their detachment. Resuspendet cells in full medium were counted in a Z2 Coulter®Particle Count and Size Analyzer and transferred in a new flask in the dilution ratio of approximately 1:5. Cells were passaging every 2-3 days.

3.2.2.2   Freezing and thawing of the cells

After detachment with trypsin and resuspension in fresh medium, cells were centrifugated (1,000 x g, 5 minutes, 4°C), cell pellet was re-suspended in a medium containing 10% DMSO. Carefully re-suspended cells were aliquoted in cryo-vials, stored in cryocontainer at -80°C overnight and finally saved in liquid nitrogen.

For re-cultivation of the frozen cell lines, they were thawed in water bath at 37°C, transferred in a cold medium and centrifuged (1,000 x g, 5 minutes, 4°C). Cell pellet was re-suspended in full medium and transferred to a 75-cm^2 cell culture flask. Next day medium was changed and when cells were reaching confluence, they were passed.

3.2.2.3   Proliferation assay

3.2.2.3.1   Principle

The proliferation assay is a simple and rapid method for estimating the extent of the toxicity of a substance or damaging conditions. Cells are treated with a substance and the proliferation factor is determinate by determination of the cell number. Untreated cells serve as a comparison for determining the toxicity of the substance.

3.2.2.3.2   Procedure

Depending on the need of the experiment, different numbers of the cells were cultured in a 25-cm^2 / 75-cm^2 cell culture flask. After 24h, the medium was changed and cells were incubated with different concentrations of H_2O_2 or MMS or $KBrO_3$ in the presence of glutathione for 15 minutes at 37°C in serum free medium. Untreated cells were always used as a controls. (Control cells were incubated in parallel in complete medium). After the treatment one sample was counted, to obtain the cell number at time t=0. Treated cells were rinsed twice with 1xPBSCMF and cultured under normal culture conditions in a full medium for another 24h. After 24h from the treatment, cells were counted at time t=1. For determination of the proliferation factor, the quotient of t1 and t0 was used.

3.2.3   Micronuclei test

3.2.3.1   Principle

The micronucleus test is a sensitive indicator for chromosomal damage and genotoxicity. Micronuclei are formed during cell division as a result of chromosomal damage or damage in the spindle apparatus. Chromosome fragments lacking a centromere or whole chromosomes that are unable to migrate with the rest of the chromosomes during the anaphase, cannot be integrated into one of the daughter nuclei, develop nuclear membranes and remain as micronuclei (Fenech et al., 2011). Micronuclei can be determined *in vivo*, e.g. in erythrocytes and *in vitro* cell culture. For *in vivo* tests, usually bone marrow or peripheral blood is used. Micronuclei detected in erythrocytes come from their precursor erythroblasts. Erythroblasts during their development into erythrocytes extrude their main nucleus.

In vitro micronucleus test, cell cultures are exposed to a substance, grown for a sufficient period (to allow cell division and thus micronuclei formation), stained, and microscopically analysed for the presence of micronuclei.

3.2.3.2 *In vitro* micronuclei

Between 300 000 and 1 million cells were cultured in a 25-cm^2 / 75-cm^2 culture flasks. After 24h, cells were treated with different concentrations of $KBrO_3$ (with or without GSH) or H_2O_2 or MMS in a serum free medium or PBS-containing Ca^{2+} and Mg^{2+} for 15 min at 37°C. After treatment, cells were washed 2x with PBSCMF and cultured for 24h in a fresh full medium so that the cells undergo at least one cell division. Afterwards, cells are washed 1x with PBSCMF, trypsinised and re-suspended in full medium. One to three drops of the cell suspension (1×10^5 cells) were fixed on a microscope slide by cytospin centrifugation and treatment with methanol at –20°C for 1 h. Cells were stained with bisbenzimide-PBSCMF solution (5 µg/ml) or acridine orange for 1 minute or 30 seconds, respectively and rinsed 2x with PBSCMF for 1 minute. Afterwards 5 µl of mounting medium was added and coverslips were applied without bubbles. One thousand cells were analysed for the presence of micronuclei with a fluorescence microscope in duplicates.

3.2.3.3 Transient transfection of HeLa cells by means of Effectene

HeLa cells were plated 16–24 hours before transfection per well of the 6-well plates. Directly before transfection, the medium was substituted with a fresh one (1.6 ml per well). Cells were transfected with 400 ng plasmid DNA with the help of Effectene. Effectene transfection mix was prepared at room temperature as indicated in Table 3.4. The transfection medium containing plasmid DNA and transfection reagent was replaced with the fresh medium after 5 hours. 24 Hours after the transfection, cells were damaged with different concentrations of $KBrO_3$ in the presence of 4 mM GSH for 15 min at 37°C in a serum free medium and used for micronuclei analyses as described above (see chapter 3.2.3.2).

Table 3.3 Pipetting chart for transfection with Effectene per well

SIRT1-GFP plasmid (100 ng/µl)	4 µl
EC Buffer	100 µl
Enhancer	3.2 µl
Effectene	10 µl

3.2.3.4 *In vivo* micronuclei

Few drops of blood from the mouse open aorta were coated on a microscope slide and air-dried for several hours. Afterwards, slides were immersed in a *May-Gruenwald* solu-

tion for 5 minutes and then rinsed with distilled H_2O for 5 minutes. Staining was performed with Giemsa solution for 20 minutes at RT. Afterwards, slides were rinsed twice with distilled H_2O. Detection of the nuclei (blue), erythrocytes (pink-red), lymphocytes (light blue-blue) and the thrombocytes (red-violet) was performed with fluorescence microscopy. One thousand erythrocytes per mouse were counted in duplicates.

3.2.4   Alkaline Elution

3.2.4.1   Principle

Alkaline elution, developed by Kohn (Lombard, 2009), is a highly sensitive method for the detection of intracellular DNA single strand breaks (SSBs). It is based on the principle that the elution of the single-stranded DNA from a polycarbonate filter depends on its length. Shorter DNA fragments as a result of many SSBs elute faster than longer DNA fragments. By modifying the method, which involves additional incubation with repair endonucleases, it is also possible to detect DNA base modifications (Martinez-Pastor & Mostoslavsky, 2012). The repair enzymes detect DNA modifications and cut at the damage site, which then is detect as a single strand break. The detection limit of alkaline elution is 0.05 lesions per 10^6 base pairs. The method is thus 200 times more sensitive than the PM2 relaxation assay (Mostoslavsky et al., 2006). The principle of the alkaline elution is illustrated in Figure3.3. The suspension of cells in which DNA damage is going to be quantified is applied to a polycarbonate filter. Immediately afterwards, the cells are lysed by adding buffer containing SDS and proteinase K, pH 10. In the following washing steps, proteins, RNA and membranes are washed and only double stranded DNA remains on the filter. In some cases, the following step is an incubation with repair endonucleases. Finally, DNA is separated into single strands by addition of an alkaline buffer (pH 12) and eluted in various fractions. The amount of DNA per fraction is quantified fluorometrically after adding bisbenzimide in a neutral buffer (pH 6). Calibration of the alkaline elution with γ-rays radiation (6 Gy=1 SSB/10^6 base pairs) allows quantification of DNA damage (Lombard, 2009).
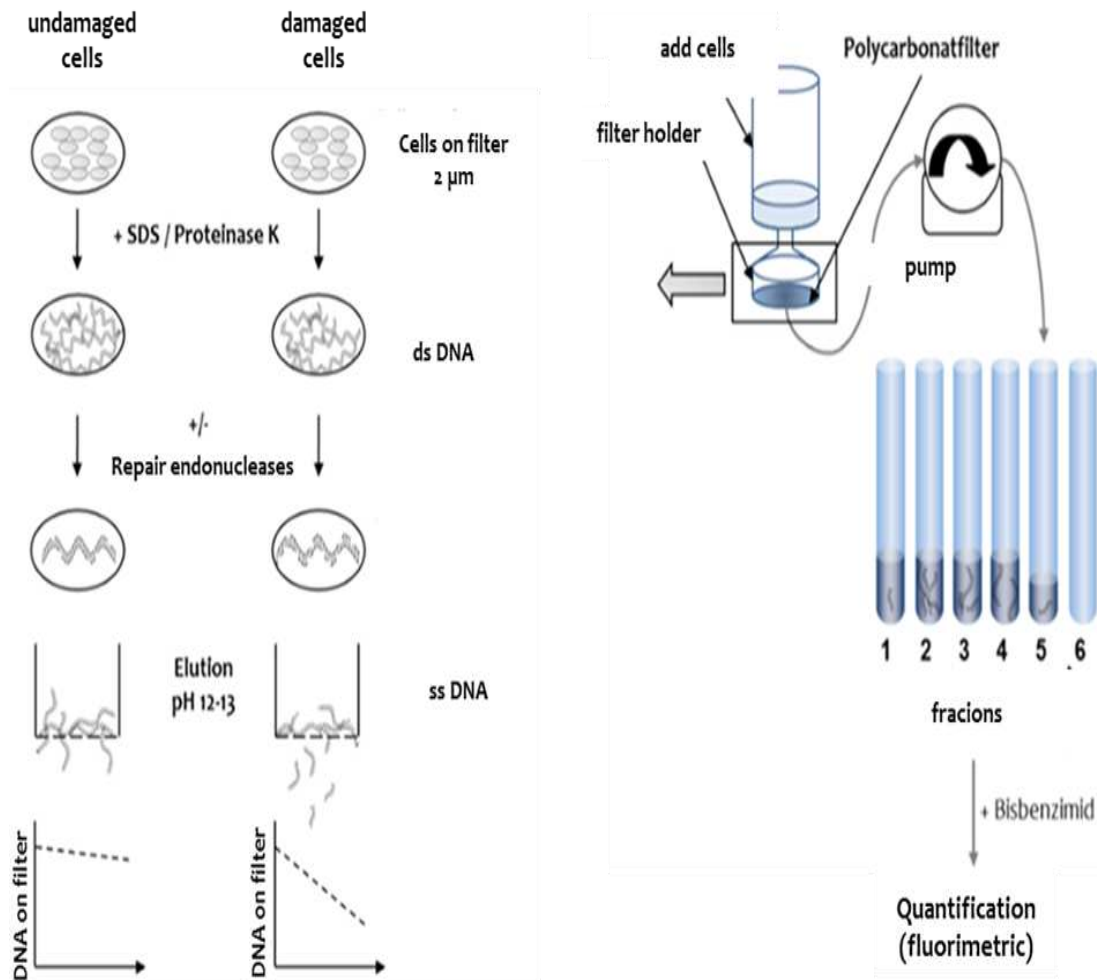
Figure 3.3 Principle of the alkaline elution assay.

3.2.4.2 Experimental setup and preparation

Alkaline elution consists of twenty 25 ml disposable syringes without pistons. All syringes are fixed at the same level and can be immersed in a temperature-controlled water bath up to the filter holder. Before applying the cell suspension, polycarbonate membrane filters (25 mm diameter, 2 μm pore size) have to be installed at the bottom end of each syringe. The structure of alkaline elution is shown in Figure 3.3. Cell suspension and buffers are pipetted into the syringes and pumped by a multichannel pump through a syringe, filter and dialyses tubes into a waste container. The waste container is replaced by a fraction collector which consists of glass tubes for collecting the eluted DNA. In order to keep the flow rate of the buffers between different samples constant, peristaltic multichannel pump is connected to the filter holder. Before starting the experiment, polycarbonate filters have to be installed to the syringes. Three syringes per sample are required for detection of DNA damage: one without and two with repair enzyme. Installed filters are placed in a bubble-free manner on the already used filter holders and are filled with dis-

tilled water. Then 2x2.5 ml of cold PBSCMF is added in the syringes and pumped through the filter holders.

3.2.4.3   Treatment of the cells

KBrO$_3$, H$_2$O$_2$ or MMS Three million glioblastoma or osteosarcoma cells were cultured in a 75-cm^2 culture flasks. After 24h cells were treated with different concentrations of KBrO$_3$ (with or without GSH) or H$_2$O$_2$ or MMS in a serum free medium or PBS-containing Ca^{2+} and Mg^{2+} for 15 min at 37°C. After treatment, cells were washed 2xPBSCMF and cultured for different recovery times, in a fresh full medium. Afterwards, cells were washed 1xPBSCMF, trypsinased and re-suspended in a full cold medium.

Ro 19-8022 photosensitizer. Three million MEFs were cultured in 75-cm^2 culture flasks. After 24h cells were damaged by exposure to the 300 nm Ro 19-8022 photosensitizer for 10 min on ice, plus visible light (38 cm, 1000W). After treatment, cells were washed 2xPBSCMF and cultured for different recovery times, in a fresh full medium. Afterwards, cells were washed 1xPBSCMF, trypsinased and re-suspended in a full cold medium.

3.2.4.4   Lysis of cells, enzyme incubation and elution

At the beginning of the experiment before applying the cell suspension, after the filters have been installed in the filter holders, syringes are filled with sterile distilled water, then rinsed twice with ice cold 2.5 ml PBSCMF and water bath is adjusted to 4°C. Depending on the cell type 1x10^6 cells are added per filter, corresponding to a 10 µg amount of DNA. There is also always one filter that doesn't contain any cells as a blank control. By washing twice with 3 ml of cold PBSCMF, residues of the cell culture medium are washed away. During the second washing step the water bath is adjusted to 25°C. Cell lysis can be started from the temperature of 15°C to avoid the SDS precipitation from the lysis buffer. Two ml of lysis buffer (2% SDS) are pumped through the filters with maximum pump speed. To complete the lysis and remove all proteins, 5 ml of the lysis buffer supplemented with 0.4 mg/ml proteinase K is slowly pumped for 90 min. Before the enzyme incubation, all residues of the lysis buffer have to be removed. For this purpose, filters are washed 7x with 5 ml of BE1 buffer taking care that the inner walls of the syringes are completely free of the lysis buffer. During these washing steps, water bath temperature is increased to 37°C for providing optimal conditions for the subsequent step, incubation with repair endonucleases. Two ml of the BE1 enzyme solution (BE1 with 1 µg/ml Fpg crude extract and 0.5 mg/ml BSA) are pipetted on the filters and 1 ml is pumped with maximum pump speed where the second ml is slowly pumped for period of 50 min. After the enzyme incubation water bath is cooled to 25°C. Enzyme remains are washed out with 2x5 ml of BE1 and 1x4 ml of washing buffer (pH 10) with maximum pump speed. The waste container is replaced

with faction collector consisting 6 glass tubes per filter and the syringes reservoirs are completely filled with elution buffer (pH 12.15). Depending on the amount of DNA damage that is going to be measured, either slow elution (DNA damage up to 0.9 lesions per 10^6 base pairs) over 11 h or fast elution (0.9 - 3 lesions per 10^6 base pairs) for 54 minutes can be started. During the elution the fraction collector changes every 120 or 9 minutes, respectively so that the 6 fractions are collected for each filter. At the end the volume left in the syringes is pumped with the maximum pump speed in the 6th fraction. All the filters and filter holders are removed and placed in the coulter counter bottles filled with the volume of the last fraction that is measured and recorded. Volumes of all other factions are measured and recorded (between 3.2-3.6 ml). In order to dissolve the DNA remaining on the filters, coulter counter bottles are incubated in the shaker water bath at 60°C for 2h.

3.2.4.5   Evaluation and quantification of DNA damage

After 2h incubation of the 6th fraction volume with the filters (filter volume), volume corresponding to the other 5 fractions (fraction volume) is taken out from the coulter counter bottle and added in the 6th glass tube. Neutralization that will allow eluted single stranded DNA molecules to assemble into a double stranded molecules is achieved by adding phosphate buffer (PP pH 6.0). The same volume of a phosphate buffer (pH 6.0) is added to each fraction and incubated for 15 min. In the next step, neutral phosphate buffer (PP pH 7.2) containing bizbenzimide (1.5 µM) is added in the same volume (fraction volume). Further incubation period of 15 min will allow dye to intercalate completely with the existing double-stranded DNA molecule. DNA amount of each fraction is quantified fluorimetrically (excitation: 360 nm, emission: 450 nm). At the beginning of the quantification, the fluorimeter has to be adjusted to a zero value using a blank (equal volumes of elution buffer, PP buffer pH 6.0. and PP buffer pH 7.2 containing 1.5 µM bizbenzimide). Sample with DNA standard is also measured and used for the calculation of the absolute amount of DNA in µg. For one million cells amount of DNA should be around 10 µg. If the quantification is more or less than 10 µg, amount of the cells applied on the filter should be optimized. The fluorescence of the fractions from the cell-free lane is measured and subtracted from the other fractions. The total DNA amount of a sample is proportional to the sum of the measured fluorescence intensity of the individual fractions. Fractions reflect eluted amount of DNA per time. Logarithm of the relative amount of DNA values plotted against the elution time gives straight line which is proportional to the single strand breaks, assuming a random distribution of single strand breaks in DNA.

The calculation of the absolute single strand breaks as well as the endonuclease-sensitive sites is is carried out according to the following formula:

$$SSB + EES = m * (-2.24*10^6)$$

Equation 3.1. Calculation of DNA damage by alkaline elution. SSB = number of single strand breaks; EES = number of endonuclease-sensitive sites; m = average slope of the straight line; Factor of slow elution 2.24

In order to calculate the absolute numbers of the SSB and ESS, the elution rates are compared with the elution rate observed with cells exposed to a defined dose of γ-irradiation at 0°C. Factor -2.24 was applied to the slow elution and was determined by calibration with ⍰-radiation (6 Gy correspond to 1 lesion per 10^6 base pairs) (Yamamoto et al., 2007)), (Rodriguez et al., 2013) and factor of -8.6 was determined for rapid elution. To quantify the ESS, a lane without repair enzyme has to be measured from the same sample. Number of these direct single strand breaks are subtracted from the ESS values. In addition for calculation of the induced damage, corresponding basal DNA damage is subtracted.

3.2.5   Microscopy

3.2.5.1   Co-transient transfection with LipoFectamine 2000

50 000 cells were plated 16–24 hours before transfection per well of the 6-well plates. Directly before transfection medium was substituted with a fresh medium containing FBS without antibiotic (400 µl per well). LipoF 2000 transfection mix was prepared at room temperature as indicated in Table 3.4. 100 µl of the mixture was added in each well. The transfection medium containing plasmid DNA and transfection reagent was replaced with the fresh medium after 5 hours.

Table 3.4 Pipeting chart for transfection with LipoFectamine 2000 per well

Mix A		
a.	OGG1-Cherry (plasmid 100 ng/µl)	2 µl
b.	OGG1-Cherry + SIRT1-GFP (plasmid 100 ng/µl)	2 µl +2 µl
Mix B		
LipoFectamine 2000		1 µl
OptiMEM		49 µl

Both mixtures from Table 3.4 were incubated separately for 5 min at RT. Mix B was added to each tube of mix A and re-incubated at RT for a further 5 min. After incubation mixture was added to each well.

3.2.5.2   Knockdown of HeLa cells with LipoRNAiMAX

For SIRT1 knockdown in HeLa cells reverse transfection was performed. In reverse trans-fection, the complexes are prepared inside the wells, after which cells and medium are added. 3 µl (µm) siRNA was added per well. Immediately after, 47 µl mix of DMEM and LipoRNAiMAX was added per well. Cells were diluted in complete growth medium with-out antibiotics so that 450 µl contains the appropriate number of cells to give 30-50% con-fluence 24 hours after plating. To each well with Lipofectamine RNAiMAX complexes, 450 µl of the diluted cells was added. Samples were mixed by rocking the plates back and forth. Cells were incubated 72h at 37°C.

Table 3.5 Pipeting chart for siRNA-Lipofectamine RNAiMAX complex per well

LipoRNAiMIX	0.25 µl
siRNA (2 µl or 25 nM)	3 µl
DMEM-FBS-PC	46.75 µl

3.2.5.3   DNA damage induction

KBrO$_3$

After transient transfection, cells were treated with 40 mM KBrO$_3$ in PBS-containing Ca^{2+} and Mg^{2+} for 45 min at 37°C. After treatment, cells were washed 2xPBSCMF and cultured for 3h, in a fresh full medium. Afterwards, cells were washed 1xPBSCMF. For the removal of soluble proteins, cells were incubated 5 min with cytoskeletal (CSK) buffer on ice. Cells were washed twice with ice-cold PBSCMF before fixation in 2% paraformaldehyde (PFA) for 30 min at room temperature. Nuclear DNA was counterstained with 1 µg/ml 4′,6′-diamidino-2-phenylindole (DAPI). The cells on the cover slips were mounted in Dako fluo-rescence mounting medium.

Ro-19-8022

HeLa cells were co-transfected with OGG1-Cherry and siCtrl / OGG1-Cherry and siSIRT1. Oxidative damage was locally induced with laser micro-irradiation and 5 µM Ro-19-8022 pre-incubation. Kinetic of OGG1 relocalization was analysed by confocal microscopy.

3.2.5.4   Microscopy and image analyses

Image acquisition was performed with a Leica confocal microscope SPE (Wetzlar, Germa-ny), using an ACS APO 40.0×, 1.15-numerical-aperture (NA) oil immersion lens. Images were analysed in Image J software [http://rsb.info.nih.gov/ij/]. Colocalization between

green and red signals, were calculated with the ImageJ plug-in JACOP. The ROI color-coded plug-in was used for the association of particle-size measurements with a color.

3.2.6   PM2-Assay / Relaxation assay

3.2.6.1   Principle

The PM2 relaxation assay allows damage detection in the cell-free DNA after exposure to DNA-damaging chemical substances and/or radiation. Supercoiled PM2 DNA can be converted into the open circular form by a SSB or through an incision by a repair endonuclease. On the other hand, a DSB leads to a linearization of the plasmid DNA. The different forms of PM2 DNA due to their different compactness differ in their migration in an agarose gel. Supercoiled DNA as more compact form will migrate faster in the gel compared with the relaxed circular form of the plasmid. By using different repair endonucleases, different DNA modifications can be converted into a SSB and detected (Epe, Mützel, & Adam, 1988).
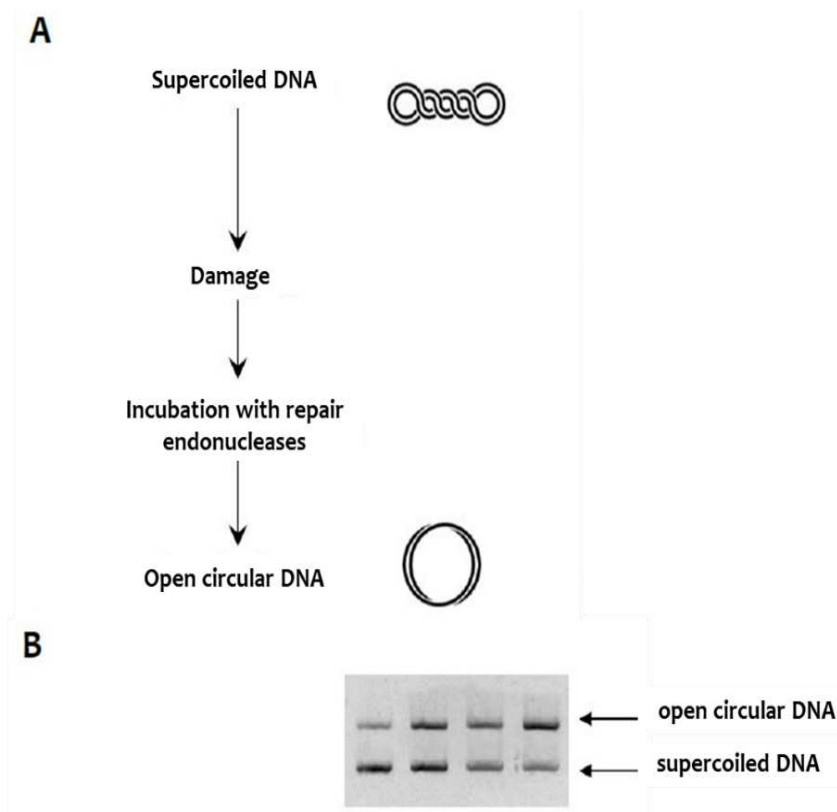

Figure 3.4 Schematic presentation of PM2 DNA relaxation assay. (A) Principle; (B) Separation of the PM2 DNA in the agarose gel

3.2.6.2   Investigation of APE1 endonuclease activity in cell extracts (PM2-DNA relaxation assay / cleavage assay)

To obtain cell extracts for the cleavage assay, 3-5 million cells were plated into a 75-cm^2 cell culture flask. After 16-24h cells were damaged with 40 mM $KBrO_3$ in the presence of 4 mM GSH for 15 min at 37°C in a serum free medium, and additionally incubated in different time points. After incubation cells were washed with 10 ml of PBSCMF, (with 0.5 mM PMSF) scraped in 10 ml PBSCMF (with 0.5 mM PMSF) with a cell scraper and centrifuged (250 g, 5 min, 4°C). Cell pellet was re-suspended in 0.5 ml lysis buffer and transferred into a 1.5 ml Eppendorf tube. The lysis was carried out by sonication of the samples, cooled on ice-cold water. Before sonication of each sample the sonicator was washed with 0.1% SDS solution and water, through sonication for 0.5 to 1 minute. The samples were sonicated in three runs with 40% power and 40% cycles for 40 seconds. If the samples were still turbid after the runs, they were sonicated in two additional runs with 40% power and 40 cycles for 40 seconds. After ultracentrifugation (50,000 g, 45min, 4°C), aliquots of the supernatant were stored at -80°C until use. One aliquot was diluted 1:100 and 1:1000 with water and the protein concentration was determined by Bradford assay (see chapter 3.7.3). For the cleavage assay, 100 ng of the PM2 DNA containing AP modifications was incubated with 5 µl cell extracts (containing various protein amount 0.25-20 µg) in 10 µl reaction buffer (10 mM Hepes pH 7.5, 1 mM MgCl2, 200 mM NaCl) for 30 minutes at 37°C. As a control reaction, 100 ng of untreated PM2 DNA was incubated with 5 µl cell extracts. As a negative control, 100 ng of PM2 DNA was incubated with 5 µl reaction buffer. As a positive control, 100 ng of PM2 DNA was incubated with 5 µl Endo IV enzyme (55U). The reaction was terminated by addition of the Stop buffer containing 0.5% SDS.

3.2.6.3   Agarose gel electrophoresis and quantification of AP lesions

For detection of DNA 1.8 % agarose gel was run. 1.8 g of agarose was completely dissolved in 100 ml 1xTAE buffer by heating in the microwave. The solution was bubble-free poured in a gel chamber equipped with combs. The entire sample volume was pipetted into the well and DNA was separated at 80 V for 90 minutes. To visualize DNA under UV light, gels were stained with 0.5 mg/L ethidium bromide in TAE buffer for 30 minutes and rinsed briefly in deionized water. Due to the different fluorescence intensities of the two DNA conformations, the number of SSBs already present or the number of SSBs generated by APE1 can be calculated. Images of the gels were taken with a BioRad Gel Doc 1000. The densitometric evaluation of the gel image was carried out with the software Image Lab®. The number of APE1-sensitive lesions was calculated by the following equation:

$$SSB + ESS = -\ln\frac{-1{,}4 * S}{1{,}4 * S + R}$$

Equation 3.2 Calculation of SSB and endonuclease-sensitive lesions SSB: single strand breaks per PM2 molecule (per 10^4 base pairs); EES: endonuclease-sensitive lesions per PM2 molecule; S: fluorescence intensity in supercoiled form; R: fluorescence intensity of the relaxed (open-circular) form; 1.4 correction factor, which takes into account the lower intercalation of ethidium bromide into the supercoiled form.

3.2.7   Western Blot

3.2.7.1   Principle

Western blot is a method for the detection of proteins from cell lysates. The first step in a western blotting procedure is to separate proteins using gel electrophoresis. After electrophoresis, the separated proteins are transferred or blotted onto a second matrix, generally a nitrocellulose or polyvinylidene (PVDF) membrane. Next, the membrane is blocked to prevent any nonspecific binding of antibodies to the surface of the membrane. Most commonly, transferred protein is complexed with an enzyme-labelled antibody as a probe. An appropriate substrate is then added to the enzyme and together they produce a detectable product such as a chromogenic precipitate on the membrane for colorimetric detection. The most sensitive detection methods use a chemiluminescent substrate that, when combined with the enzyme, produces light as a by-product. The light output can be captured using a film that is designed for chemiluminescent detection. Alternatively, fluorescently tagged antibodies can be used, which are directly detected with the aid of a fluorescence imaging system. Whatever system is used the intensity of the signal should correlate with the abundance of the antigen on the membrane.

3.2.7.2   Protein extraction from the cells

Ten to fifteen million cells were plated and cultured for 16-48h in a 125-cm^2 culture flask. Before reaching confluence, medium was removed, cells were washed twice with PBSCMF and RIPA buffer was added (shortly before use it was mixed with 1 mM PMSF, dissolved in isopropanol) in a way that entire surface was in contact with the buffer. After 15 min gentle shaking on ice, adherent cells were scraped using a cell scraper, lysate was transferred in a 2 ml tube and incubated on ice for 30 minutes. Afterwards lysate was centrifuged (time 10, 000x g, 10 min 4°C) and the supernatant was mixed with the complete mini protease inhibitor cocktail and stored in aliquots at -80. One aliquot without protein-ase inhibitor was used for determination of the protein concentration.

3.2.7.3   Bradford assay

For determination of the protein concentration, 800 µl of the samples (diluted 1:100 and 1:1000 in water) and a blank sample consisting of water were mixed with 200 µl of the Bio-Rad protein assay Dye Reagents. After 5 minutes incubation at room temperature, the absorbance was measured at 595 nm. Different dilutions of BSA in water (0.78-25 ng/µl) served for calibration of the test.

3.2.7.4   SDS-PAGE

Proteins were separated in a SDS-polyacrylamide gel electrophoresis by their molecular weight, as the smaller proteins will travel more easily and hence rapidly than larger proteins. For the large SIRT1 protein (82 kDa) a separation gel containing 10% acrylamide was used, while for the OGG1 and APE1 the polyacrylamide concentration was 12%. Gels were made by pouring the solutions into the space between two glass plates, using the solution shown in Table 3.6. Shortly before loading into the gel pockets samples (15-20 µg) were mixed with 4X loading buffer and boiled for 5-10 minutes in a water bath. PageRuler Prestained Protein Ladder was used as a marker. Electrophoresis was performed in 1X running buffer, initially at 80 V, after migration of the proteins into the separation gel voltage was increased to 180 V.

Table 3.6 Pipetting scheme for preparing the polyacrylamide gels for SDS-PAGE

Component	10% Running gel		12% Running gel		Stacking Gel	
H2O	3.85	ml	3.25	ml	3.425	ml
1,5 M Tris-HCl pH 8.8	2.6	ml	2.6	ml	-	
1 M Tris-HCl pH 6.8	-		-		650	µl
20% SDS	50	µl	50	µl	25	µl
10% APS	100	µl	100	µL	50	µl
TEMED	4	µl	4	µL	5	µl
sume	**10**	**ml**	**10**	**ml**	**5**	**ml**

3.2.7.5   Blotting

After separating, the protein mixture was transferred to a membrane. Gel was carefully washed in a de-ionized water to remove the electrophoresis buffer. Gel, nitrocellulose membrane, two filter pads (sponges) and two filter papers were placed in a cold transfer buffer for 30 minutes. The transfer was done using an electric field oriented perpendicular to the surface of the gel, causing proteins to move out of the gel onto the membrane. The membrane was placed between the gel surface and the positive electrode in a sand-

wich. The sandwich included a fiber pad at each end, and filter papers to protect the gel and blotting membrane. For SIRT1, a transfer buffer containing SDS was used, while for the other proteins the transfer buffer was without SDS. After the protein transfer at 100V for 1 hour, the membrane was briefly washed with de-ionized water, and proteins were stained with Ponceau red for 5-10 minutes. When clear transfer of proteins was observed, a photo was taken and the membrane was several times washed with de-ionised water and prepared for immunodetection. In order to investigate if the protein transfer was complete, gel was additionally incubated with Coomassie Briliant Blue solution for 1 hour, washed with de-ionised water, and incubated with discoloration solution overnight.

3.2.7.6   Blocking, washing and antibody incubation

Blocking is a very important step of western blotting as it prevents antibodies from binding to the membrane non-specifically. Blocking was made with 5% BSA for 1h at RT / overnight at 4°C on shaker. After the blocking membrane was briefly washed in 0.1% TBST and then washed three more times with 0.5% TBST as follows: 15, 10 and 5 minutes. Incubation with primary antibodies was performed overnight at 4°C on shaker. After primary antibody incubation, membrane was washed three times with 0.5% TBST for 15, 10 and 5 minutes. Incubation with secondary antibodies labelled with horseradish peroxidase (HRP) was performed at RT for 1-2h.

Table 3.7 Primary and secondary antibodies for the detection of SIRT1, APE1, OGG1 and AcOGG1 protein as well as β –actin as loading control

	Primary antibody	Optimal dilution	Secondary antibody	Optimal dilution
SIRT1	Rabbit monoclonal SIRT1 antibody:E104:ab32441	1:5000	Goat anti-rabbit IgG-HRP: sc 2004	1:2000
SIRT1	Rabbit monoclonal SIRT1 antibody:E104:ab32441	1:5000	Goat anti-rabbit IgG (H+L), Alexa Fluor 594	1:1000
Ref-1	Mouse monoclonal Ref-1 antibody (C4):sc-17774	1:2000	Goat anti-mouse IgG-HRP: sc-2005	1:2000
OGG1	Monoclonal rabbit OGG1 antibody: EPR4664(2)	1:2000	Goat anti-rabbit IgG-HRP: sc-2004	1:2000
Ac-OGG1	Rabbit polyclonal OGG1 acetyl K338+K341 antibody:ab-93670	1:500	Goat anti-rabbit IgG-HRP: sc-2004	1:2000
β-Actin	Mouse monoclonal β-actin antibody (C4):sc-47778	1:2000	Goat anti-mouse IgG-HRP: sc-2005	1:2000

3.2.7.7   Immunodetection

For the detection of the proteins, an indirect detection method was performed, first adding a primary antibody to bind to the antigen. This was followed by an incubation with an enzyme-conjugated secondary antibody that is directed against the primary antibody. The secondary antibody was bond with an enzyme-conjugated antibody as a probe. When a chemiluminescent substrate (luminol reagent) was added to the enzyme, light was produced as a by-product of the oxdiation that was captured using a film. Membrane and corresponding piece of film were fixed together and kept in an autoradiography cassette. The intensity of the signal correlated with the abundance on the antigen on the blotting membrane. For quantification, a photo was made using Bio-Rad Gel Doc 1000. The densiometric measurement was performed by Image Lab™ software.

3.2.8   Statistics

All statistical calculations for this work were done with Microsoft Excel 2013. The Student's T-Test was used to compare two mean values. To indicate the significance, a classification was made according to the following probabilities (p-value):

* $p < 0.05$: statistically significant
** $p < 0.005$: statistically very significant
*** $p < 0.0005$: statistically highly significant

4   Results

4.1   SIRT1

4.1.1   Influence of SIRT1 on genomic (in)stability - generation of micronuclei

4.1.1.1   SIRT1 overexpression has protective role on the formation of micronuclei

Various mechanistic considerations and experimental observations suggest that SIRT1 activity has an influence on genomic stability (see chapter 1.2.2). To directly test this influence, the micronucleus test was used as an indicator for genomic instability. Micronuclei are formed during cell division as result of directly or indirectly generated DSB or damage in the spindle apparatus. Chromosome fragments lacking centromere or whole chromosomes that are unable to migrate with the rest of the chromosomes during the anaphase do not integrate into the nucleus of one of the daughter cells, develop nuclear membranes, and remain as micronuclei (Fenech et al., 2011).

To investigate the influence of SIRT1 overexpression on the generation of micronuclei, two osteosarcoma (U2OS) cell lines were used that stably express biologically functional SIRT1-GFP or a control protein, Ctrl-GFP. The U2OS cells were exposed to three different types of DNA damaging agents, each one inducing a different type of lesion. Potassium bromate ($KBrO_3$) in the presence of 4 mM glutathione (GSH) predominantly generates 8-oxoG, H_2O_2 generates SSB, and AP sites were induced by MMS.
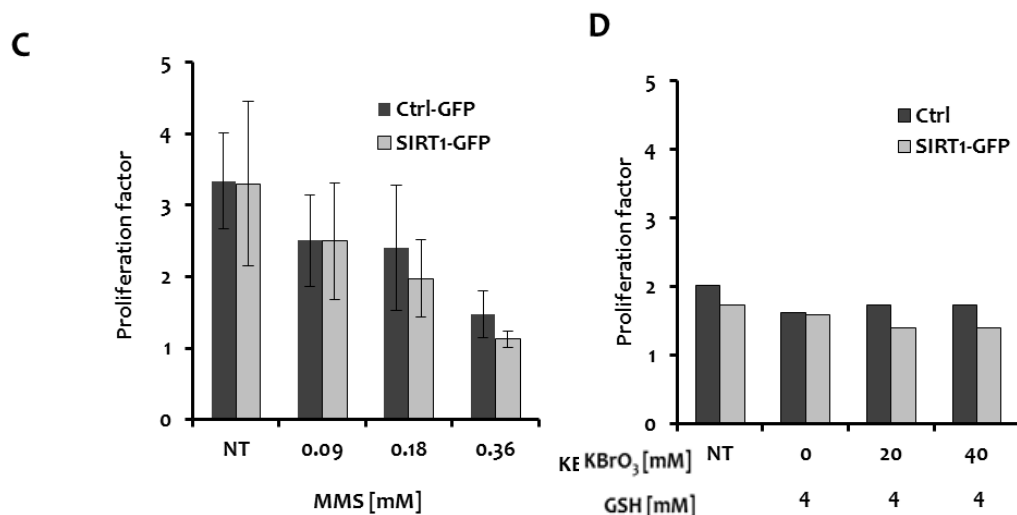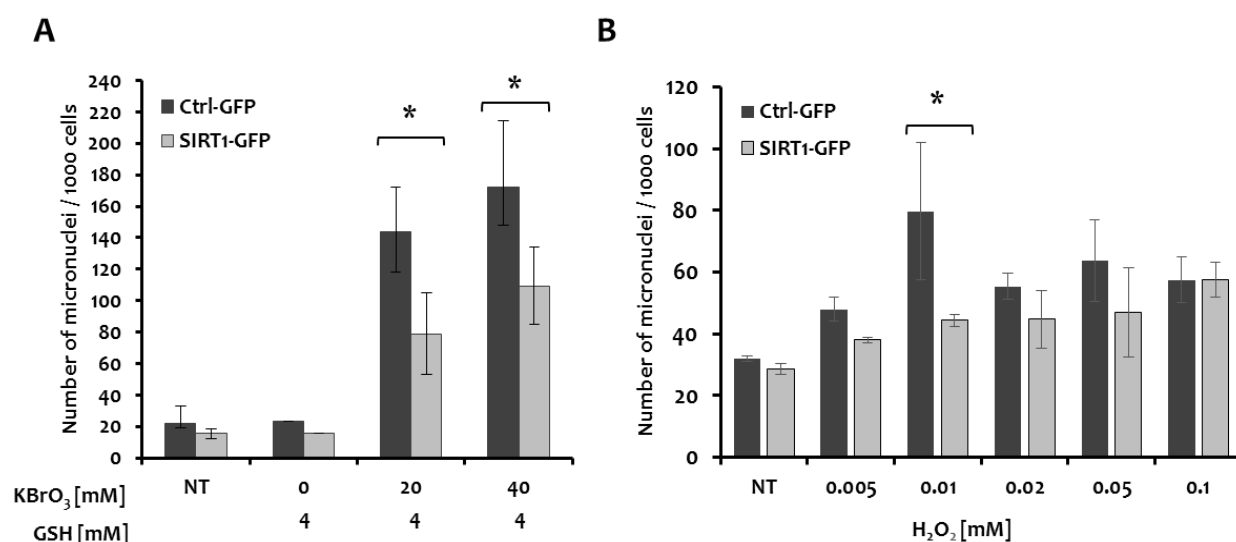
C

D
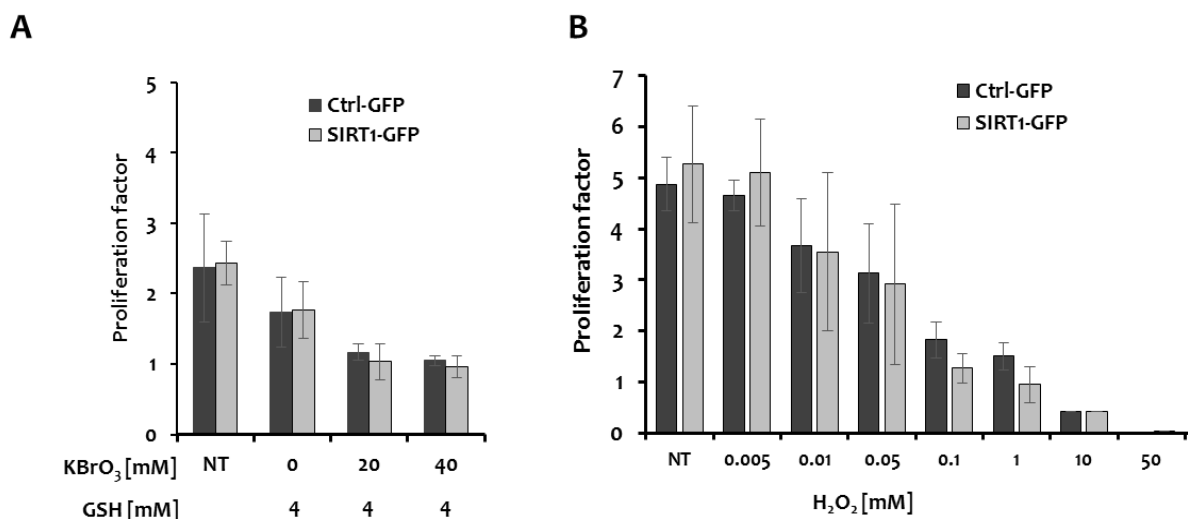
Figure 4.1 Effect of KBrO₃, H₂O₂ and MMS on the cell proliferation. SIRT1-GFP and Ctrl-GFP osteosarcoma cells were treated with different concentrations of (A) KBrO₃ in the presence of 4 mM GSH for 15 min at 37°C, n=3; (B) H₂O₂ for 15 min at 37°C, n=1-4; (C) MMS for 15 min at 37°C, n=2. (D) HeLa cells were treated with KBrO₃ in the presence of 4 mM GSH for 15 min at 37°C, n=1. Trypsinized cells were re-suspended in full culture medium and counted 24h (A), (B), (D) or 48h (C) after treatment with a coulter counter (see chapter 3.2.2.3). NT=non-treated. Bars represent the means of 2-4 experiments ± SD.

Cell division is important for micronuclei production. Therefore, before counting micronuclei, the proliferation of the cells after treatment with KBrO₃, H₂O₂ and MMS was investigated first (Figure 4.1. A, B, C). No difference in the cell numbers between SIRT1 overexpressing and control cells was observed after treatment at toxic and non-toxic doses, indicating that SIRT1 overexpression has no influence on the cell proliferation with and without damage.
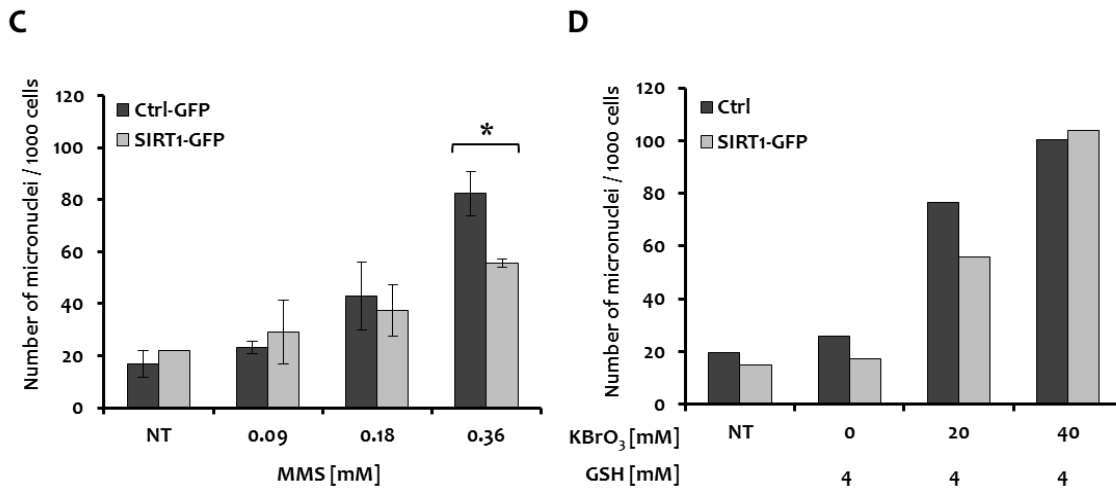
A

B

C

D

Figure 4.2 Influence of SIRT1 overexpression on the micronuclei generation. SIRT1-GFP and Ctrl-GFP osteosarcoma cells were treated with different concentrations of (A) $KBrO_3$ in the presence of 4 mM GSH for 15 min at 37°, n=3; (B) H_2O_2 for 15 min at 37°C, n=2-3; (C) MMS for 15 min at 37°C, n=3. (D) HeLa cells were treated with $KBrO_3$ in the presence of 4 mM GSH for 15 min at 37°C, n=1. 24h (A), (B), (D) or 48h (C) after the treatment trypsinized cells were re-suspended in full culture medium and ~1 × 10^5 cells were fixed on a microscope slide by cytospin centrifugation and treatment with methanol for 1h at –20°C. After staining with bizbenzimide / acridine orange in Ca^{2+}- and Mg^{2+}-free PBS, 1000 cells were analysed for the presence of micronuclei with a fluorescence microscope (see chapter 3.2.3). NT=non-treated. Bars represent the means of 2-3 experiments ± SD. Statistical significance of the difference between SIRT1-GFP and Ctrl-GFP cells was determined using a two tailed Student's t test (* p<0.05).

In Figure 4.2 a significant dose dependent increase of micronuclei generation after treatment with $KBrO_3$ (A) and MMS (C) can be observed in both cell lines. However, in H_2O_2 treated cells (Figure 4.2.B) the increase of micronuclei generation is significant only up to 0.01 mM. In general, relatively toxic concentrations of an agent will not generate micronuclei since they are only formed during cell division. Concentrations of H_2O_2 higher than 0.01 mM indeed reduce cell proliferation significantly as shown in (Figure 4.1.B). Importantly, SIRT1-GFP overexpressing cells showed significantly lower number of micronuclei generation after treatment with all three damaging agents in comparison with the control cells (Figure 4.2. A, B, and C).

In addition to U2OS cells, HeLa cells were transiently transfected with SIRT1-GFP plasmid, exposed to $KBrO_3$ in the presence of 4 mM GSH and micronuclei were counted. As in the case of the U2OS cells, SIRT1 overexpression had no influence on the proliferation (4.1.D). A lower number of micronuclei was counted in cells transfected with SIRT1-GFP after treatment with 20 mM $KBrO_3$ while the number of micronuclei after treatment with 40 mM $KBrO_3$ was the same between transfected and non-transfected cells (Figure 4.2.D). More experiments need to be done to confirm the significance of this observation.

In summary, these data (Figure 4.2) suggest that SIRT1 overexpression has a protective role on genome stability after DNA damage induction with $KBrO_3$, H_2O_2 and MMS.

4.1.1.2 SIRT1 inhibition causes higher micronuclei formation

To investigate the influence of SIRT1 deficiency on the generation of micronuclei, osteosarcoma (U2OS Ctrl-GFP) cells, glioblastoma SIRT1 knockdown (LN428-SIRT1sh) and control (LN428) glioblastoma cells were used. Ctrl-GFP cells were pre-incubated with 10 mM nicotinamide (NAM), a well-established SIRT1 inhibitor (Hwang & Song, 2017). Cell lines were exposed to different concentrations of MMS or $KBrO_3$ in the presence of 4 mM GSH.
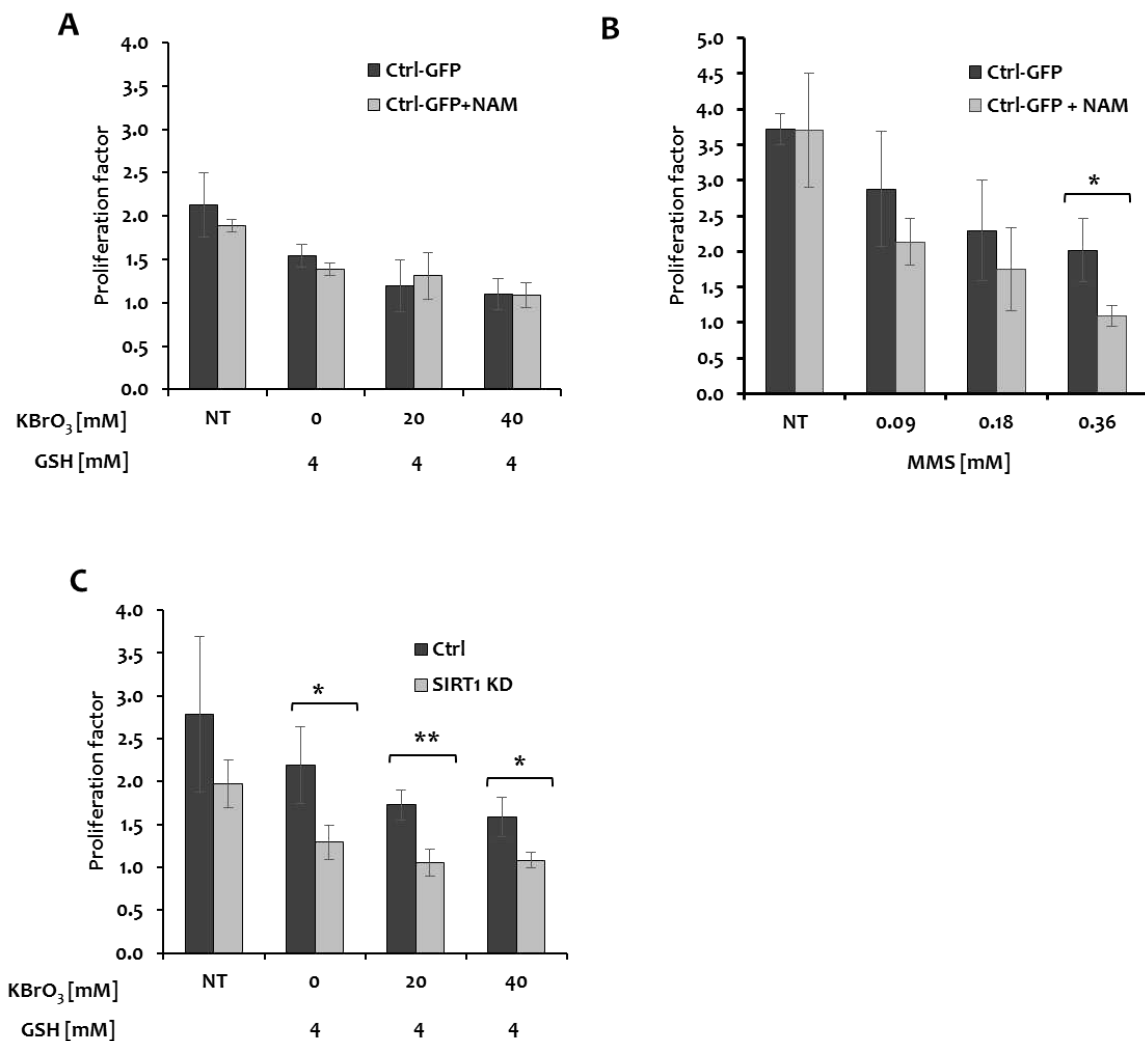

Figure 4.3 Effect of $KBrO_3$ and MMS on the cell proliferation. Ctrl-GFP osteosarcoma cells were preincubated with 10 mM NAM and treated with different concentrations of (A) $KBrO_3$ in the presence of 4 mM GSH for 15 min at 37°C, n=5; (B) MMS for 15 min at 37°C, n=4. (C) Glioblastoma cells were treated with $KBrO_3$ in the presence of 4 mM GSH for 15 min at 37°C, n=4. Trypsinized cells were re-suspended in full culture medium and counted 24h (A), (C) or 48h (B) after treatment with a coulter counter (see chapter 3.2.2.3). NT=non-treated. Bars represent the means of 4-5 experiments ± SD. Statistical significance was determined using a two tailed Student's t test (* p<0.05; ** p<0.01).

Proliferation analysis of Ctrl-GFP cells pre-incubated with NAM and subsequently treated with $KBrO_3$, showed no difference of the cell growth in comparison with the control cells

(Figure 4.3.A). However, after MMS treatment, NAM pre-incubated Ctrl-GFP cells showed lower proliferation then cells in the absence of the SIRT1 inhibitor. The difference reached statistical significance at 0.36 mM MMS (Figure 4.3.B).

The SIRT1 knockdown in glioblastoma cells caused a reduction of cell proliferation even without damage induction (Figure 4.3.C). The difference appears to be even more significant after damage by 20 mM $KBrO_3$ plus 4 mM GSH (Figure 4.3.C). Surprisingly, GSH treatment alone appears to cause lower cell proliferation in both SIRT1 KD and control cells. Taken together, the data (Figure 4.3.B, C) demonstrates a protective role of SIRT1 against cytotoxic stress and a role in cell proliferation.

The results of the micronuclei tests with cells with reduced SIRT1 activity are shown in Figure 4.4. Ctrl-GFP cells inhibited with NAM showed slightly lower number of micronuclei after $KBrO_3$ treatment. However, the effect was not significantly different (Figure 4.4.A). The dose dependence of micronuclei generation in U2OS cells by MMS is shown in Figure 4.4. B. Up to 0.18 mM, the induction by MMS is much higher in control cells than in cells in which SIRT1 activity in inhibited by NAM. This is in accordance with the opposite effect observed by SIRT1 overexpression (Figure 4.2.C). At 0.36 mM MMS, however, micronuclei generation in the inhibited cells (but not in the control cells) is even lower then at 0.18 mM MMS. Most probably, the strong reduction of cell proliferation observed in the inhibited cells (but not the control cells) (Figure 4.3.B) inhibits micronuclei generation (because cell division is required for micronuclei generation).

In glioblastoma cells, the knock-down of SIRT1 caused an inhibition of micronuclei formation even in undamaged cells. The effect appears slightly higher after DNA damage induction by $KBrO_3$ (Figure 4.4.C). Again, the reduction of micronuclei generation in the SIRT1-deficient cells may be best explained by the reduced cell proliferation showed in (Figure 4.3.C).

In summary, the result obtained with SIRT1-deficient and inhibited cells supports the previous finding (Figure 4.2) that SIRT1 plays a protective role on genome stability in particular after induction of AP sites by MMS.
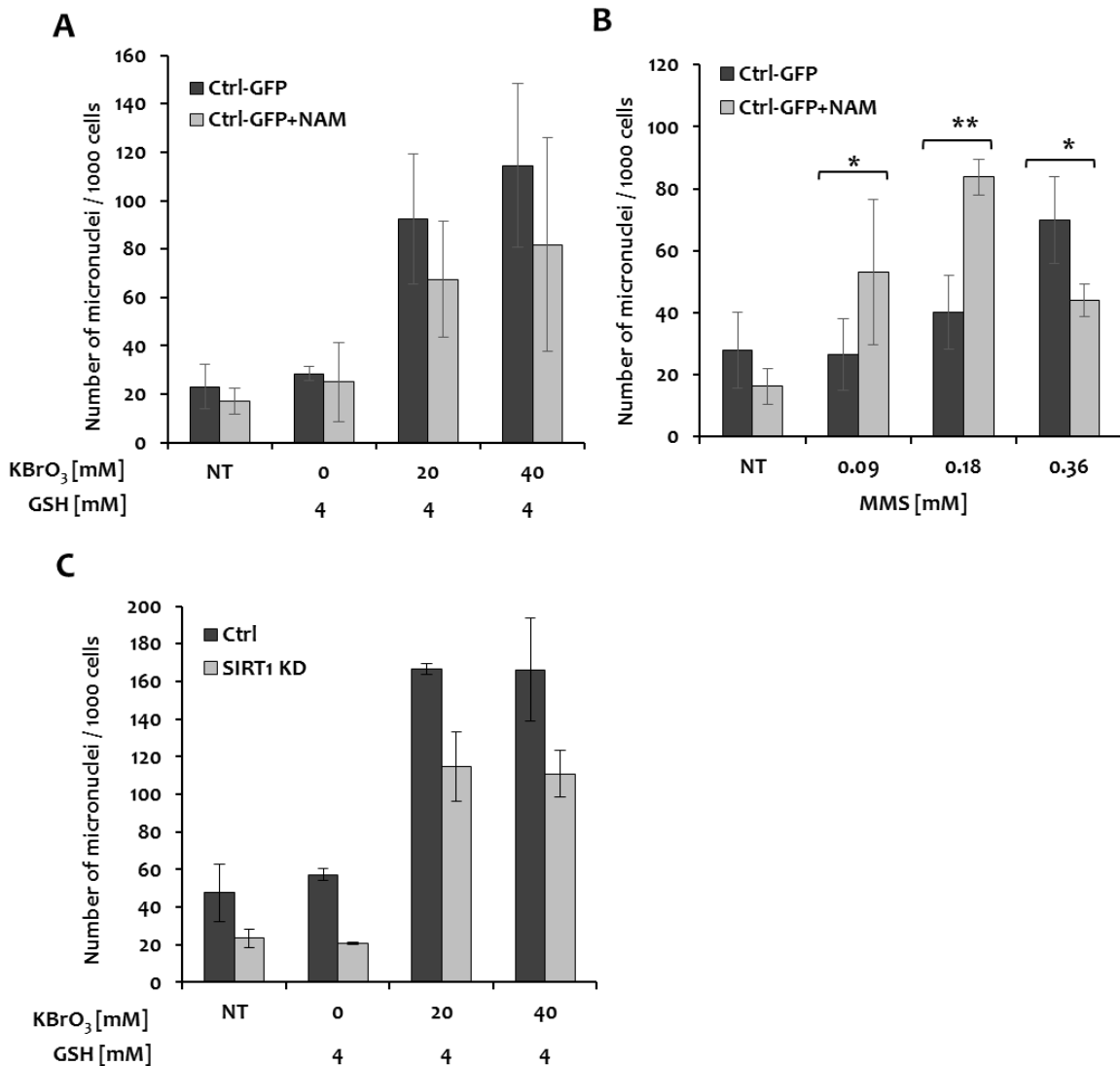
Figure 4.4 Influence of SIRT1 deficiency on the micronuclei generation. Ctrl-GFP osteosarcoma cells were were pre-incubated with 10 mM NAM and treated with different concentrations of (A) $KBrO_3$ in the presence of 4 mM GSH for 15 min at 37°C, n=2; (B) MMS for 15 min at 37°C, n=3-4. (C) SIRT1 KD and control glioblastoma cells were treated with $KBrO_3$ in the presence of 4 mM GSH for 15 min at 37°C, n=2. 24h (A), (C) or 48h (B) after the treatment trypsinized cells were re-suspended in full culture medium and ~1 × 10^5 cells were fixed on a microscope slide by cytospin centrifugation and treatment with methanol for 1h at –20°C. After staining with bizbenzimide / acridine orange in Ca^{2+}- and Mg^{2+}-free PBS, 1000 cells were analysed for the presence of micronuclei with a fluorescence microscope (see chapter 3.2.3). NT=non-treated. Bars represent the means of 2-4 experiments ± SD. Statistical significance was determined using a two tailed Student's t test (* $p<0.05$; **$p<0.01$).

4.1.2   Influence of SIRT1 on the generation and repair of different types of DNA modifications

As a histone deacetylase, SIRT1 has long been known to act as an important regulator of chromatin condensation and therefore the accessibility of chromosomal DNA. Therefore, SIRT1 in theory could have differential effects on DNA damage and repair and, in consequence, genome stability (see chapter 1.1). Its overexpression either could lead to

higher protection against endogenous/exogenous damage generation and/or less accessibility for DNA repair enzymes to the site of damage (slower repair). Similarly, SIRT1 deficiency could lead to less protection against damage and/or higher accessibility for DNA repair enzymes (better repair).

To explain the observed influence of SIRT1 overexpression/deficiency on the genome stability, and considering that micronuclei might arise from a defective DNA repair mechanism (see chapter 1.1), the next aim of my study was to analyse the influence of SIRT1 on the repair of DNA damage. As for the micronuclei analysis, SIRT1 overexpressing (U2OS) and SIRT1 knockdown (LN428) glioblastoma cell lines were used, and the same damaging agents (KBrO$_3$, H$_2$O$_2$, MMS) were used for preferential induction of 8-oxoG, SSB and AP sites, respectively. Damage was measured by alkaline elution assay.

4.1.2.1   SIRT1 overexpression has no influence on the induction and repair of 8-oxoG

In order to investigate the influence of a SIRT1 overexpression on the induction and repair of 8-oxoG lesions, U2OS cells, SIRT1-Flag tagged and their control cells were incubated with 15 mM KBrO$_3$ for 15 min at 37°C in serum-free medium. The removal of the oxidatively generated base modifications (8-oxoG) during different repair incubations was followed by an alkaline elution assay using Fpg protein as a probe (see chapter 3.2.4). Fpg protein, the bacterial homologue of OGG1 recognizes 8-oxoG and some other oxidative purine modifications in DNA. The Fpg-generated SSB can be used for the quantification of these lesions in the nuclear DNA of cells. Figure 4.5.B shows no difference between cell lines in the induction and repair of Fpg lesions after different recovery times.

In addition, U2OS osteosarcoma cells that stably express biologically functional SIRT1-GFP or a control protein Ctrl-GFP were used. For induction of 8-oxoG in cellular DNA, cells were incubated with 10 mM KBrO3 in the presence of 4 mM GSH, for 15 min at 37°C in serum free medium. Less than 50% of the lesions were repaired in both cell lines after 4h recovery time. Figure 4.5.A shows no significant difference between cell lines in the induction or repair of Fpg lesions, confirming previous observation (Figure 4.5.B). There were also no significant differences between genotypes in the induction and repair of SSB (Fig.4.5.A).
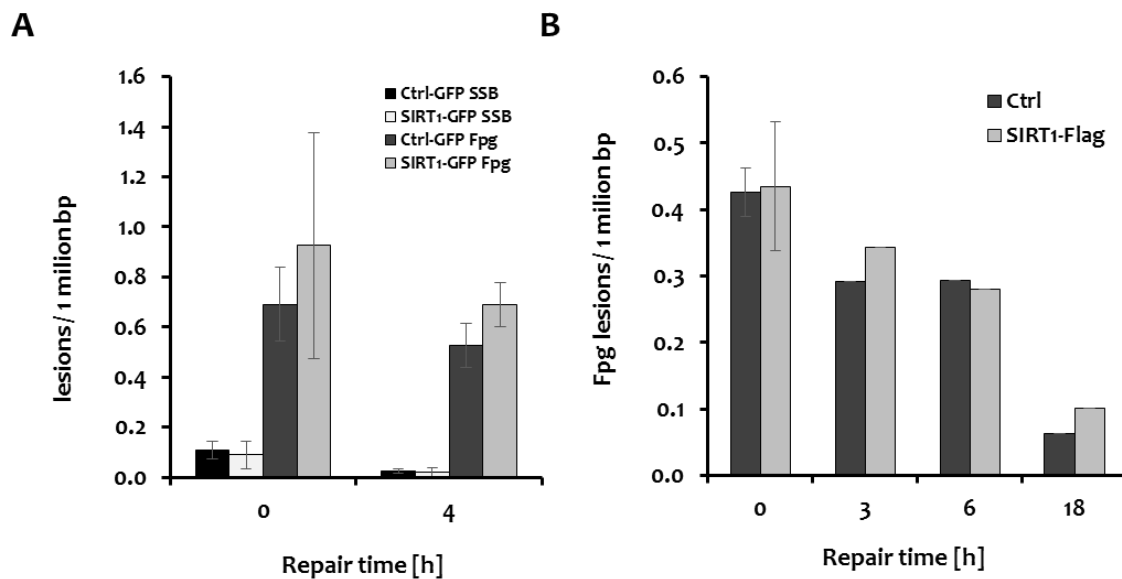
Figure 4.5 Influence of SIRT1 overexpression on the induction and repair of SSB and Fpg lesions after KBrO3 treatment. (A) SIRT1-GFP and Ctrl-GFP U2OS osteosarcoma cells were exposed to KBrO$_3$ (10 mM in the presence of 4 mM GSH for 15 min at 37°C, n=3; (B) SIRT1-Flag and control U2OS osteosarcoma cells were exposed to KBrO$_3$ 15 mM for 15 min at 37°C, n=1-3. The numbers of modifications were determined by alkaline elution after different recovery times under standard culture conditions (see chapter 3.2.4). Bars represent the means of 3 experiments ± SD.

Taken together, data from Figure 4.5.A and Figure 4.5.B allow to conclude that the rate-limiting step in base excision repair, 8-oxoG excision, (Deyo, 2001) is not affected by SIRT1 overexpression, indicating that SIRT1 overexpression has no influence on the repair of KBrO$_3$ induced 8-oxoG. In addition, results show that SIRT1 overexpression has no influence on the induction of the 8-oxoG lesions.

4.1.2.2   SIRT1 deficiency causes slower repair kinetic of 8-oxoG

As a second approach to analyse the influence of SIRT1 on the repair I used SIRT1 knockdown (LN428-SIRT1sh) and control (LN428) glioblastoma cell lines. Again oxidized purines (8-oxoG) were induced by incubation of the cells with 10 mM KBrO$_3$ in the presence of 4 mM GSH for 15 min at 37°C in a serum free medium and again removal of the induced oxidative guanine modifications during the repair incubation was followed by the alkaline elution assay in the presence of Fpg.

The result (Figure 4.6) shows that SIRT1 has no influence on the induction of the Fpg lesions. However, analysis of the repair kinetics showed that SIRT1 knockdown causes significantly delayed repair. Four hours after their appearance Fpg-sensitive modifications induced by oxidative treatment persisted by more than 90%, while in the control cells 40% were repaired. Interestingly, 50% of the lesions were removed 2h later in both cell lines.

This result suggests that SIRT1 influences the repair of oxidatively induced DNA damage only at early time points (Figure 4.6).
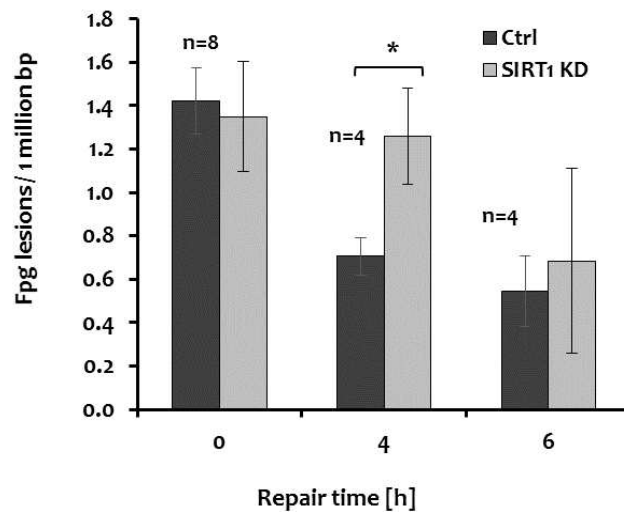

Figure 4.6 Influence of SIRT1 deficiency on the induction and repair of Fpg lesions after KBrO$_3$ treatment. SIRT1 KD and control glioblastoma cells were exposed to KBrO$_3$ (10 mM in the presence of 4 mM GSH for 15 min at 37°C). The number of modifications were determined by alkaline elution after 4h and 6h of incubation under standard culture conditions (see chapter 3.2.4). Bars represent the means of 4-8 experiments ± SD. Statistical significance was determined using a two tailed Student's t test (* p<0.05).

4.1.2.3   SIRT1 overexpression has no influence on the repair of SSB

In principle, SSB can be formed as intermediates during BER, or by radical attack at the sugar-phosphate backbone of the DNA, or by spontaneous cleavage of the sugar-phosphate bond, e.g. at an AP site (see chapter 1.3.4). To analyse the influence of SIRT1 overexpression on the repair kinetic of SSBs, SSBs were induced directly in SIRT1-GFP overexpressing U2OS cells and their control cells by treatment with 50 µM H$_2$O$_2$ for 15 min at 37°C. Data presented in Figure 4.7 show the repair kinetics of induced SSBs in the SIRT1-GFP overexpressing cells in comparison with their control. There is no significant influence of SIRT1 overexpression on the repair of SSB.
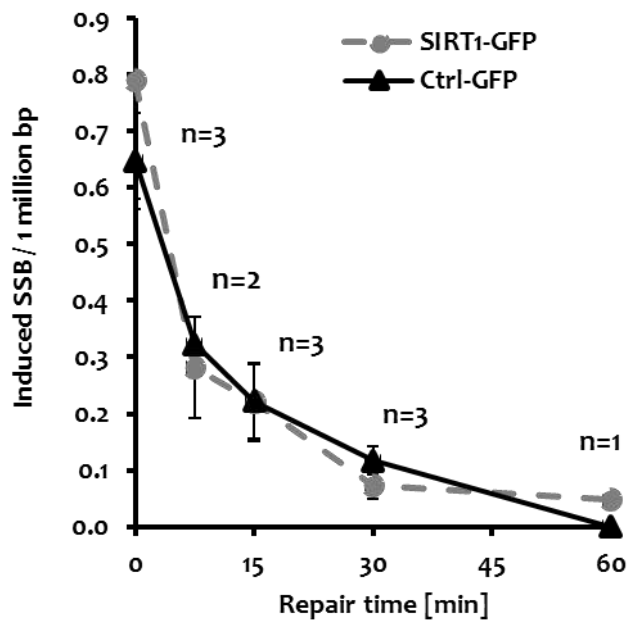
Figure 4.7 Repair of SSB in U2OS. U2OS-GFP and U2OS GFP-SIRT1 were exposed to H_2O_2 (50 µM for 15 min at 37°C). The numbers of modifications were determined by alkaline elution after various times of incubation under standard culture conditions (see chapter 3.2.4). Plot represent the means of 2-3 experiments ± SD.

4.1.2.4   SIRT1 deficiency has no influence on the repair of SSB

In a second approach SIRT1 knockdown and control glioblastoma cells were exposed to 100 µM H_2O_2 for 15 min at 37°C to test whether there is a difference in the repair kinetics of SSBs between these two cells lines. After damage induction cells were incubated in full medium for different recovery times. Data shown in Figure 4.8 indicate that SIRT1 deficiency has no significant influence on the repair kinetic of SSB.
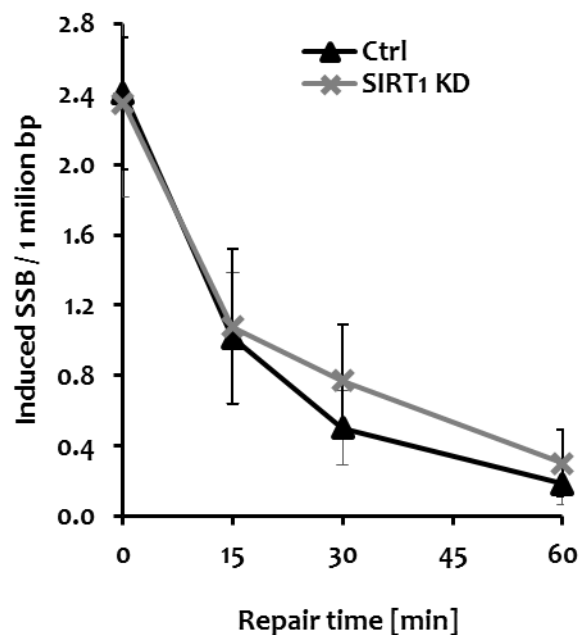
Figure 4.8 Repair of SSB in glioblastoma cells. SIRT1 KD and control glioblastoma cells were exposed to H_2O_2 (100 μM for 15 min at 37°C). The numbers of modifications were determined by alkaline elution after various times of incubation under standard culture conditions (see chapter 3.2.4). Plot represent the means of 2 experiments ± SD.

4.1.2.5   SIRT1 overexpression causes retarded repair of AP sites

As described in chapter 1.1, micronuclei can arise from DSBs that are indirectly produced from SSBs during BER. Data so far obtained didn't show significant influence of SIRT1 overexpression or deficiency on the induction or repair of ROS-induced SSB. MMS as alkylating agent generates high levels of AP sites, both by spontaneous depurination and as intermediates of the base excision repair of alkylated DNA bases such as N7-methylguanine. SIRT1-GFP and Ctrl-GFP cell lines were damaged with 0. 33 mM MMS for 15 min at 37°C (see chapter 3.2.4). The accumulation of AP sites and SSBs produced during the repair of AP sites, were analysed with alkaline elution in the presence of Fpg protein. Fpg, besides 8-oxoG modifications, also recognizes AP sites. When compared with control cells, SIRT1-GFP cells showed higher levels of AP sites, both before repair incubation and at all repair times analysed (Figure 4.9). Thus, there is significant higher generation and / or slower processing of the AP sites in SIRT1 overexpressing cells, indicating that SIRT1 overexpression has an influence on the accumulation of AP sites in the genome after MMS exposure. In accordance with the result obtained in H_2O_2-treated cells, the processing of the low number of SSB observed after treatment with MMS seems not to be affected by SIRT1 overexpression (Figure 4.9).
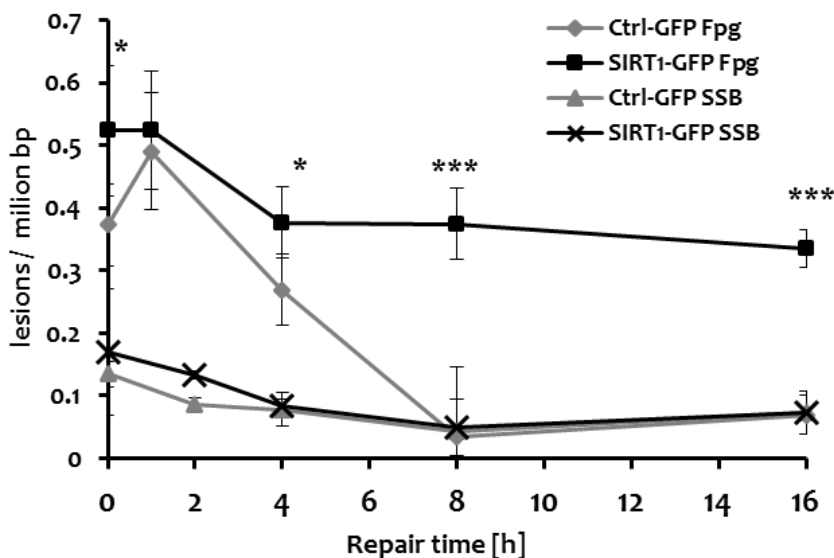
Figure 4.9 Influence of SIRT1 overexpression on the induction and repair of SSB and AP lesions after MMS treatment. SIRT1-GFP and control U2OS osteosarcoma cells were exposed to MMS (0.33 mM for 15 min at 37°C). The number of modifications were determined by alkaline elution after different recovery times under standard culture conditions (see chapter 3.2.4). Plot represent the means of 2-6 experiments ± SD. (Ctrl-GFP n=5 for 0h and 8h, n=2 for 1h, 2h and 16h repair time; SIRT1-GFP n=6 for 0h and 8h, n=3 for 1h, 2h and 16h repair time). Statistical significance was determined using a two tailed Student's t test (* p<0.05; * * * p<0.005).

4.1.2.6 SIRT1 deficiency causes retarded repair of AP sites

To complete the comparison of repair kinetics, I investigated the influence of SIRT1 deficiency on the induction and repair of AP lesions. In order to induce AP sites, SIRT1 KD and control glioblastoma cells were again incubated with 0.3 mM MMS at 37°C for 15 min (see chapter 3.2.4) and SSBs and AP lesions were measured with the alkaline elution assay using Fpg. Damage induction (AP sites and SSBs) was significantly higher in SIRT1 KD cells (Figure 4.10). Moreover, SIRT1 deficient cells showed significantly slower repair of SSBs and AP lesions in comparison with their controls (Figure 4.10). Nevertheless, after 5h repair time, more than 70% of the AP lesions were repaired in both cell lines. SSBs were completely repaired in both cell lines after 5h recovery time. This result indicates that SIRT1 deficiency leads to slower processing of AP sites. At early time points (i.e. directly at the damage induction and after 2h) SSBs seem to accumulate as well.
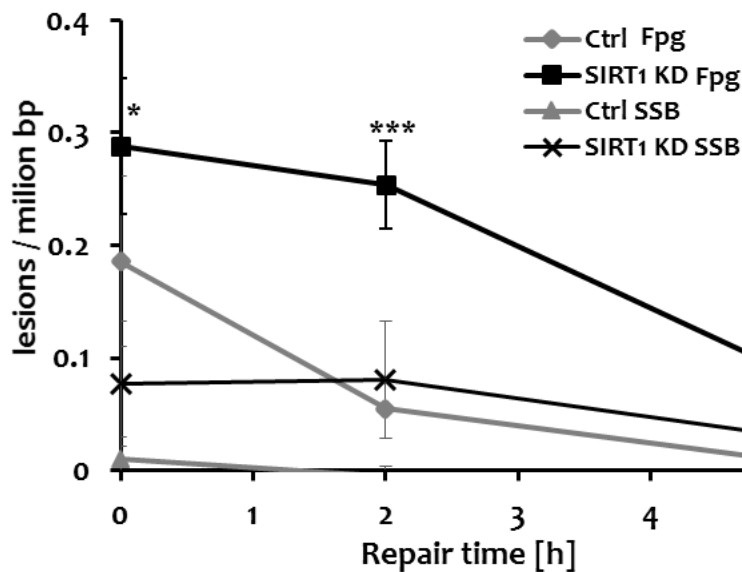
Figure 4.10 Influence of SIRT1 deficiency on the induction and repair of AP lesions after MMS treatment. SIRT1 KD and control glioblastoma cells were exposed to MMS (0.3 mM for 15 min at 37°C). The number of modifications induced by the treatment were determined by alkaline elution after different recovery times under standard culture conditions (see chapter 3.2.4). Plot represent the means of 2-4 experiments ± SD. (Ctrl n=3 for 0h and 5h, n=2 for 2h repair time; SIRT1-KD n=4 for 0h and 5h, n=3 for 2h repair time). Statistical significance was determined using a two tailed Student's *t* test (*p<0.05; ***p≤0.005).

In summary, results described so far indicate a protective role of SIRT1 overexpression on the genome stability. However, SIRT1 overexpression is not involved in the rate-limiting step of BER, 8-oxoG excision (Figure 4.5). In contrary, SIRT1 overexpression is involved in the accumulation of AP lesions as indicated by the fact that SIRT1 overexpressing cells showed significant retardation in the repair after MMS treatment (Figure 4.9).

On the other hand, SIRT1 deficiency leads to higher genome instability (Figure 4.4), slower cell proliferation (Figure 4.3) and significantly slower repair kinetics of oxidatively generated purine modification at early time points (Figure 4.6). Surprisingly, AP sites and SSBs accumulated in MMS-treated cells not only in SIRT1-overexpressing cells, but also in SIRT1-deficient cells (Figure 4.10).

Next step in this study was to analyse the influence of SIRT1 on the subnuclear re-distribution of proteins initiating BER (OGG1 and APE1) after induction of oxidative stress. This type of experiments should give information whether the accessibility of the chromatin for repair proteins is influenced by SIRT1.

4.1.3   Influence of SIRT1 deficiency and overexpression on the recruitment of proteins initiating BER to the chromatin

4.1.3.1   Co-localization of SIRT1-GFP and OGG1-Cherry in the same nuclear regions in KBrO$_3$ treated cells

To test for a possible co-localization of SIRT1 and OGG1, both glioblastoma cells (Figure 4.11) and U2OS (Figure 4.12) were used. SIRT1-GFP overexpressing U2OS cells were transfected with plasmid expressing OGG1-Cherry, while control glioblastoma cells were co-transfected with OGG1-Cherry and SIRT1-GFP plasmids. In order to induce oxidative damage, 24h after transfection cells were treated with 40 mM KBrO$_3$ for 45 min at 37°C and allowed to recover in fresh medium for 3h. After the recovery period, they were washed with CSK (cytoskeleton buffer containing 0.5 % triton) to remove soluble proteins (not bound to chromatin/nuclear matrix). Previously, it had already been shown that OGG1 after oxidative damage is recruited to euchromatin (Amouroux et al., 2010). While in non-treated cells OGG1 and SIRT1 are both soluble in the nucleoplasm and therefore removed by CSK washes (Figure 4.11-4.12), treatment with KBrO$_3$ induces SIRT1 re-localization to the chromatin into the euchromatin areas in the same way as OGG1. This result shows that SIRT1 and OGG1 co-localize in response to oxidative DNA damage.
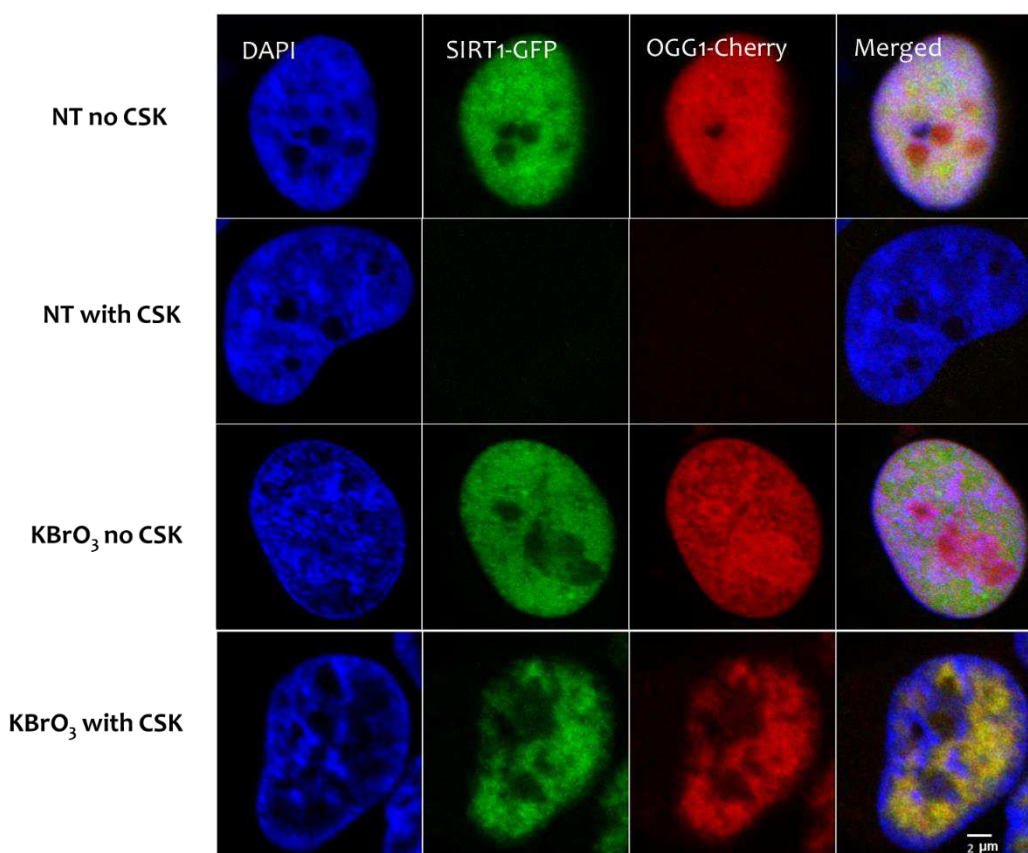

Figure 4.11 Co-localization of SIRT1 and OGG1 in glioblastoma cells. Glioblastoma cells were co-transfected with SIRT1-GFP and OGG1-Cherry and treated with 40 mM KBrO$_3$ when indicated. After 3h recovery in a fresh

medium, cells were washed with cytoskeleton buffer (CSK), if indicated, and fixed with 2% PFA, DAPI stained to visualize DNA and analysed by confocal microscopy. Scale bare = 2 µm. NT=non-treated.
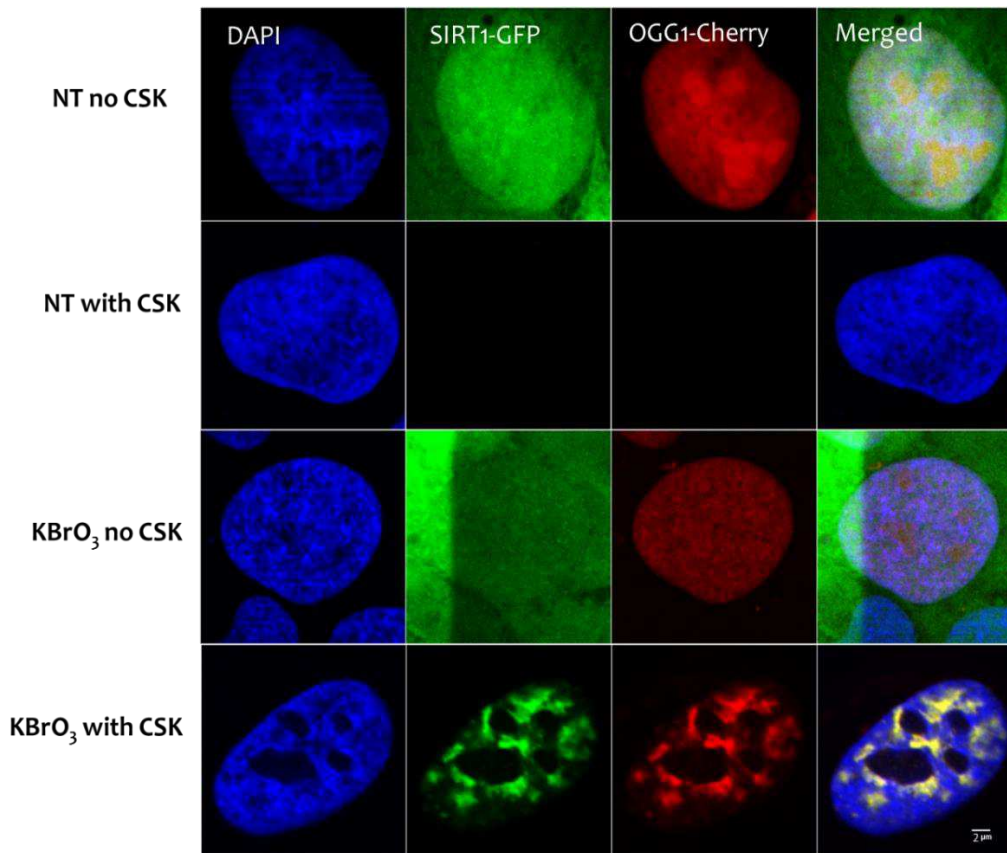

Figure 4.12 Co-localization of SIRT1 and OGG1 in U2OS cells. SIRT1-GFP osteosarcoma cells were transfected OGG1-Cherry and treated with 40 mM KBrO$_3$ when indicated. After 3 h recovery in a fresh medium, cells were washed with cytoskeleton buffer (CSK), if indicated, and fixed with 2% PFA, DAPI stained to visualize DNA and analysed by confocal microscopy. Scale bare = 2 µm. NT=non-treated.

4.1.3.2   SIRT1 has no influence on the recruitment of OGG1 and APE1 to the chromatin

To further determine the influence of SIRT1 on the recruitment of BER enzymes, HeLa cells were co-transfected with siSIRT1, APE1-YFP and OGG1-Cherry. When KBrO$_3$ treated cells were washed with CSK buffer, both OGG1-Cherry and APE1-YPF signals were observed, suggesting that recruitment of APE1 and OGG1 to the chromatin is independent of the presence of SIRT1 (Figure 4.13. A). As a control, HeLa cells were co-transfected with siCtrl1, APE1-YFP and OGG1-Cherry (Figure 4.13. B).
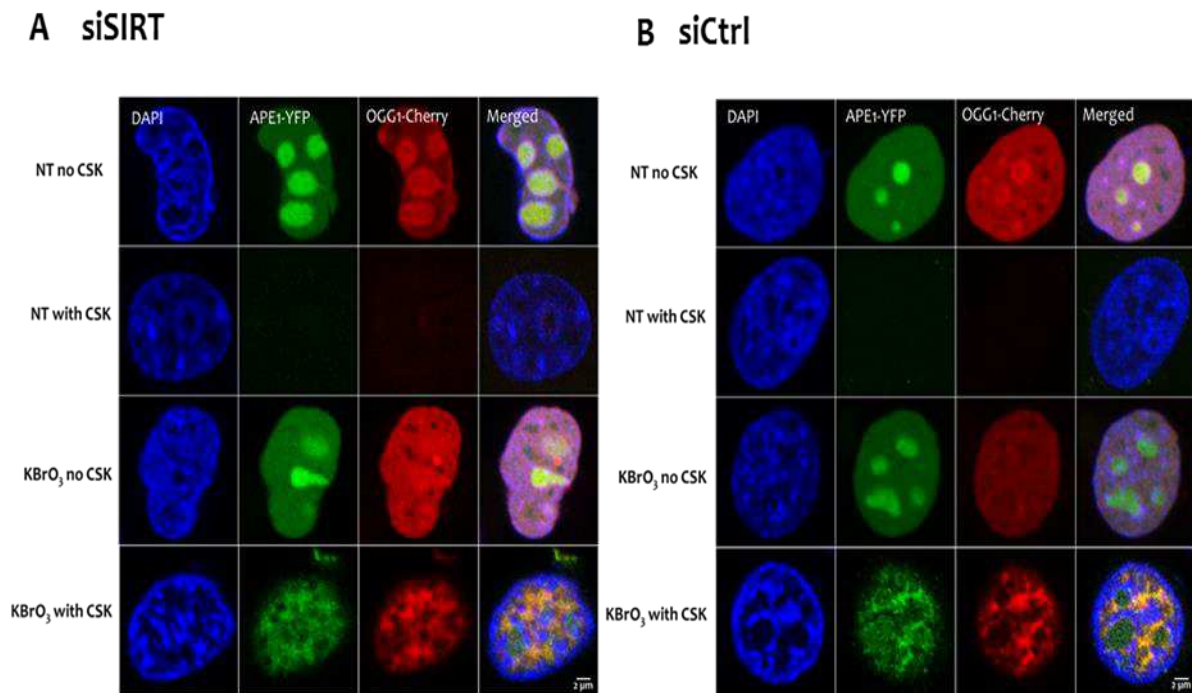
Figure 4.13 Recruitment of OGG1 and APE1 in HeLa cells. HeLa cells were co-transfected with (A) siSIRT1, APE1-YFP and OGG1-Cherry (B) siCtrl, APE1-YFP and OGG1-Cherry treated with 40 mM KBrO₃ when indicated. After 3h recovery in a fresh medium, cells were washed with cytoskeleton (CSK) buffer, if indicated and fixed with 2% PFA, DAPI stained to visualize DNA and analysed by confocal microscopy. Scale bare = 2 μm. NT=non-treated.

Taken together, single cell analysis showed that recruitment of BER enzymes is independent of SIRT1. In order to quantify this finding (Figure 4.13) HeLa cells stably overexpressing OGG1-GFP were transiently transfected with either siOGG1 or siSIRT1 or siCtrl (Figure 4.14). As expected, in the siOGG1 transfected cells (non-treated or with KBrO₃ treated) no OGG1-GFP fluorescence was observed (Figure 4.14. A-C). In the siCtrl and siSIRT1 transfected non-treated cells, OGG1 was soluble in the nucleoplasm and therefore removed by CSK washes (Figure 4.14. A-B). In KBrO₃ treated cells, the OGG1 signal was observed not only in siCtrl-transfected but also in siSIRT1-transfected cells indicating its recruitment to euchromatin independently of SIRT1 (Figure 4.14. C). Again, this result demonstrates that SIRT1 has no influence on the recruitment of OGG1 to the chromatin. Cells transfected with siSIRT1 and siCtrl were additionally incubated with an antibody against SIRT1. Quantifications of SIRT1 and OGG1 fluorescence intensities from each groups are represented in Figure 4.14. E and 4.14. D, respectively.
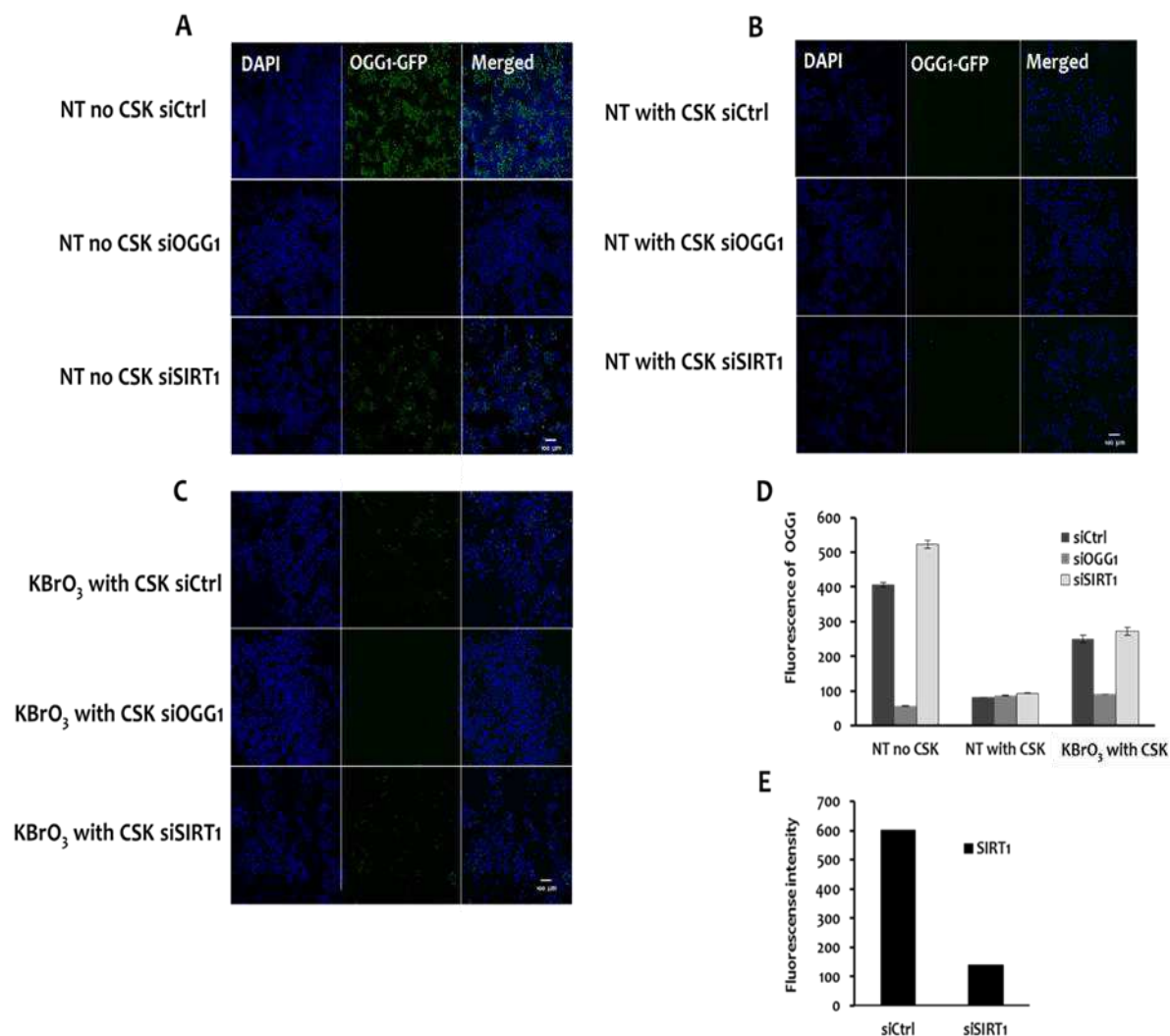
Figure 4.14 Recruitment of OGG1 in HeLa OGG1-GFP cells. (A), (B), (C) HeLa OGG1-GFP cells were transfected with siCtrl or siOGG1 or siSIRT1 and treated with 40 mM KBrO$_3$ if indicated. After 3h recovery in a fresh medium, cells were washed with cytoskeleton (CSK) buffer, if indicated and fixed with 2% PFA, DAPI stained to visualize DNA and analysed by confocal microscopy. Scale bare 100 µm. (D) Bars indicate the average of the fluorescence intensities of cells showed in (A), (B), and (C) ± SEM (n > 1000). (E) Fluorescence intensity of SIRT1 after incubation with an antibody against SIRT1. NT=non-treated.

4.1.3.3   Influence of SIRT1 on the kinetic of OGG1

Next, we investigated the kinetics of the OGG1 re-localization after damage induction i.e., its appearance at the site of damage and its release in the presence and absence of SIRT1. HeLa cells were transiently co-transfected with OGG1-Cherry and siSIRT1 or with OGG1-Cherry and siCtrl. Local oxidative damage in single cells was induced by laser irradiation in the presence of 5 µM Ro 18-8022 (see chapter 3.2.5). The kinetics of OGG1 was followed by confocal microscopy. Fluorescence intensities of OGG1 followed for 180 seconds from 13 cells are presented in Figure 4.15. Few seconds after damage induction, OGG1 accumulates to the site of damage (Figure 4.15). In the siSIRT1 transfected cells a slightly delay of OGG1 recruitment and release after oxidative damage can be observed in

comparison with the control cells. This is an indication that both the appearance of OGG1 at the site of damage and its release is retarded in the absence of SIRT1.
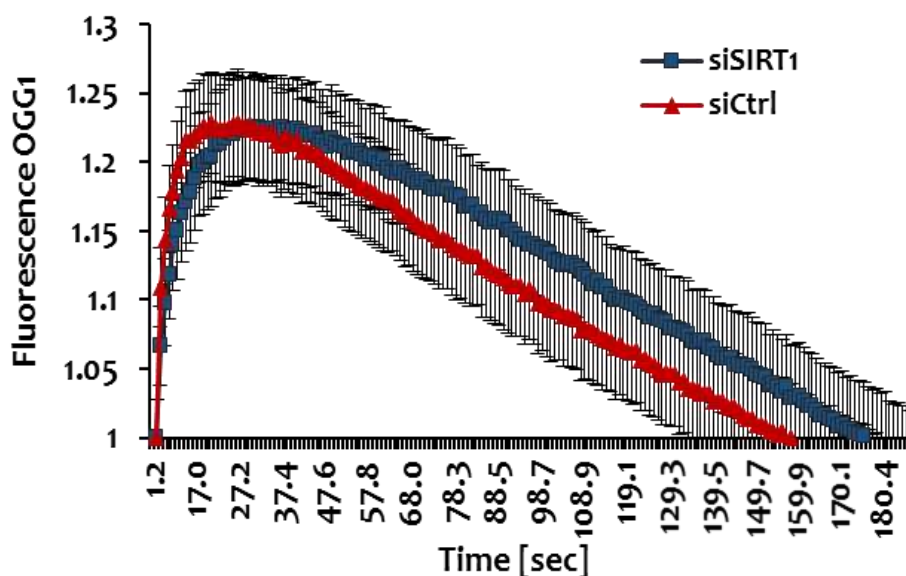

Figure 4.15 Kinetic of OGG1 relocalisation. HeLa cells were co-transfected with OGG1-Cherry and siCtrl / OGG1-Cherry and siSIRT1. Oxidative damage was locally induced with laser microirradiation and 5 µM Ro-19-8022 preincubation. Kinetic of OGG1 relocalization was analysed by confocal microscopy. Plot represent the mean of the OGG1-Cherry fluorescence intensities ± SEM (n=13 cells).

4.1.4   Influence of SIRT1 on the activity of APE1

4.1.4.1   Influence of SIRT1 overexpression on the cleavage activity of APE1

In theory, SIRT1 can influence not only the chromatin compaction (and thus its accessibility to repair-proteins), but also reduce the acetylation status (and thereby activity) of certain repair proteins. In the results described above, I found that SIRT1 and OGG1 co-localize at euchromatin in response to oxidative damage, and that OGG1 and APE1 co-localize after oxidative damage independent of the presence of SIRT1. To investigate if there might be a functional, besides physical interaction between SIRT1 and BER factors, I compared the APE1 cleavage activity in protein extracts from SIRT1 overexpressing and SIRT1 deficient cells.

I performed a DNA relaxation assay to investigate whether SIRT1 overexpression affects APE1 cleavage activity in untreated cells or after application of oxidative stress (see chapter 3.2.6). SIRT1-GFP and control osteosarcoma cells were treated with 40 mM $KBrO_3$ in the presence of 4 mM GSH for 15 min at 37°C in a serum free medium. After 4h recovery time, total protein extracts were prepared and AP endonuclease activity was measured using PM2 DNA containing AP sites as a substrate (see chapter 3.2.6). In non-treated cell extracts, I observed strongly reduced APE1 activity in SIRT1 overexpressing cells in

comparison with control cells (Figure 4.16. B). Oxidative stress did not influence the cleavage activity in the SIRT1-overexpressing cells but strongly decreased APE1 cleavage activity in control cell extracts prepared directly after damage induction (Figure 4.16. C). Four hours after oxidative stress, APE1 activity was found to be further decreased in the control cells, down to the same low level of cleavage activity observed in the SIRT1 overexpressing cell extracts (Figure 4.16. D). PM2 DNA without AP sites was used as a control for analysing unspecific cleavage of the cell extracts. As shown in Figure 4.16. A, no unspecific cleavage of the cell extracts was observed.
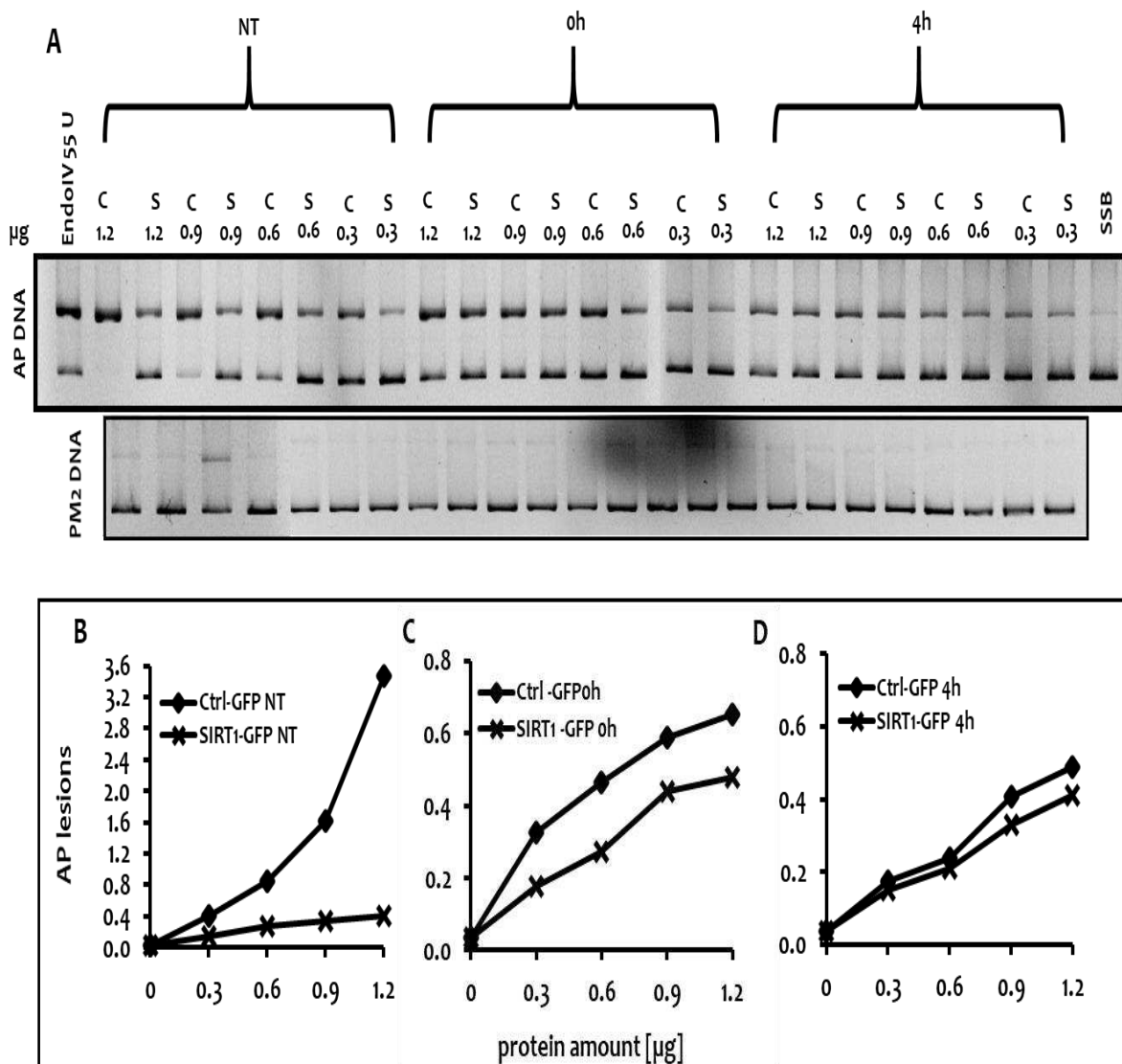
Figure 4.16 Cleavage activity of APE1 in U2OS cells. U2OS cells were treated with 40 mM KBrO$_3$ in the presence of 4 mM GSH, for 15 min at 37°C, left to recover in full medium for 4h. Various amount of cell extracts were incubated with 100 ng AP or PM2 DNA at 37°C for 30 min and the cleaved product was analysed as described in chapter 3.2.6. (A) Representative agarose gel. (B), (C), (D) The intensity of the bands (number of AP lesions) was quantitated using Image Lab software. (lane 1): complete cleavage by 55U endonuclease-IV = positive control; (last lane): SSB, no extract enzyme added = negative control; C: extract from Ctrl-GFP cells; S: extract from SIRT1-GFP overexpressing cells. NT=non-treated.

In summary, the data show that control cells have higher APE1 activity then SIRT1 overexpressing cells. Oxidative stress caused a decrease of APE1 cleavage activity in control cell extracts, while the activity of SIRT1 overexpressing cells after damage induction remain unchanged. The results could best be explained by the assumption that oxidative stress results in a SIRT1-mediated deacetylation of APE1, which strongly decreases its activity (Figure 4.16. B-D).

4.1.4.2   Influence of SIRT1 deficiency on the cleavage activity of APE1

To verify the observed influence of SIRT1 on the cleavage activity of APE1, I conducted similar experiments with SIRT1 deficient and control glioblastoma cells, again under normal conditions and after application of oxidative stress. The results indicate that the APE1 activity without oxidative damage is the same in cell extracts from SIRT1 knockdown and control cells (Figure 4.17. A). After oxidative stress, a decrease of APE1 activity can be observed in both cell lines (Figure 4.17. B). Four hours after damage induction, this decrease of APE1 activity is clearly higher in control cells than in SIRT1-deficient cells. These findings confirm the conclusions from the experiments with the SIRT1-overexpressing cells (chapter 4.1.4.1) and again indicate that SIRT1 is required for a down-regulation of APE1 activity by oxidative stress.
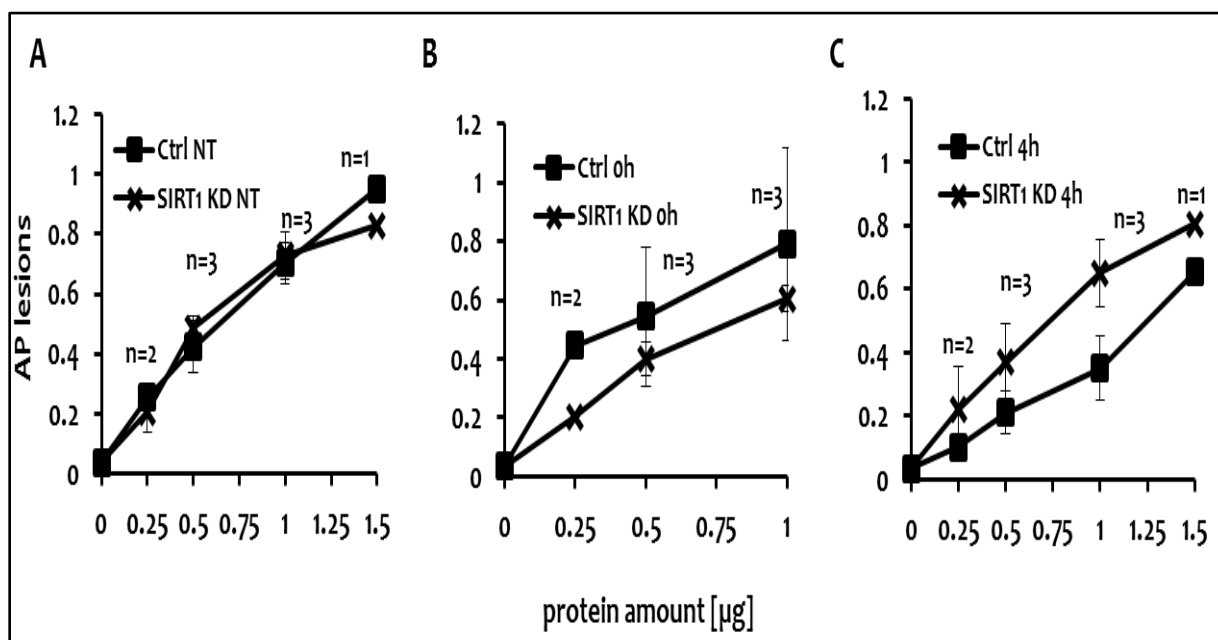
Figure 4.17 Cleavage activity of APE1 in glioblastoma cells. Glioblastoma cells were treated with 40 mM KBrO$_3$ in the presence of 4 mM GSH for 15 min at 37°C, left to recover in full medium for 4h. Various amount of cell extracts were incubated with 100 ng AP DNA at 37°C for 30 min and the cleaved product was analysed as described in chapter 3.2.6. (A), (B), (C) The intensity of the bands (number of AP lesions) was quantitated using Image Lab software and plotted ± SD from 2-3 independent experiments. NT=non-treated.

4.1.5   Influence of SIRT1 on the protein level of BER enzymes after oxidative damage

The previous findings (chapter 4.1.4) - demonstrated that the reduction of APE1 activity after oxidative stress is SIRT1 dependent.

In the next experiments, I wanted to investigate whether oxidative stress affects the expression levels of OGG1, APE1 and AcOGG1, and whether their expression is SIRT1 dependent.

OGG1 and APE1 protein levels were detected by Western blots using specific antibodies for OGG1 and APE1, respectively. Cell lysates were obtained from osteosarcoma cells either untreated or after oxidative damage induction with $KBrO_3$, followed by different recovery times (see chapter 3.2.7). In the blots (Figure 4.18. A-B) it can clearly be seen that the expression levels of OGG1 and APE1 are not affected by the SIRT1 overexpression in the absence of damage. Furthermore, protein levels of OGG1 and APE1 do not appear to be significantly affected by the $KBrO_3$ treatment, neither in SIRT1 overexpressing nor in control cells (Figure 4.18).

Figure 4.18 Protein expression of OGG1 and APE1 after oxidative damage. Protein levels of (A) OGG1 and (B) APE1 were measured by Western blot in U2OS either untreated (NT) or treated with 40 mM $KBrO_3$, after expressions times of 4 or 6 h. Specific antibodies for OGG1 and APE1 were used. 20 µg of total protein extracts were applied and β-actin was used as a loading control; n=1. Lower panels: the intensity of the bands was quantitated using Image Lab software.

Similar results were obtained with glioblastoma cells. In untreated cells, there was no influence of SIRT1 deficiency on the expression levels of OGG1 and APE1 protein levels (Figure 4.19 lane 1 and 5). Moreover, protein levels of OGG1 and APE1 remain unchanged 6h after oxidative stress, suggesting that oxidative damage induction has no influence on

the expression levels of these BER proteins (Figure 4.19). Also, SIRT1 KD had no influence on the protein levels of APE1 and OGG1 after oxidative stress (Figure 4.19).

In conclusion, SIRT1 overexprerssion or deficiency does not influence protein level of OGG1 and APE1 with or without oxidative damage.
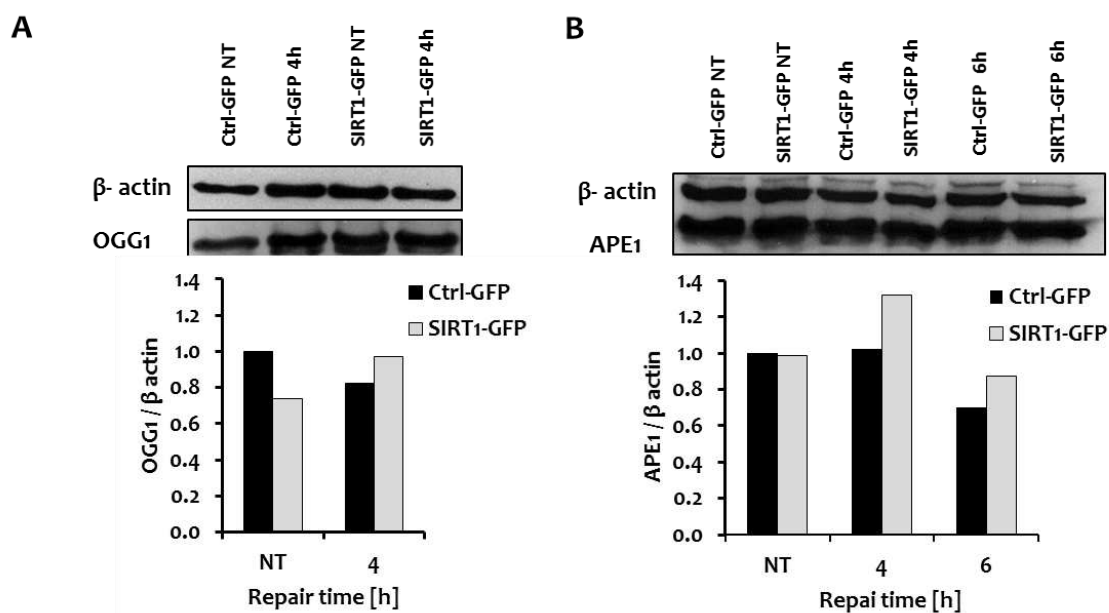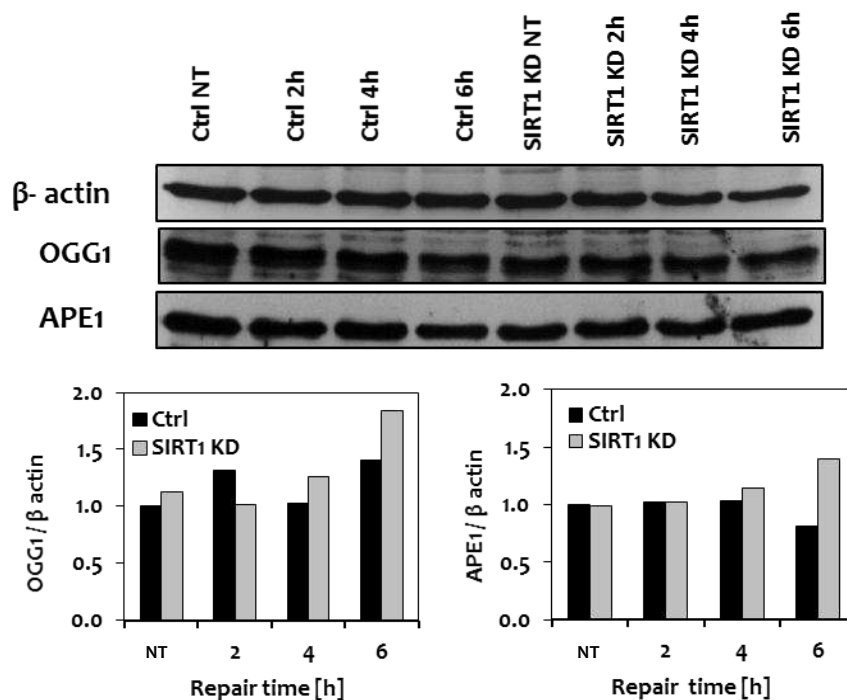

Figure 4.19 Protein expression of OGG1 and APE1 after oxidative damage. Protein levels of (A) OGG1 and (B) APE1 were measured by Western blot in glioblastoma cells either untreated (NT) or treated with 40 mM KBrO$_3$ and different recovery times 2-6h. Specific antibodies for OGG1 and APE1 were used. 20 µg of total protein extract was applied and β-actin was used as a loading control; n=1. Lower panels: the intensity of the bands was quantitated using Image Lab software.

In the next step, I wanted to test whether the acetylation level of OGG1 is influenced by SIRT1 overexpression in the presence or absence of oxidative damage.

Western blot was performed with extracts from both damaged and undamaged osteosarcoma cells. After blotting, the membrane was divided. One part was incubated with an antibody for OGG1 and the other was incubated with an antibody for AcOGG1. Thus, comparison was made between the relative concentrations of total and acetylated OGG1. Figure 4.20 shows no influence of SIRT1 overexpression on the level of AcOGG1 between the cell lines (Figure 4.20 lane 1 and 3). Furthermore, neither oxidative stress alone nor its combination with SIRT1 overexpression influenced the acetylation status of OGG1 in the cell extracts (Figure 4.20).

This result indicates that SIRT1 overexpression has little or no influence on the OGG1-acetylation status, with or without oxidative stress. It has to be mentioned, however, that the specificity of the AcOGG1 antibody was not verified.
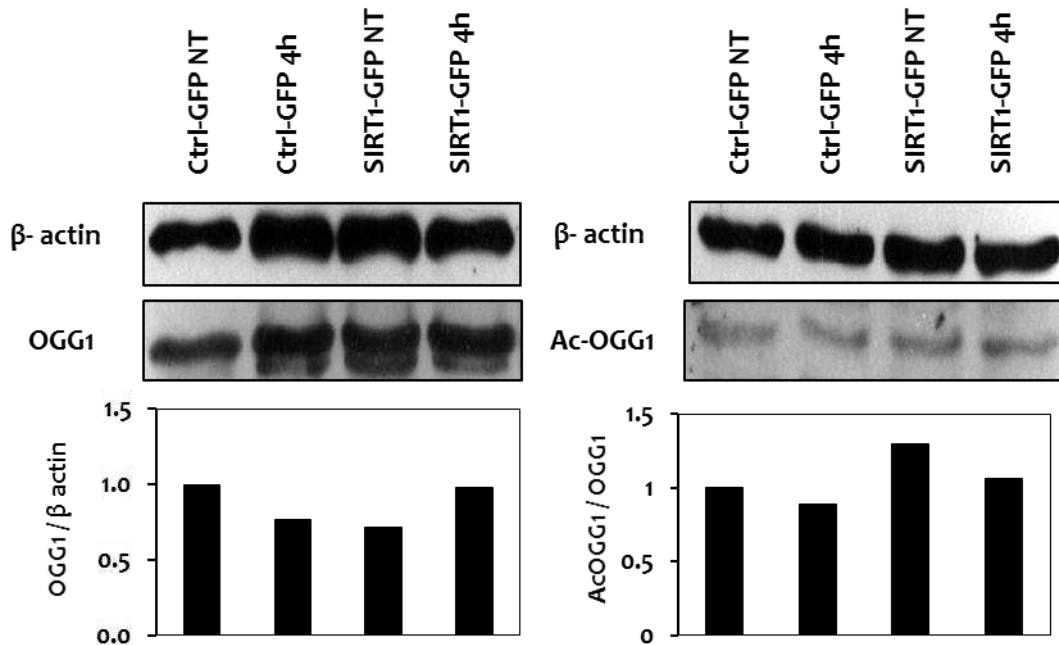
Figure 4.20 AcOGG1 in U2OS cells after oxidative damage. Protein levels of OGG1 and AcOGG1 were measured by Western blot in U2OS cells either untreated (NT) or treated with 40 mM KBrO$_3$ and 4h recovery times. Specific antibodies for OGG1 (left) and AcOGG1 (right) were used. 20 µg of total protein extract was applied and β-actin was used as a loading control; n=1. Lower panels: the intensity of the bands was quantitated using Image Lab software.

4.2   SIRT6

4.2.1   Influence of SIRT6 on genome stability

4.2.1.1   SIRT6 has no influence on micronuclei generation

To analyse the influence of SIRT6 on genomic stability *in vivo*, the mammalian micronucleus test (see chapter 3.2.3.4) was again applied as an indicator of chromosome damage and genetic instability. Sirt6 deficient and control mice were bred from the commercially available heterozygous strain 129-Sirt6$^{tm1Fwa/J}$ (see chapter 3.1.9). The level of micronuclei was determined in peripheral erythrocytes from SIRT6 deficient, heterozygous and wild type mice. The number of micronuclei in SIRT6 deficient mice was found to be slightly higher than in wild type and heterozygous mice (Figure 4.21). This result indicates that SIRT6 could have influence on the genome stability. However, for confirmation of the significance of this result more SIRT6 deficient and wild type mice are needed.

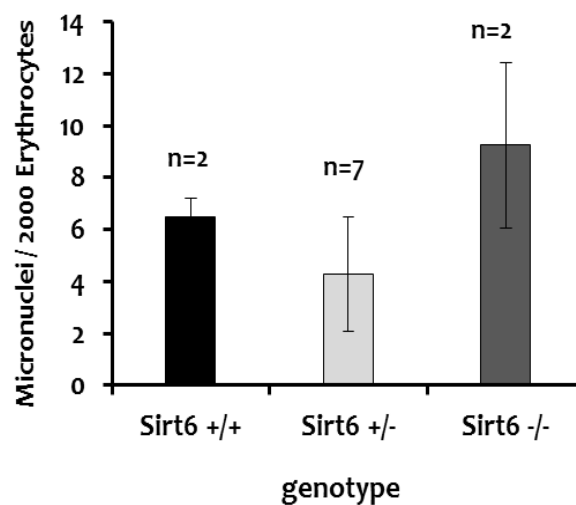**Figure 4.21 Influence of SIRT6 on the micronuclei generation.** Micronuclei formation of peripheral blood erythrocytes was analysed by Pappenheim staining of blood slides. Mice were sacrificed and one drop of blood from the Arteria carotis was used to perform a blood smear on a glass slide (see chapter 3.2.3.4). The numbers of the individual animals per each genotype are indicated above the columns. Bars represent the means ± SD.

4.2.2   Influence of SIRT6 on the generation and repair of oxidative DNA damage

4.2.2.1   SIRT6 has no influence on the repair of SSB in the presence or absence of a PARP inhibitor

To establish whether there is influence of SIRT6 on the repair kinetics of SSB, primary *Sirt6$^{-/-}$* and *wild type* mouse embryonic fibroblasts (MEFs), were prepared (see chapter 3.2.1.7) and exposed to 50 µM H$_2$O$_2$ for 15 min. Since it has been shown that SIRT6 interacts with PARP1 and stimulates poly-ADP-ribosylation activity upon oxidative stress (during DSB repair) (Mao et al., 2011), I measured the repair kinetic of SSB in the presence or absence of the PARP inhibitor DPQ (10 µM). The data shown in (Figure 4.22) indicates that the repair kinetics of SSB generated in both cell lines is the same. Cells treated with DPQ showed slower repair compared with the untreated cells, indicating the influence of PARP in the repair of SSB. However, the same retardation was observed with *wild type* and *Sirt6$^{-/-}$* MEFs, indicating that PARP activity stimulates repair in a SIRT6-independent manner.

Figure 4.22 Repair of SSB in primary MEFs from SIRT6$^{-/-}$ and SIRT6$^{+/+}$ – embryos. Mouse embryonic fibroblasts were prepared from 13.5 day old embryos by using standard methods (see chapter 3.2.1.7). *Sirt6$^{-/-}$* MEFs and *Sirt6$^{+/+}$* MEFs were exposed to H$_2$O$_2$ (50 µM; 15 min; 37°C) and subsequently treated with DPQ (10 µM). The numbers of SSB were determined by alkaline elution after various times of incubation under standard culture conditions (see chapter 3.2.4). Plot represents the means of 3 experiments ± SD.

4.2.2.2   SIRT6 has no influence on the repair kinetic of 8-oxoG

In order to measure if a SIRT6 deficiency affects the repair kinetics of 8-oxoG, primary MEFs were exposed to the photosensitizer 300 nM Ro 19-8022 plus visible light, for 10 min

on ice. In this way, 8-oxoG was generated in the DNA. The removal of the induced oxidative guanine modifications during the repair incubation was followed by alkaline elution assay using Fpg protein as a probe.

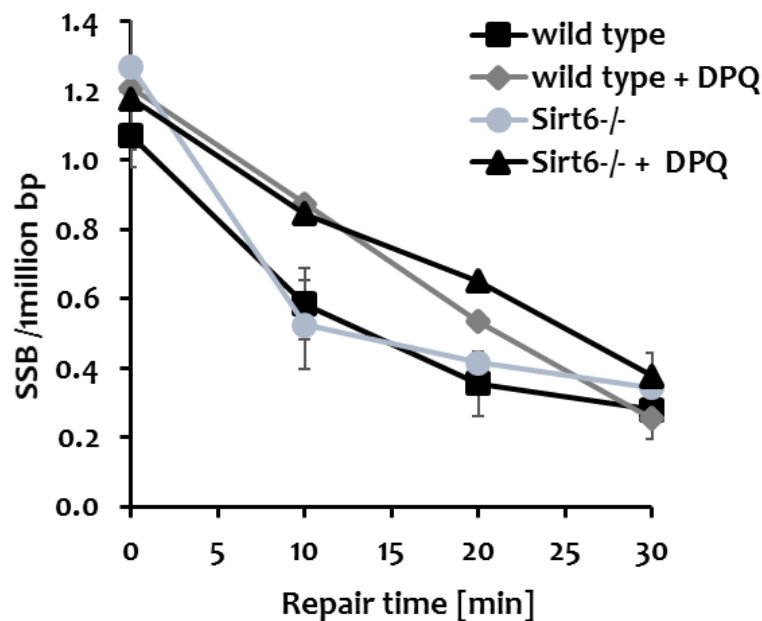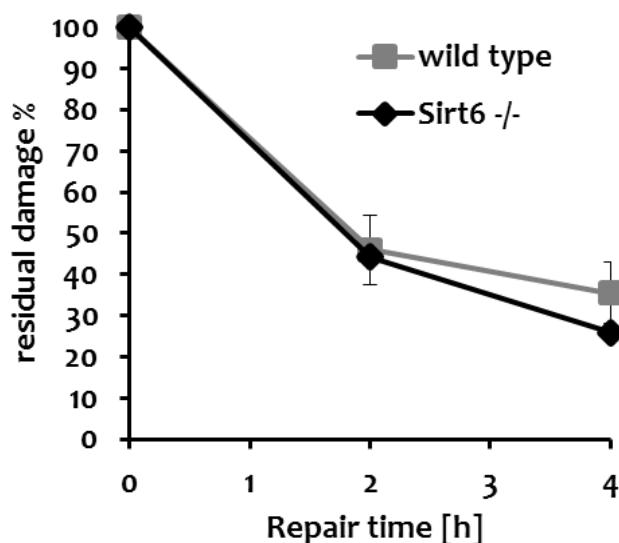**Figure 4.23. Repair of induced Fpg-sensitive lesions in primary MEFs from SIRT6^{-/-} and SIRT6^{+/+} – embryos.** Mouse embryonic fibroblasts were prepared from 13.5 day old embryos by using standard method (see chapter 3.2.1.7). *Sirt6^{-/-}* MEFs and *Sirt^{+/+}*MEFs were exposed to Ro 19-8022 (300 nM; 10 min; 38 cm; 1000W) and visible light. The numbers of modifications induced by the treatment were determined by alkaline elution after 0, 2 and 4h of incubation under standard culture conditions (see chapter 3.2.4). Plot represents the means of 2 experiments ± SD.

Sirt6^{-/-} MEFs showed no impaired repair of Fpg-sensitive DNA lesions compared to *wild type* MEFs. This indicates that SIRT6 has no influence on the repair of oxidatively induced DNA damage in primary MEFs (Figure 4.23).

4.2.2.3   SIRT6 has no influence on the basal levels of oxidative base modifications

Basal levels of oxidative base modifications reflect the steady-state between continuous generation of the modifications in the oxygen metabolism and a concomitant removal by DNA repair enzyme. To analyse the influence of SIRT6 on the basal levels of oxidative base modifications in spleen cells of SIRT6 deficient and wild type mice, an alkaline elution assay in combination with the repair glycosylase Fpg protein was used.

Figure 4.24. Basal level of Fpg-sensitive lesions in spleen cells derived from SIRT6$^{-/-}$, SIRT6$^{+/+}$ and SIRT6$^{+/-}$ – mice. Spleen cells were isolated from SIRT6 deficient, wild and heterozygous type mice (see chapter 3.2.1.6). The numbers of Fpg modifications were determined by alkaline elution. The numbers of the individual animals per each genotype are indicated above the columns. Bars represent the means of ± SD.
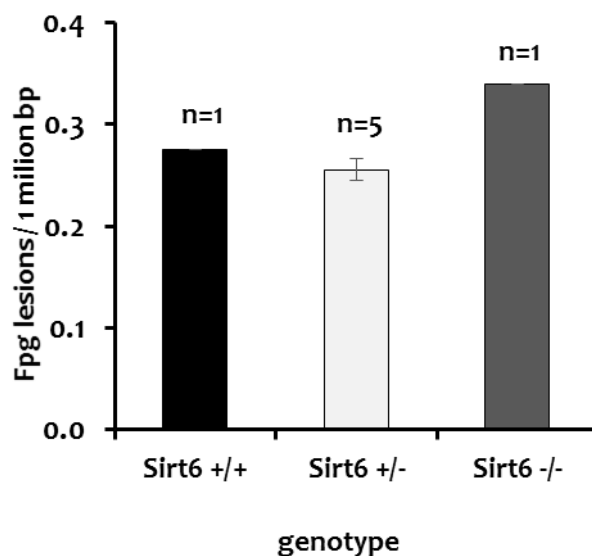
The results indicate similar levels of Fpg-sensitive oxidative base modifications in the nuclear DNA of cells from all three genotypes (SIRT6 deficient, wild and heterozygous type) (Figure 4.24). Therefore, there is no increased endogenous oxidative stress in result of a SIRT6 deficiency. For confirmation of the significance of this result more SIRT6 deficient and wild type mice are needed.

4.2.3 Influence of SIRT6 on the genome stability in *Sirt6$^{-/-}$/Ogg1$^{-/-}$* double knockout mouse

To test whether SIRT6 has a role in the generation of endogenous oxidative damage *Sirt6$^{-/-}$/Ogg1$^{-/-}$* double knockout mice were generated. *Ogg1*-defective mice are expected to respond to any change in the generation of 8-oxoG very sensitively, since the lesions cannot be rapidly removed by BER. As described in Material and methods (chapter 3.2.1.2), homozygous *Sirt6$^{-/-}$/Ogg1$^{-/-}$* double knockout mice were bred from *Sirt6$^{+/-}$/Ogg1$^{+/-}$* mice. Firstly, SIRT6 heterozygous mice from 129-Sirt6$^{tm1Fwa/J}$ strain with heterozygous Ogg1 Big Blue mice were crossed and *Sirt6$^{+/-}$Ogg1$^{+/-}$* mice were generated. Then in the second breading step, *Sirt6$^{+/-}$Ogg1$^{+/-}$* mice were crossed. In F2 generation, nine genotypes were generated: *Sirt6$^{+/+}$Ogg1$^{+/+}$, Sirt6$^{+/-}$Ogg1$^{+/+}$, Sirt6$^{+/+}$Ogg1$^{-/-}$, Sirt6$^{+/+}$Ogg1$^{+/-}$, Sirt6$^{+/+}$Ogg1$^{-/-}$, Sirt6$^{+/-}$Ogg1$^{+/-}$, Sirt6$^{-/-}$Ogg1$^{+/+}$, Sirt6$^{-/-}$Ogg1$^{+/-}$, Sirt6$^{-/-}$Ogg1$^{-/-}$* (see Figure 3.1). Homozygous *Sirt6$^{-/-}$Ogg1$^{-/-}$* double knockout and *Sirt6$^{+/+}$Ogg1$^{-/-}$* mice as a control were used for further experiments.

4.2.3.1 In the absence of OGG1, SIRT6 exhibits a protective influence on genome stability

To compare the genome stability in $Sirt6^{-/-}/Ogg1^{-/-}$ double knockout and $Ogg1^{-/-}$ mice, the mammalian *in vivo* micronucleus test was used. Untreated $Sirt6^{-/-}/Ogg1^{-/-}$ mice showed lower number of micronuclei in erythrocytes in comparison with $Sirt6^{+/+}/Ogg1^{-/-}$ mice (Figure 4.25). This data suggests that SIRT6 has a protective role on genome stability in the absence of OGG1.
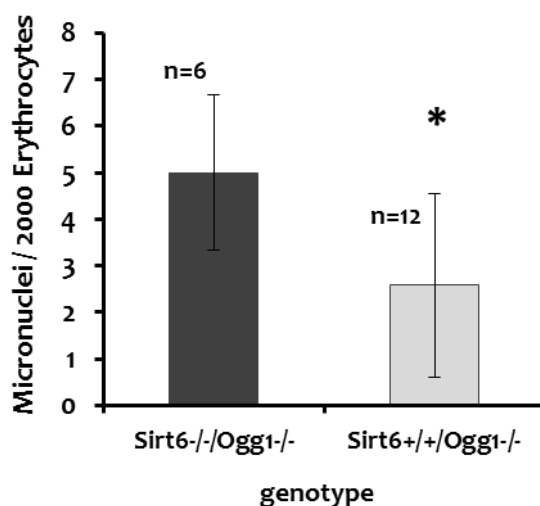
Figure 4.25 Influence of SIRT6 on the micronuclei generation in $Sirt6^{-/-}/Ogg1^{-/-}$ double knockout mice. Micronuclei formation of peripheral blood erythrocytes was analyzed by Pappenheim staining of blood slides. Mice were sacrificed and one drop of blood from the Arteria carotis was used to perform a blood smear on a glass slide (see chapter 3.2.3.4). The numbers of the animals per each genotype are indicated above the columns. Bars represent the means ± SD. Statistical significance of the difference between $Sirt6^{-/-}/Ogg1^{-/-}$ and $Sirt6^{+/+}/Ogg1^{-/-}$ genotypes was determined using a two tailed Student's t test (* $p<0.05$).

4.2.4 Influence of SIRT6 on the generation and repair of oxidative DNA damage in $Sirt6^{-/-}/Ogg1^{-/-}$ *double* knockout mouse

4.2.4.1 SIRT6 has no influence on the basal levels of oxidative base modifications in $Sirt6^{-/-}/Ogg1^{-/-}$ double knockout mouse

Previous analysis (Figure 4.24) of the basal level of oxidative base modifications in $Sirt6^{-/-}$ spleen cells showed no accumulation of endogenous oxidative base damage. As outlined above, a more sensitive approach to test whether SIRT6 has a role in the generation of endogenous oxidative damage is to analyse the basal steady-state levels of oxidative DNA modifications in $Ogg1^{-/-}$ cells. The levels of endogenous oxidative DNA base damage sensitive to Fpg protein were determined in splenocytes by alkaline elution. The results obtained from 7 animals of the two genotypes $Sirt6^{-/-}/Ogg1^{-/-}$ and $Sirt6^{+/+}/Ogg1^{-/-}$ are shown in Figure 4.26. The observed 8-oxoG levels in both genotypes were not statistically

different, indicating again that SIRT6 has no influence on the generation of endogenous oxidative DNA base damage (Figure 4.26).
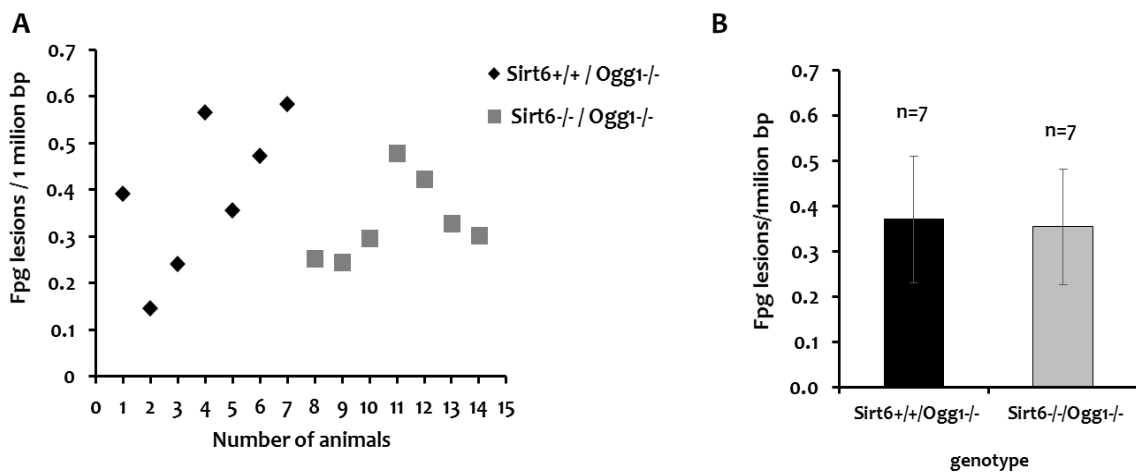
Figure 4.26 Basal level of Fpg-sensitive lesions in spleen cells derived from $Sirt6^{-/-}/Ogg1^{-/-}$ and $Sirt6^{+/+}/Ogg1^{-/-}$ – mice. Spleen cells were isolated from $Sirt6^{-/-}/Ogg1^{-/-}$ and $Sirt6^{+/+}/Ogg1^{-/-}$ mice (see chapter 3.2.1.6). The numbers of Fpg modifications were determined by alkaline elution. (A) Fpg lesions in individual animal. (B) Fpg lesions in the two genotypes. The number of animals per genotype is indicated above the columns. Bars represent the means ± SD.

4.2.4.2   SIRT6 has no influence on the repair of 8-oxoG in $Sirt6^{-/-}/Ogg1^{-/-}$ double knockout mouse

To analyse the OGG1-independent back-up repair, oxidative DNA damage was induced in the primary $Sirt6^{-/-}/Ogg1^{-/-}$ and $Sirt6^{+/+}/Ogg1^{-/-}$ MEFs by exposure to the photosensitizer Ro 19-8022 (300 nm) for 10 min on ice, plus visible light. The number of unrepaired 8-oxoG modifications was determined 3h after the treatment by alkaline elution. The result (Figure 4.27) shows that there is no difference in the repair of Fpg-sensitive lesions between the two cell lines. However, experiments with longer repair time are needed to exclude a SIRT6 involvement in OGG1-independent backup repair.

Another finding interesting to mention is related to the generation of $Sirt6^{-/-}/Ogg1^{-/-}$ double knockout MEFs. An unexpected ratio of the genotypes was observed in the MEFs when crossing the $Ogg1^{-/-}Sirt6^{+/-}$ mice, as shown in Table 4.1. From 36 embryos generated only 1 was double knockout. Crossings of $Sirt6^{+/-}$ heterozygous mice gave normal Mendel ratio of the embryonic genotypes (not shown). This finding indicates that SIRT6 only in the combination with OGG1 is important for embryonic development and perhaps genome stability.
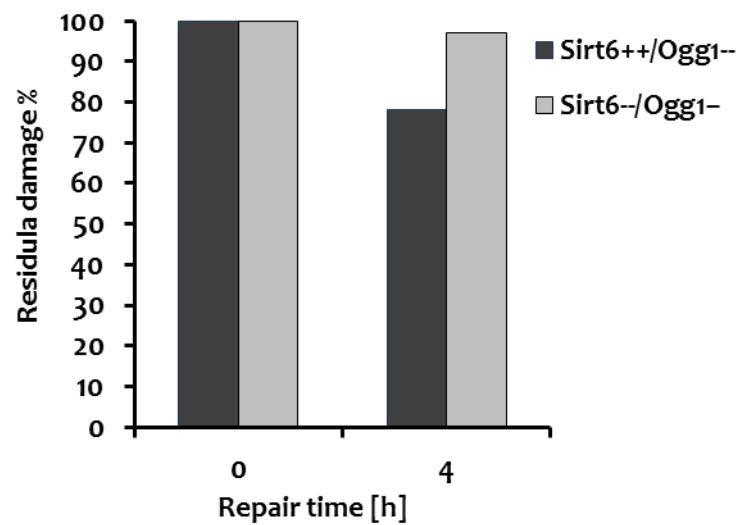
Figure 4.27 Repair of induced Fpg-sensitive lesions in primary MEFs from *Sirt6^{-/-}/Ogg1^{-/-}* and *Sirt6^{+/+}/Ogg1^{-/-}* – embryos. Mouse embryonic fibroblasts were prepared from 13.5 day old embryos by using standard methods (see chapter 3.2.1.7). $Sirt6^{-/-}/Ogg1^{-/-}$ MEFs and $Sirt^{+/+}/Ogg1^{-/-}$ MEFs were exposed to Ro 19-8022 (300 nM; 10 min; 38 cm; 1000W) and visible light. The numbers of modifications induced by the treatment were determined by alkaline elution after 4h of incubation under standard culture conditions (see chapter 3.2.4). n=1

Table 4.1 Establishment of MEFs from *Sirt6^{+/-}/Ogg1^{-/-}* - mice

MEFs						
Expected genotypes (Sirt6) (MENDEL)			Actual genotype (Sirt6) distribution			Number of embryos
+/+	+/-	-/-	+/+	+/-	-/-	
9	18	9	9	26	1	36

5   Discussion

5.1   SIRT1

SIRT1 could affect genome stability either by influencing the chromatin accessibility (via histone deacetylation) or by modifying enzymes involved in DNA repair. The aim of this study was to test these hypotheses and to investigate possible mechanisms.

The analysis of micronuclei generation in SIRT1 overexpressing U2OS or SIRT1 deficient glioblastoma cells confirmed the assumed relevance of SIRT1 for the integrity of the genome. SIRT1 overexpressing cells after damage induction with three different agents ($KBrO_3$, H_2O_2 and MMS) showed lower numbers of micronuclei than the control cells (Figure 4.2). Accordingly, inhibition of SIRT1 activity by NAM in U2OS cells increased to micronuclei generation after MMS treatment (Figure 4.4.B).

Firstly, I tested the hypothesis that SIRT1 influences the accessibility of the chromatin for repair proteins. According this hypothesis, an involvement of SIRT1 in histone deacetylation could influence both: DNA damage induction and the recruitment of repair proteins to the chromatin.

SIRT1 deacetylation activity is associated with more condensed chromatin (see chapter 1.2.2), thus I tested the idea that SIRT1 deficiency (highly acetylated chromatin) will lead to higher DNA damage induction and better repair while SIRT1-overexpression (highly condensed chromatin) should lead to less damage induction and slower repair. However, DNA damage induction analysis after oxidative stress did not show higher damage induction in the SIRT1-knockdown cells (Figure 4.6) or lower damage induction in SIRT1 overexpressing cells (Figure 4.5). In addition, the repair of 8-oxoG (induced by $KBrO_3$) was retarded rather than accelerated in the SIRT1-deficient cells (see also below) and not affected in the SIRT1 overexpressing cells (Figure 4.5-6). Radicella et al. (2010) demonstrated that chromatin compaction by sucrose, delayed the repair of 8-oxoG lesions induced by $KBrO_3$. This supports the assumption that a significant influence of SIRT1 on chromatin accessibility indeed would have affected the repair rates, in contrast to my results. Another line of evidence was obtained from co-localization studies with fluorescent proteins (chapter 4.1.3). I demonstrated that the recruitment of APE1 and OGG1 to the chromatin after oxidative stress is independent of the presence of SIRT1 (Figure 4.13.A). Taken together, the findings discussed above clearly show that a putative SIRT1-modulated chromatin compaction is not an explanation for the observed influence of SIRT1 on micronuclei generation.

An interesting additional finding from the fluorescence experiments was the demonstration of a clear co-localization between SIRT1 and OGG1 in osteosarcoma and

glioblastoma cells after oxidative stress in the euchromatin regions (Figure 4.11-4.12). Interestingly, SIRT1 and APE1 were previously shown to co-localize in nuclei (Yamamori et al., 2010). The findings point to a role of SIRT1 in the orchestration of the repair process, which in theory also could explain the observed impact of SIRT1 on genome stability. Therefore, the influence of SIRT1 on three subsequent steps of BER, namely base removal (and concomitant AP site formation), AP site incision and SSB ligation was analysed in greater detail.

It can be anticipated that an efficient and rapid resealing of SSBs after the initiation of repair is crucial for maintaining genome integrity. More micronuclei generation in control osteosarcoma cells could be due to defects in the ligation of SSBs generated directly or as repair intermediates. Indeed, it was shown that impaired resealing of BER-induced SSB leads to genome instability. Cells expressing the XRCC1 (R194W) variant, which is unable to recruit LigIII to the sites of BER, accumulated higher number of micronuclei after exposure to oxidative stress than control cells (Campalans et al., 2015). However, my analyses of the repair kinetics of SSBs directly induced by H_2O_2 did not show an influence of an SIRT1 overexpression or deficiency on the repair of SSBs (Figure 4.7-8).

PARP1 rapidly recognises SSB and initiates the recruitment of other repair proteins to the damage sites, such as XRCC1, Pol-β and LigIII (Hill, 1991). In the study of the repair of H_2O_2 induced SSB, I observed a small, but significant influence of PARP1 on the repair of H_2O_2-induced SSBs (Figure 4.22) which makes PARP1 another candidate for posttranslational modification by SIRT1. SIRT1 and PARP1 are functionally connected due to their use of a common co-substrate, nicotinamide adenine dinucleotide (NAD^+). Several studies suggested that activation of PARP1 causes a depletion in NAD^+ levels, which inhibits SIRT1 activity, whereas SIRT1 is capable of deacetylating and deactivating PARP1 (Cheung & New, 1985). However, the results shown in (Figure 4.7-8) suggest that SIRT1 does not influence the activity of PARP1 significantly.

Theoretically, slower excision of 8-oxoG by OGG1 will lead to less AP-site formation and less SSBs generation. SIRT1 deficient cells indeed had slower repair kinetics of $KBrO_3$-induced 8-oxoG lesions (Figure 4.6) which could explain the slightly lower number of micronuclei observed (Figure 4.4.C). However, as already pointed out (Figure 4.4.C), the reduced cell proliferation of the SIRT1-deficient glioblastoma cells is a more likely explanation. Moreover, I did not observe impaired 8-oxoG repair in SIRT1 overexpressing cells (Figure 4.5), and yet these cells had lower micronuclei generation (Figure 4.2.A).

The influence of acetylation on the activity of OGG1 was studied by several groups. *In vitro* analyses of the enzymatic activity (by means of a cleavage assay) demonstrated that acetylated OGG1 (AcOGG1) has better base excision activity than unmodified OGG1 (Bhakat et al., 2006). Since acetylation of OGG1 decreases its affinity for the AP site produced, an acetylation / deacetylation loop might be crucial for a balanced enzymatic

activity (Bhakat et al., 2006). Sarga et al. (2013) demonstrated an inverse correlation between SIRT1 and AcOGG1 level. Under conditions of oxidative stress (animal exercises), neuronal cells showed increased SIRT1 expression and decreased AcOGG1 level. Additionally, both the SIRT1 inhibitor NAM and a transfection with siSIRT1 increased the acetylation of OGG1 (Sarga et al., 2013). Bhakat et al. (2006) measured the basal levels of 8-oxoG in MEFs using immunofluorescence techniques. Cells treated with TSA (a class-I and class-II HDAC inhibitor) also showed lower 8-oxoG levels in comparison with non-treated cells. The repair kinetics of induced 8-oxoG was better in cells transfected with wild type OGG1 than in cells transfected with mutant (non-acetyable) OGG1 (Bhakat et al., 2006).

The reported findings that acetylation modulates OGG1's activity suggest that SIRT1 modulates 8-oxoG repair. Indeed, I observed slower repair kinetics of 8-oxoG lesions in SIRT1 deficient cells (Figure 4.6), but the repair in SIRT1 overexpressing cells was not affected (Figure 4.5) despite the elevated level of micronuclei (Figure 4.2). Moreover, the level of AcOGG1 was not affected in SIRT1 overexpressing cells, neither under normal nor under oxidative stress conditions (Figure 4.20). These data suggest that the influence of SIRT1 on the micronuclei generation is not mediated by a modulation of OGG1 activity.

Finally, I investigated the assumption that the influence of SIRT1 on micronuclei generation is a consequence of a role of SIRT1 in the processing of AP sites, due to a putative deacetylation of APE1. Higher acetylation level in the absence of SIRT1 might increase APE1-cleavage activity that will lead to higher SSBs generation, as products of APE1, and, in consequence, higher micronuclei generation. SIRT1 overexpression, decreasing APE1 activity by deacetylation is expected to decrease micronuclei generation due to less SSBs generation from AP sites. For an analysis of the processing of AP sites, methyl-methane sulphonate (MMS) was used, an alkylating agents that generates high levels of AP sites, both by spontaneous depurination and base excision repair of alkylated DNA bases. In accordance with the expectations mentioned above, SIRT1 overexpressing cells had higher levels of AP sites at all repair times analysed (Figure 4.9). Moreover, the relatively high number of SSBs detected in SIRT1 deficient glioblastoma cells directly after MMS treatment, which may reflect a rapid (unbalanced) incision of AP sites by APE1, was not observed in the control cells, consistent with higher APE1 activity due to a higher acetylation level in result of SIRT1 deficiency (Fig.4.10).

Unexpectedly, however, SIRT1 knockdown cells showed a slower (rather than accelerated) removal of AP sites after MMS treatment (Figure 4.10). A putative explanation is that the activity of the methylpurine DNA glycosylase (MPG), which generates AP sites from the major base modifications induced by MMS in the first step of BER, is also increased by acetylation (Jacobs & Schär, 2012). Higher MPG activity in SIRT1 knockdown cells then would lead to higher AP site generation and could explain the observed accumulation of AP sites. (Figure 4.10). In accordance with my data, Yamamori

et al. (2010) demonstrated that SIRT1 knockdown increased AP site induction by MMS treatment in HeLa cells. Conceivably, MPG is already fully deacetylated in control osteosarcoma cells, so that SIRT1 overexpression has no influence on the rate of AP site generation. The accumulation of AP sites in the SIRT1 overexpressing cells (Figure 4.9) then results only from of the higher deacetylation and thus impaired activity of APE1. Reduced APE1 activity could also explain the diminished micronuclei generation in SIRT1 overexpressing cells after $KBrO_3$ and H_2O_2 induction.

Although $KBrO_3$ and H_2O_2 generate 8-oxoG and SSBs, respectively, as the predominant direct lesions, both compounds also induce small amounts of AP sites as by-products. These contribute less to the generation of micronuclei if less rapidly converted into SSBs by less active (deacetylated) APE1. In the case of $KBrO_3$, AP sites generated as repair intermediates are also less rapidly converted into SSBs if APE1 activity is reduced by SIRT1 overexpression and concomitantly more efficient deacetylation.

To verify the assumption that SIRT1 activity reduces the APE1 activity, I directly quantified APE1 activity in cell extracts, both under normal conditions and following oxidative stress. Extracts from SIRT1 overexpressing cells (not exposed to oxidative stress) had strongly reduced APE1 activity in comparison with extracts from the control cells (Figure 4.16.B). APE1 therefore appears to exist predominantly in acetylated (active) state and can be inactivated by additional SIRT1. This is in agreement with the finding that the knockdown of SIRT1 in glioblastoma cells has little influence on the APE1 activity, as the acetylation level cannot be further increased (Figure 4.17.A). Directly after oxidative damage, a strong reduction of the APE1 cleavage activity was observed in osteosarcoma cells (Figure 4.16.B). Four hours after damage induction, APE1 cleavage was further decreased in both control osteosarcoma (Figure 4.16.C) and control glioblastoma (Figure 4.17.C) cells. APE1 activity in SIRT1 overexpressing cells after oxidative stress remained unchanged, since it was already low from the beginning (Figure 4.16). The glioblastoma SIRT1 knockdown cells appear protected from the influence of oxidative stress, i.e. 4h after $KBrO_3$ treatment they showed better APE1 cleavage activity than control cells (Figure 4.17.C). The results can best be explained by an increase of SIRT1 activity following oxidative stress, which gives rise to a pronounced deacetylation and thereby inactivation of APE1. In accordance with these findings, Yamamory et al. (2010) have demonstrated that SIRT1 expression is increased after oxidative stress and in the model proposed by Sengupta et al. (2016) SIRT1 by deacetylation of Lys 6/7 of APE1 is decreasing APE1's cleavage activity (Sarga et al., 2013). With these data I demonstrated that oxidative stress is a signal for induction of APE1-deacetylation by SIRT1 which strongly decreases its activity (Figure 4.16-4.17).

Finally, I showed that APE1 repair activity was affected by deacetylation without a concomitant change of the amount of the protein. As shown in (Figure 4.18-19), the expression levels of APE1 and OGG1 were not affected by SIRT1 overexpression or

deficiency in the basal conditions. Also after oxidative stress SIRT1 overexpression or deficiency had no significant influence on the protein levels of APE1 and OGG1 (Figure 4.18-19).

In this study I demonstrated that a SIRT1-mediated deacetylation and thereby inactivation of the DNA repair enzymes, in particular APE1, is a previously unknown regulatory mechanism of genetic instability (micronuclei formation). According to the proposed model, in SIRT1 deficient cells (Figure 5.1.A), glycosylase (MPG) activity is increased by acetylation under conditions of oxidative / genotoxic stress (not verified). Higher glycosylase (MPG) activity will lead to higher AP site generation and accumulation of AP sites, as observed (Figure 4.10). Importantly, higher acetylation level in the absence of SIRT1 (Figure 4.17) will also increase APE1-cleavage activity that will lead to higher SSBs generation as products of APE1 activity, as observed in Figure 4.10, and, in consequence, higher micronuclei generation, as observed in Figure 4.4.B. In SIRT1 overexpressing cells on the other hand (Figure 5.1.B), glycosylase (MPG) is already fully deacetylated (not verified) and doesn't have any further influence on the rate of AP site generation. Higher deacetylation by SIRT1 overexpression will reduce activity of APE1, as observed in Figure 4.16, and results in an accumulation of AP sites (observed in Figure 4.9). As a result of the lower number of SSB, less micronuclei are generated (observed in Figure 4.2).

A

SIRT1 deficiency
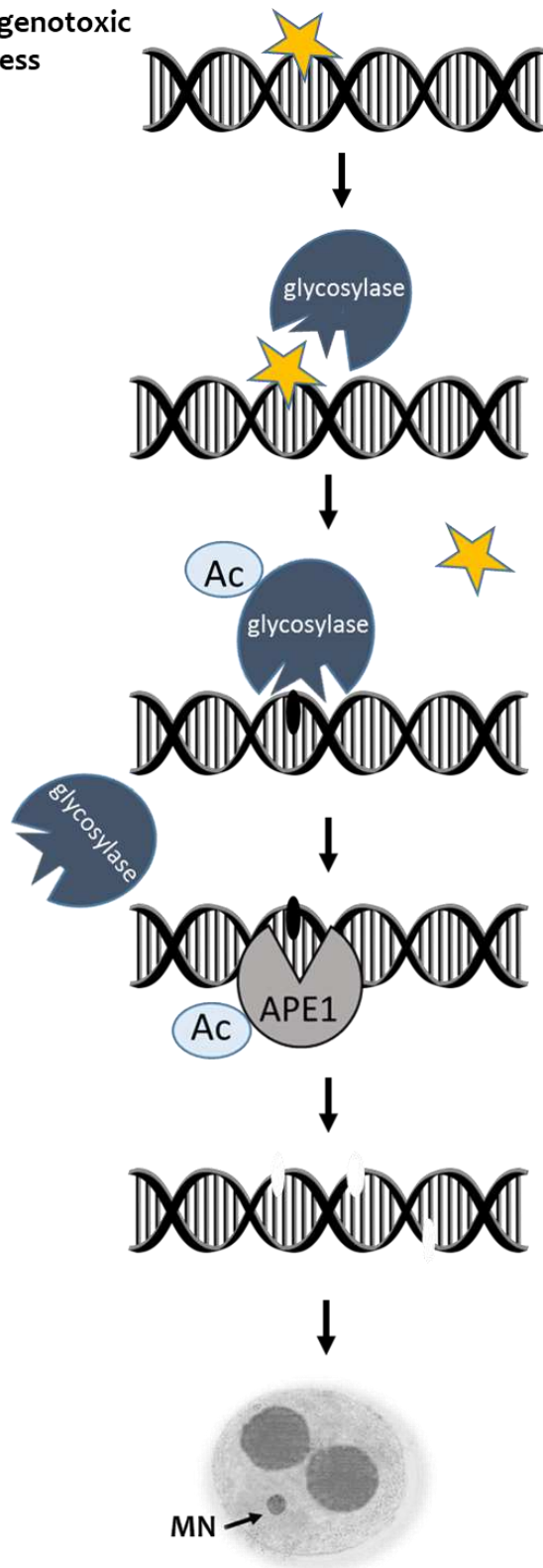
oxidative/genotoxic stress

Higher glycosylase activity (not verified)

accumulation of AP sites (Fig.4.10)
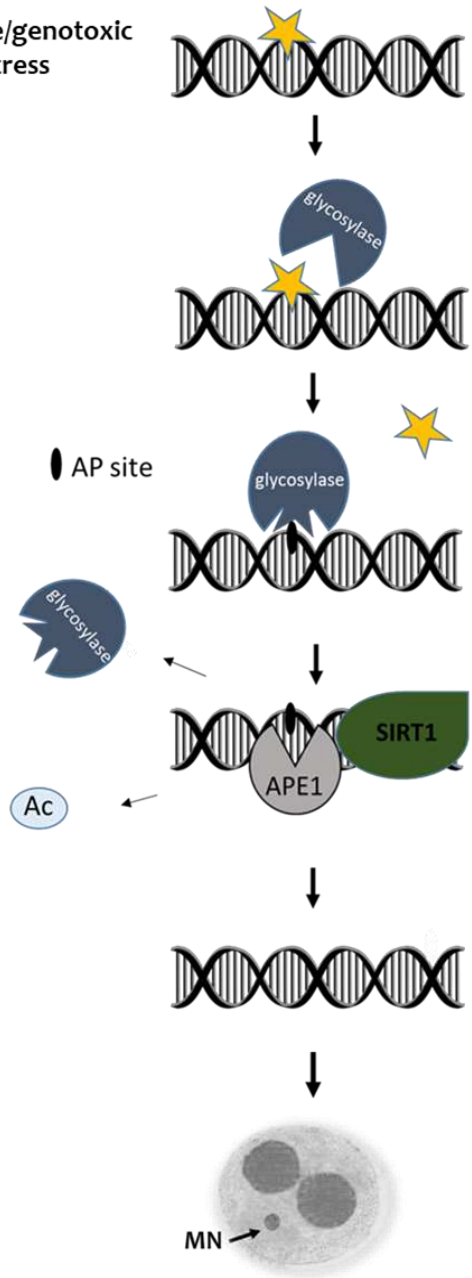
Higher APE1 activity (Fig.4.17.C)

accumulation of SSBs (Fig.4.10)

Higher number of micronuclei formation (Fig.4.4.B)

Figure 5.1 Model for micronuclei generation due to SIRT1-mediated deacetylation of APE1 in (A) SIRT1 deficient cells; (B) SIRT1 overexpressing cells

5.2   SIRT6

SIRT6 is another histone deacetylase that in principle could have an influence on genome stability and DNA repair pathways by the mechanism described above for SIRT1. According to findings described in the literature (see chapter 1.2.3), another putative way for SIRT6 to alter DNA repair is by affecting metabolism and ROS production that will increase DNA damage load. Aim of this part of the study was to investigate the influence of SIRT6 on the endogenous level of oxidatively generated DNA base modifications.

A good model for the investigation of the influence of SIRT6 on the accumulation of oxidative DNA damage and on DNA repair are $Sirt6^{-/-}$ knock-out mice. While SIRT6 heterozygous mice appear normal, SIRT6 deficient mice show a severe phenotype as already described by Mostoslavsky et al. (2006). They are smaller, show growth retardation and die 3-4 weeks after birth.

An *in vivo* mammalian micronucleus test showed elevated numbers of micronuclei in erythrocytes from SIRT6 deficient mice, although only 2 animals could be analysed (Figure 4.21). This could indicate that SIRT6 has indeed an influence on genome stability (Figure 4.21). As mentioned above, a putative explanation for such an influence is that metabolic defects in SIRT6 deficient mice that lead increased ROS generation (e.g. via increased Insulin / IGF1–like signalling) and in consequence - DNA damage accumulation and higher micronuclei generation.

Liver is the best organ for investigating the steady-state levels of oxidative generated DNA base modifications, which reflect the equilibrium between the continuous generation of oxidative damage and its continuous removal by DNA repair. However, due to growth retardation of SIRT6 deficient mice and small organs, I had to use spleen cells for the analysis of the basal levels of 8-oxoG. The data indicated that the basal levels of oxidative base modifications in spleen cells were not influenced by SIRT6 (Figure 4.24). SIRT6 has no influence on the repair of SSBs (Figure 4.22), neither in the absence nor in the presence of an PARP inhibitor (Figure 4.22). Also the removal of induced 8-oxoG modifications in primary MEFs was not affected by the deficiency of SIRT6 (Figure 4.23).

However, the repair of AP sites still has not been investigated so far and remains as a possible explanation for the increased genetic instability in SIRT6 deficient mice. In accordance with this idea are the findings described in Introduction (chapter 1.2.3) (Mostoslavsky et al., 2006) in which SIRT6 deficient MEFs showed a hypersensitivity against MMS, H_2O_2, and ionizing radiation that was rescued by expression of the dRP-lyase domain of DNA polymerase β (polβ). After MPG recognition of the lesion, APE1 leaves 5'-deoxyribose phosphate (dRP) at the SSB, which is subsequently removed by Polβ.

A more sensitive approach to investigate the influence of SIRT6 on the generation of oxidative DNA damage is the analysis of $Sirt6^{-/-}/Ogg1^{-/-}$ - double knockout mice, since the additional OGG1 deficiency prevents a rapid repair of the lesions (see chapter 1.3.8.1). My finding (Figure 4.25) that less micronuclei were counted in erythrocytes from $Sirt6^{-/-}/Ogg1^{-/-}$ - double knockout mice than in erythrocytes from $Sirt6^{+/+}/Ogg1^{-/-}$ mice was unexpected.

Measurements of basal levels of oxidative damage in spleen cells from $Sirt6^{-/-}/Ogg1^{-/-}$ - double knockout (Figure 4.26) showed that SIRT6 has no influence on the generation of oxidative damage. In summary, neither the analyses of the influence of SIRT6 on repair in MEFs (Figure 4.27) nor the analysis of the basal levels of oxidative damage, couldn't explain the finding of less micronuclei formation in $Sirt6^{-/-}/Ogg1^{-/-}$ - double knockout.

6   Summary

Genome stability is very important for all living organisms and is constantly under threat because of the exposure to different environmental and endogenous DNA damaging agents. Genome instability, for example in consequence of defective DNA repair, is an important risk factor for the initiation of carcinogenesis. Aim of this study was to investigate the influence of SIRT1 and SIRT6 on genome stability. Sirtuins are NAD^+-dependent deacetylases of histones and other proteins that could influence base excision repair (BER) by modulating chromatin accessibility, by modifying enzymes involved in DNA repair or by affecting metabolism and the production of reactive oxygen species (ROS) that will increase DNA damage load.

For investigation of these hypotheses, SIRT1 overexpressing and deficient cells were used, as well as $Sirt6^{-/-}$ knock-out and $Sirt6^{-/-}/Ogg1^{-/-}$ double knock-out. The micronucleus assay was used as indicator for genome instability. DNA damage and repair were measured by an alkaline elution assay. A DNA relaxation assay was used for the analyses of APE1 activity.

Results showed that SIRT1 overexpression has a protective role on genome stability and SIRT1 deficiency leads to genome instability. Chromatin accessibility analyses did not show an influence of SIRT1, neither on DNA damage induction nor on the recruitment of repair proteins to the chromatin, as demonstrated by immune fluorescence techniques. Co-localization of SIRT1 with BER enzymes to euchromatin regions suggested a role of SIRT1 in the coordination of the BER. The resealing of single strand breaks (SSBs) as a crucial step for maintaining genome integrity was not affected by SIRT1. Further analyses of the removal of modified DNA bases and AP site incision showed that AP site incision is the main event in micronuclei generation that is influenced by SIRT1. More detailed investigation of APE1 activity showed that SIRT1-mediated deacetylation inhibits APE1-endonuclease activity. Accordingly, decreased APE1 activity causes an accumulation of AP sites in SIRT1 overexpressing cells after MMS treatment. Accumulation of SSBs in MMS-treated SIRT1 knockdown cells, generated from base excision repair-intermediates, was the result of higher APE1 activity.

In this study, a mechanism for micronuclei generation from SSBs as a result of impaired base excision repair pathway due to SIRT1-modulated APE1 activity was proposed. More SSBs in SIRT1 deficient cells lead to higher number of micronuclei, as result of increased APE1 cleavage activity and genomic instability. Reduced APE1-endonuclease activity in SIRT1 overexpressing cells results in less SSBs generation and lower number of micronuclei, suggesting a protective role of SIRT1 on genome stability. Interestingly, the activity of SIRT1 was found to be stimulated by oxidative stress. Thus the APE1 activity in cell extracts was reduced after treatment with bromate in normal, but not in SIRT1 deficient cells, while SIRT1-overexpressing cells exhibit low APE1 activity, independent of oxidative

stress. An unexpected accumulation of AP sites and SSBs in MMS-treated SIRT1-deficient cells suggests an additional influence of SIRT1 on the activity of methyl purine glycosylase (MPG), another repair enzyme.

In summary, the results demonstrate that SIRT1 plays a previously unknown role in the preservation of the genetic stability of cells. By its influence on the processing of AP sites (via a regulation of APE1 activity) it prevents an unbalanced base excision repair, in particular an accumulation of SSBs as repair intermediates, which would cause chromosome breaks and micronuclei formation.

Many questions regarding the relevance of SIRT6 for genetic stability remain unanswered due to the low number and early death of SIRT6 deficient animals that could be generated. However, results in this study clearly demonstrate that SIRT6 has no influence on the resealing of SSBs. An unexpected protective role of SIRT6 deficiency on genome stability, which was only observed in combination with OGG1 deficiency, raises new questions about a mechanistic interaction / interplay of these two proteins. Further investigations (and more animals) are needed for any conclusions about the role of SIRT6 on genome stability and the proteins involved.

7 References

Allgayer, J., Kitsera, N., Bartelt, S., Epe, B., & Khobta, A. (2016). Widespread transcriptional gene inactivation initiated by a repair intermediate of 8-oxoguanine. *Nucleic acids research*, *44*(15), 7267–7280. https://doi.org/10.1093/nar/gkw473

Amouroux, R., Campalans, A., Epe, B., & Radicella, J. P. (2010). Oxidative stress triggers the preferential assembly of base excision repair complexes on open chromatin regions. *Nucleic acids research*, *38*(9), 2878–2890. https://doi.org/10.1093/nar/gkp1247

Antoniali, G., Lirussi, L., D'Ambrosio, C., Dal Piaz, F., Vascotto, C., Casarano, E.,. . . Tell, G. (2014). SIRT1 gene expression upon genotoxic damage is regulated by APE1 through nCaRE-promoter elements. *Molecular biology of the cell*, *25*(4), 532–547. https://doi.org/10.1091/mbc.E13-05-0286

Arumugham, R. G., Hsieh, T. C., Tanzer, M. L., & Laine, R. A. (1986). Structures of the asparagine-linked sugar chains of laminin. *Biochimica et biophysica acta*, *883*(1), 112–126.

Ballmaier, D., & Epe, B. (1995). Oxidative DNA damage induced by potassium bromate under cell-free conditions and in mammalian cells. *Carcinogenesis*, *16*(2), 335–342.

Ballmaier, D., & Epe, B. (2006). DNA damage by bromate: mechanism and consequences. *Toxicology*, *221*(2-3), 166–171. https://doi.org/10.1016/j.tox.2006.01.009

Baute, J., & Depicker, A. (2008). Base excision repair and its role in maintaining genome stability. *Critical reviews in biochemistry and molecular biology*, *43*(4), 239–276. https://doi.org/10.1080/10409230802309905

Beauharnois, J. M., Bolívar, B. E., & Welch, J. T. (2013). Sirtuin 6: A review of biological effects and potential therapeutic properties. *Molecular bioSystems*, *9*(7), 1789–1806. https://doi.org/10.1039/c3mb00001j

Beneke, S., & Bürkle, A. (2007). Poly(ADP-ribosyl)ation in mammalian ageing. *Nucleic acids research*, *35*(22), 7456–7465. https://doi.org/10.1093/nar/gkm735

Bhakat, K. K., Mokkapati, S. K., Boldogh, I., Hazra, T. K., & Mitra, S. (2006). Acetylation of human 8-oxoguanine-DNA glycosylase by p300 and its role in 8-oxoguanine repair in vivo. *Molecular and cellular biology*, *26*(5), 1654–1665. https://doi.org/10.1128/MCB.26.5.1654-1665.2006

Bialostozky, L. (1974). Letter: Painless removal of sutures. *Surgery*, *76*(2), 356–357.

Bjelland, S., & Seeberg, E. (2003). Mutagenicity, toxicity and repair of DNA base damage induced by oxidation. *Mutation research*, *531*(1-2), 37–80.

Boiteux, S., O'Connor, T. R., & Laval, J. (1987). Formamidopyrimidine-DNA glycosylase of Escherichia coli: cloning and sequencing of the fpg structural gene and overproduction of the protein. *The EMBO journal*, *6*(10), 3177–3183.

Boiteux, S., & Guillet, M. (2004). Abasic sites in DNA: Repair and biological consequences in Saccharomyces cerevisiae. *DNA repair*, *3*(1), 1–12.

Bradbury, C. A., Khanim, F. L., Hayden, R., Bunce, C. M., White, D. A., Drayson, M. T.,. . . Turner, B. M. (2005). Histone deacetylases in acute myeloid leukaemia show a distinctive pattern of expression that changes selectively in response to deacetylase inhibitors. *Leukemia*, *19*(10), 1751–1759. https://doi.org/10.1038/sj.leu.2403910

Busso, C. S., Iwakuma, T., & Izumi, T. (2009). Ubiquitination of mammalian AP endonuclease (APE1) regulated by the p53-MDM2 signaling pathway. *Oncogene*, *28*(13), 1616–1625. https://doi.org/10.1038/onc.2009.5

Caldecott, K. W. (2008). Single-strand break repair and genetic disease. *Nature reviews. Genetics*, *9*(8), 619–631. https://doi.org/10.1038/nrg2380

Campalans, A., Moritz, E., Kortulewski, T., Biard, D., Epe, B., & Radicella, J. P. (2015). Interaction with OGG1 is required for efficient recruitment of XRCC1 to base excision repair and mainte-

nance of genetic stability after exposure to oxidative stress. *Molecular and cellular biology*, *35*(9), 1648–1658. https://doi.org/10.1128/MCB.00134-15

Cannan, W. J., & Pederson, D. S. (2016). Mechanisms and Consequences of Double-Strand DNA Break Formation in Chromatin. *Journal of cellular physiology*, *231*(1), 3–14. https://doi.org/10.1002/jcp.25048

Chailley, B., Bork, K., Gounon, P., & Sandoz, D. (1986). Immunological detection of actin in isolated cilia from quail oviduct. *Biology of the cell*, *58*(1), 43–52.

Chatterjee, N., & Walker, G. C. (2017). Mechanisms of DNA damage, repair, and mutagenesis. *Environmental and molecular mutagenesis*, *58*(5), 235–263. https://doi.org/10.1002/em.22087

Cheng, H.-L., Mostoslavsky, R., Saito, S.'i., Manis, J. P., Gu, Y., Patel, P.,. . . Chua, K. F. (2003). Developmental defects and p53 hyperacetylation in Sir2 homolog (SIRT1)-deficient mice. *Proceedings of the National Academy of Sciences of the United States of America*, *100*(19), 10794–10799. https://doi.org/10.1073/pnas.1934713100

Cheng, Y., Ren, X., Gowda, A. S. P., Shan, Y., Zhang, L., Yuan, Y.-S.,. . . Yang, J.-M. (2013). Interaction of Sirt3 with OGG1 contributes to repair of mitochondrial DNA and protects from apoptotic cell death under oxidative stress. *Cell death & disease*, *4*, e731. https://doi.org/10.1038/cddis.2013.254

Cheung, Y. W., & New, P. K. (1985). Missionary doctors vs Chinese patients: Credibility of missionary health care in early twentieth century China. *Social science & medicine (1982)*, *21*(3), 309–317.

Cohen, H. Y., Miller, C., Bitterman, K. J., Wall, N. R., Hekking, B., Kessler, B.,. . . Sinclair, D. A. (2004). Calorie restriction promotes mammalian cell survival by inducing the SIRT1 deacetylase. *Science (New York, N.Y.)*, *305*(5682), 390–392. https://doi.org/10.1126/science.1099196

Crade, M., & Taylor, K. J. (1979). Ultrasound diagnosis of pancreatic pathology. *Journal of clinical gastroenterology*, *1*(2), 171–181.

Csibi, A., Fendt, S.-M., Li, C., Poulogiannis, G., Choo, A. Y., Chapski, D. J.,. . . Blenis, J. (2013). The mTORC1 pathway stimulates glutamine metabolism and cell proliferation by repressing SIRT4. *Cell*, *153*(4), 840–854. https://doi.org/10.1016/j.cell.2013.04.023

Dai, Y., & Faller, D. V. (2008). Transcription Regulation by Class III Histone Deacetylases (HDACs)-Sirtuins. *Translational oncogenomics*, *3*, 53–65.

Dai, Z.-J., Wang, X.-J., Kang, A.-J., Ma, X.-B., Min, W.-L., Lin, S.,. . . Kang, H.-F. (2014). Association between APE1 Single Nucleotide Polymorphism (rs1760944) and Cancer Risk: A Meta-Analysis Based on 6,419 Cancer Cases and 6,781 Case-free Controls. *Journal of Cancer*, *5*(3), 253–259. https://doi.org/10.7150/jca.8085

Damsma, G. E., & Cramer, P. (2009). Molecular basis of transcriptional mutagenesis at 8-oxoguanine. *The Journal of biological chemistry*, *284*(46), 31658–31663. https://doi.org/10.1074/jbc.M109.022764

Dantzer, F., Luna, L., Bjørås, M., & Seeberg, E. (2002). Human OGG1 undergoes serine phosphorylation and associates with the nuclear matrix and mitotic chromatin in vivo. *Nucleic acids research*, *30*(11), 2349–2357.

Davidovic, L., Vodenicharov, M., Affar, E. B., & Poirier, G. G. (2001). Importance of poly(ADP-ribose) glycohydrolase in the control of poly(ADP-ribose) metabolism. *Experimental cell research*, *268*(1), 7–13. https://doi.org/10.1006/excr.2001.5263

Deyo, R. A. (2001). A key medical decision maker: The patient. *BMJ (Clinical research ed.)*, *323*(7311), 466–467.

Dherin, C., Radicella, J. P., Dizdaroglu, M., & Boiteux, S. (1999). Excision of oxidatively damaged DNA bases by the human alpha-hOgg1 protein and the polymorphic alpha-hOgg1(Ser326Cys) protein which is frequently found in human populations. *Nucleic acids research*, *27*(20), 4001–4007.

Dizdaroglu, M. (1992). Oxidative damage to DNA in mammalian chromatin. *Mutation research*, *275*(3-6), 331–342.

Dyrkheeva, N. S., Lebedeva, N. A., & Lavrik, O. I. (2016). AP Endonuclease 1 as a Key Enzyme in Repair of Apurinic/Apyrimidinic Sites. *Biochemistry. Biokhimiia*, *81*(9), 951–967. https://doi.org/10.1134/S0006297916090042

Entman, M. L. (1990). Alprazolam withdrawal. *Texas medicine*, *86*(9), 122.

Epe, B. (1996). DNA damage profiles induced by oxidizing agents. *Reviews of physiology, biochemistry and pharmacology*, *127*, 223–249.

Epe, B., Mützel, P., & Adam, W. (1988). DNA damage by oxygen radicals and excited state species: a comparative study using enzymatic probes in vitro. *Chemico-biological interactions*, *67*(1-2), 149–165.

Epe, B., Pflaum, M., & Boiteux, S. (1993). DNA damage induced by photosensitizers in cellular and cell-free systems. *Mutation research*, *299*(3-4), 135–145.

Fan, W., & Luo, J. (2010). SIRT1 regulates UV-induced DNA repair through deacetylating XPA. *Molecular cell*, *39*(2), 247–258. https://doi.org/10.1016/j.molcel.2010.07.006

Fenech, M., Kirsch-Volders, M., Natarajan, A. T., Surralles, J., Crott, J. W., Parry, J.,... Thomas, P. (2011). Molecular mechanisms of micronucleus, nucleoplasmic bridge and nuclear bud formation in mammalian and human cells. *Mutagenesis*, *26*(1), 125–132. https://doi.org/10.1093/mutage/geq052

Fenech, M. (2002). Chromosomal biomarkers of genomic instability relevant to cancer. *Drug discovery today*, *7*(22), 1128–1137.

Fridovich, I. (1995). Superoxide radical and superoxide dismutases. *Annual review of biochemistry*, *64*, 97–112. https://doi.org/10.1146/annurev.bi.64.070195.000525

Frosina, G., Fortini, P., Rossi, O., Carrozzino, F., Raspaglio, G., Cox, L. S.,... Dogliotti, E. (1996). Two pathways for base excision repair in mammalian cells. *The Journal of biological chemistry*, *271*(16), 9573–9578.

Gallagher, J. D., Bianchi, J. J., & Gessman, L. J. (1989). Halothane antagonizes ouabain toxicity in isolated canine Purkinje fibers. *Anesthesiology*, *71*(5), 695–703.

Gonfloni, S., Iannizzotto, V., Maiani, E., Bellusci, G., Ciccone, S., & Diederich, M. (2014). P53 and Sirt1: Routes of metabolism and genome stability. *Biochemical pharmacology*, *92*(1), 149–156. https://doi.org/10.1016/j.bcp.2014.08.034

Grabowska, W., Sikora, E., & Bielak-Zmijewska, A. (2017). Sirtuins, a promising target in slowing down the ageing process. *Biogerontology*. Advance online publication. https://doi.org/10.1007/s10522-017-9685-9

Haigis, M. C., Mostoslavsky, R., Haigis, K. M., Fahie, K., Christodoulou, D. C., Murphy, A. J.,... Guarente, L. (2006). SIRT4 inhibits glutamate dehydrogenase and opposes the effects of calorie restriction in pancreatic beta cells. *Cell*, *126*(5), 941–954. https://doi.org/10.1016/j.cell.2006.06.057

Halliwell, B., & Aruoma, O. I. (1991). DNA damage by oxygen-derived species. Its mechanism and measurement in mammalian systems. *FEBS letters*, *281*(1-2), 9–19.

Hashiguchi, K., Stuart, J. A., de Souza-Pinto, N C, & Bohr, V. A. (2004). The C-terminal alphaO helix of human Ogg1 is essential for 8-oxoguanine DNA glycosylase activity: the mitochondrial beta-Ogg1 lacks this domain and does not have glycosylase activity. *Nucleic acids research*, *32*(18), 5596–5608. https://doi.org/10.1093/nar/gkh863

Herskovits, A. Z., & Guarente, L. (2013). Sirtuin deacetylases in neurodegenerative diseases of aging. *Cell research*, *23*(6), 746–758. https://doi.org/10.1038/cr.2013.70

Hida, Y., Kubo, Y., Murao, K., & Arase, S. (2007). Strong expression of a longevity-related protein, SIRT1, in Bowen's disease. *Archives of dermatological research*, *299*(2), 103–106. https://doi.org/10.1007/s00403-006-0725-6

Hill, A. C. (1991). Mycoplasma oxoniensis, a new species isolated from Chinese hamster conjunctivas. *International journal of systematic bacteriology*, *41*(1), 21–25. https://doi.org/10.1099/00207713-41-1-21

Hill, J. W., Hazra, T. K., Izumi, T., & Mitra, S. (2001). Stimulation of human 8-oxoguanine-DNA glycosylase by AP-endonuclease: Potential coordination of the initial steps in base excision repair. *Nucleic acids research*, *29*(2), 430–438.

Houtkooper, R. H., Pirinen, E., & Auwerx, J. (2012). Sirtuins as regulators of metabolism and healthspan. *Nature reviews. Molecular cell biology*, *13*(4), 225–238. https://doi.org/10.1038/nrm3293

Hu, J., Imam, S. Z., Hashiguchi, K., de Souza-Pinto, Nadja C, & Bohr, V. A. (2005). Phosphorylation of human oxoguanine DNA glycosylase (alpha-OGG1) modulates its function. *Nucleic acids research*, *33*(10), 3271–3282. https://doi.org/10.1093/nar/gki636

Hwang, E. S., & Song, S. B. (2017). Nicotinamide is an inhibitor of SIRT1 in vitro, but can be a stimulator in cells. *Cellular and molecular life sciences : CMLS*, *74*(18), 3347–3362. https://doi.org/10.1007/s00018-017-2527-8

Jacobs, A. L., & Schär, P. (2012). DNA glycosylases: in DNA repair and beyond. *Chromosoma*, *121*(1), 1–20. https://doi.org/10.1007/s00412-011-0347-4

Jena, N. R., & Mishra, P. C. (2005). Mechanisms of formation of 8-oxoguanine due to reactions of one and two OH* radicals and the H_2O_2 molecule with guanine: A quantum computational study. *The journal of physical chemistry. B*, *109*(29), 14205–14218. https://doi.org/10.1021/jp050646j

Jeong, J., Juhn, K., Lee, H., Kim, S.-H., Min, B.-H., Lee, K.-M.,. . . Lee, K.-H. (2007). SIRT1 promotes DNA repair activity and deacetylation of Ku70. *Experimental & molecular medicine*, *39*(1), 8–13. https://doi.org/10.1038/emm.2007.2

Jeong, S. M., Hwang, S., & Seong, R. H. (2016). SIRT4 regulates cancer cell survival and growth after stress. *Biochemical and biophysical research communications*, *470*(2), 251–256. https://doi.org/10.1016/j.bbrc.2016.01.078

Jeong, S. M., Xiao, C., Finley, L. W. S., Lahusen, T., Souza, A. L., Pierce, K.,. . . Haigis, M. C. (2013). SIRT4 has tumor-suppressive activity and regulates the cellular metabolic response to DNA damage by inhibiting mitochondrial glutamine metabolism. *Cancer cell*, *23*(4), 450–463. https://doi.org/10.1016/j.ccr.2013.02.024

Jung, S.-B., Kim, C.-S., Kim, Y.-R., Naqvi, A., Yamamori, T., Kumar, S.,. . . Irani, K. (2013). Redox factor-1 activates endothelial SIRTUIN1 through reduction of conserved cysteine sulfhydryls in its deacetylase domain. *PloS one*, *8*(6), e65415. https://doi.org/10.1371/journal.pone.0065415

Kaplan, J. E. (1971). A survey of dentistry. *Contact point*, *49*(4), 88–91.

Kawanishi, S., & Murata, M. (2006). Mechanism of DNA damage induced by bromate differs from general types of oxidative stress. *Toxicology*, *221*(2-3), 172–178. https://doi.org/10.1016/j.tox.2006.01.002

Kim, E.-J., & Um, S.-J. (2008). SIRT1: Roles in aging and cancer. *BMB reports*, *41*(11), 751–756.

Kim, H.-S., Vassilopoulos, A., Wang, R.-H., Lahusen, T., Xiao, Z., Xu, X.,. . . Deng, C.-X. (2011). SIRT2 maintains genome integrity and suppresses tumorigenesis through regulating APC/C activity. *Cancer cell*, *20*(4), 487–499. https://doi.org/10.1016/j.ccr.2011.09.004

Kitsera, N., Stathis, D., Lühnsdorf, B., Müller, H., Carell, T., Epe, B., & Khobta, A. (2011). 8-Oxo-7,8-dihydroguanine in DNA does not constitute a barrier to transcription, but is converted into transcription-blocking damage by OGG1. *Nucleic acids research*, *39*(14), 5926–5934. https://doi.org/10.1093/nar/gkr163

Klungland, A., & Lindahl, T. (1997). Second pathway for completion of human DNA base excision-repair: reconstitution with purified proteins and requirement for DNase IV (FEN1). *The EMBO journal*, *16*(11), 3341–3348. https://doi.org/10.1093/emboj/16.11.3341

Klungland, A., Rosewell, I., Hollenbach, S., Larsen, E., Daly, G., Epe, B.,. . . Barnes, D. E. (1999). Accumulation of premutagenic DNA lesions in mice defective in removal of oxidative base damage. *Proceedings of the National Academy of Sciences of the United States of America*, 96(23), 13300–13305.

Kruszewski, M., & Szumiel, I. (2005). Sirtuins (histone deacetylases III) in the cellular response to DNA damage--facts and hypotheses. *DNA repair*, 4(11), 1306–1313. https://doi.org/10.1016/j.dnarep.2005.06.013

Kugel, S., & Mostoslavsky, R. (2014). Chromatin and beyond: The multitasking roles for SIRT6. *Trends in biochemical sciences*, 39(2), 72–81. https://doi.org/10.1016/j.tibs.2013.12.002

Kunz, C., Saito, Y., & Schär, P. (2009). DNA Repair in mammalian cells: Mismatched repair: variations on a theme. *Cellular and molecular life sciences : CMLS*, 66(6), 1021–1038. https://doi.org/10.1007/s00018-009-8739-9

Lain, S., Hollick, J. J., Campbell, J., Staples, O. D., Higgins, M., Aoubala, M.,. . . Westwood, N. J. (2008). Discovery, in vivo activity, and mechanism of action of a small-molecule p53 activator. *Cancer cell*, 13(5), 454–463. https://doi.org/10.1016/j.ccr.2008.03.004

Larsson, S. (2003). A career in oncology. *BMJ (Clinical research ed.)*, 327(7426), s169-70. https://doi.org/10.1136/bmj.327.7426.s169-a

Li, H., Rajendran, G. K., Liu, N., Ware, C., Rubin, B. P., & Gu, Y. (2007). SirT1 modulates the estrogen-insulin-like growth factor-1 signaling for postnatal development of mammary gland in mice. *Breast cancer research : BCR*, 9(1), R1. https://doi.org/10.1186/bcr1632

Lindahl, T., & Barnes, D. E. (2000). Repair of endogenous DNA damage. *Cold Spring Harbor symposia on quantitative biology*, 65, 127–133.

Lirussi, L., Antoniali, G., Vascotto, C., D'Ambrosio, C., Poletto, M., Romanello, M.,. . . Tell, G. (2012). Nucleolar accumulation of APE1 depends on charged lysine residues that undergo acetylation upon genotoxic stress and modulate its BER activity in cells. *Molecular biology of the cell*, 23(20), 4079–4096. https://doi.org/10.1091/mbc.E12-04-0299

Lombard, D. B., Schwer, B., Alt, F. W., & Mostoslavsky, R. (2008). SIRT6 in DNA repair, metabolism and ageing. *Journal of internal medicine*, 263(2), 128–141. https://doi.org/10.1111/j.1365-2796.2007.01902.x

Lombard, D. B. (2009). Sirtuins at the breaking point: SIRT6 in DNA repair. *Aging*, 1(1), 12–16. https://doi.org/10.18632/aging.100014

Mao, Z., Hine, C., Tian, X., van Meter, M., Au, M., Vaidya, A.,. . . Gorbunova, V. (2011). SIRT6 promotes DNA repair under stress by activating PARP1. *Science (New York, N.Y.)*, 332(6036), 1443–1446. https://doi.org/10.1126/science.1202723

Martinez-Pastor, B., & Mostoslavsky, R. (2012). Sirtuins, metabolism, and cancer. *Frontiers in pharmacology*, 3, 22. https://doi.org/10.3389/fphar.2012.00022

Martínez-Redondo, P., & Vaquero, A. (2013). The diversity of histone versus nonhistone sirtuin substrates. *Genes & cancer*, 4(3-4), 148–163. https://doi.org/10.1177/1947601913483767

Masumi, A., Suzuki, T., Iijima, S., & Tsukada, K. (1990). Enhanced phosphorylation of a nucleolar 110-kDa protein in rat liver by dietary manipulation. *European journal of biochemistry*, 192(1), 63–68.

McBurney, M. W., Yang, X., Jardine, K., Hixon, M., Boekelheide, K., Webb, J. R.,. . . Lemieux, M. (2003). The mammalian SIR2alpha protein has a role in embryogenesis and gametogenesis. *Molecular and cellular biology*, 23(1), 38–54.

McCord, R. A., Michishita, E., Hong, T., Berber, E., Boxer, L. D., Kusumoto, R.,. . . Chua, K. F. (2009). SIRT6 stabilizes DNA-dependent protein kinase at chromatin for DNA double-strand break repair. *Aging*, 1(1), 109–121. https://doi.org/10.18632/aging.100011

Mei, Z., Zhang, X., Yi, J., Huang, J., He, J., & Tao, Y. (2016). Sirtuins in metabolism, DNA repair and cancer. *Journal of experimental & clinical cancer research : CR*, *35*(1), 182. https://doi.org/10.1186/s13046-016-0461-5

Michan, S., & Sinclair, D. (2007). Sirtuins in mammals: Insights into their biological function. *The Biochemical journal*, *404*(1), 1–13. https://doi.org/10.1042/BJ20070140

Michishita, E., Park, J. Y., Burneskis, J. M., Barrett, J. C., & Horikawa, I. (2005). Evolutionarily conserved and nonconserved cellular localizations and functions of human SIRT proteins. *Molecular biology of the cell*, *16*(10), 4623–4635. https://doi.org/10.1091/mbc.E05-01-0033

Mostoslavsky, R., Chua, K. F., Lombard, D. B., Pang, W. W., Fischer, M. R., Gellon, L.,. . . Alt, F. W. (2006). Genomic instability and aging-like phenotype in the absence of mammalian SIRT6. *Cell*, *124*(2), 315–329. https://doi.org/10.1016/j.cell.2005.11.044

Nishioka, K., Ohtsubo, T., Oda, H., Fujiwara, T., Kang, D., Sugimachi, K., & Nakabeppu, Y. (1999). Expression and differential intracellular localization of two major forms of human 8-oxoguanine DNA glycosylase encoded by alternatively spliced OGG1 mRNAs. *Molecular biology of the cell*, *10*(5), 1637–1652.

Osterod, M., Hollenbach, S., Hengstler, J. G., Barnes, D. E., Lindahl, T., & Epe, B. (2001). Age-related and tissue-specific accumulation of oxidative DNA base damage in 7,8-dihydro-8-oxoguanine-DNA glycosylase (Ogg1) deficient mice. *Carcinogenesis*, *22*(9), 1459–1463.

Pereira, C. V., Lebiedzinska, M., Wieckowski, M. R., & Oliveira, P. J. (2012). Regulation and protection of mitochondrial physiology by sirtuins. *Mitochondrion*, *12*(1), 66–76. https://doi.org/10.1016/j.mito.2011.07.003

Pikor, L., Thu, K., Vucic, E., & Lam, W. (2013). The detection and implication of genome instability in cancer. *Cancer metastasis reviews*, *32*(3-4), 341–352. https://doi.org/10.1007/s10555-013-9429-5

Radicella, J. P., Dherin, C., Desmaze, C., Fox, M. S., & Boiteux, S. (1997). Cloning and characterization of hOGG1, a human homolog of the OGG1 gene of Saccharomyces cerevisiae. *Proceedings of the National Academy of Sciences of the United States of America*, *94*(15), 8010–8015.

Robertson, A. B., Klungland, A., Rognes, T., & Leiros, I. (2009). DNA repair in mammalian cells: Base excision repair: the long and short of it. *Cellular and molecular life sciences : CMLS*, *66*(6), 981–993. https://doi.org/10.1007/s00018-009-8736-z

Rodriguez, R. M., Fernandez, A. F., & Fraga, M. F. (2013). Role of sirtuins in stem cell differentiation. *Genes & cancer*, *4*(3-4), 105–111. https://doi.org/10.1177/1947601913479798

Sancar, A., Lindsey-Boltz, L. A., Unsal-Kaçmaz, K., & Linn, S. (2004). Molecular mechanisms of mammalian DNA repair and the DNA damage checkpoints. *Annual review of biochemistry*, *73*, 39–85. https://doi.org/10.1146/annurev.biochem.73.011303.073723

Sarga, L., Hart, N., Koch, L. G., Britton, S. L., Hajas, G., Boldogh, I.,. . . Radak, Z. (2013). Aerobic endurance capacity affects spatial memory and SIRT1 is a potent modulator of 8-oxoguanine repair. *Neuroscience*, *252*, 326–336. https://doi.org/10.1016/j.neuroscience.2013.08.020

Scalabrino, R., & Grimaldi, M. G. (1967). Applicabilità di particolari metodiche di immunofluorescenza sui leucociti circolanti in corso di affezioni post-streptococciche [Use of special immunofluorescent methods on circulating leukocytes during post-streptococcal infections]. *Giornale di malattie infettive e parassitarie*, *19*(5), 296–298.

Sengupta, S., Mantha, A. K., Song, H., Roychoudhury, S., Nath, S., Ray, S., & Bhakat, K. K. (2016). Elevated level of acetylation of APE1 in tumor cells modulates DNA damage repair. *Oncotarget*, *7*(46), 75197–75209. https://doi.org/10.18632/oncotarget.12113

Shen, Z. (2011). Genomic instability and cancer: an introduction. *Journal of molecular cell biology*, *3*(1), 1–3. https://doi.org/10.1093/jmcb/mjq057

Sies, H. (1991). Role of reactive oxygen species in biological processes. *Klinische Wochenschrift*, *69*(21-23), 965–968.

Sies, H. (1993). Strategies of antioxidant defense. *European journal of biochemistry*, *215*(2), 213–219.

Szabó, G., Hoffmann, J., & Bogáts, L. (1972). Postoperative Erscheinungen nach der Thermokoagulation des Ganglion Gasseri [Postoperative symptoms after thermo-coagulation of the gasserian ganglion]. *Deutsche Stomatologie*, *22*(3), 178–183.

Toiber, D., Erdel, F., Bouazoune, K., Silberman, D. M., Zhong, L., Mulligan, P.,. . . Mostoslavsky, R. (2013). SIRT6 recruits SNF2H to DNA break sites, preventing genomic instability through chromatin remodeling. *Molecular cell*, *51*(4), 454–468. https://doi.org/10.1016/j.molcel.2013.06.018

Valko, M., Rhodes, C. J., Moncol, J., Izakovic, M., & Mazur, M. (2006). Free radicals, metals and antioxidants in oxidative stress-induced cancer. *Chemico-biological interactions*, *160*(1), 1–40. https://doi.org/10.1016/j.cbi.2005.12.009

van Meter, M., Mao, Z., Gorbunova, V., & Seluanov, A. (2011). Repairing split ends: SIRT6, mono-ADP ribosylation and DNA repair. *Aging*, *3*(9), 829–835. https://doi.org/10.18632/aging.100389

van Meter, M., Mao, Z., Gorbunova, V., & Seluanov, A. (2011). SIRT6 overexpression induces massive apoptosis in cancer cells but not in normal cells. *Cell cycle (Georgetown, Tex.)*, *10*(18), 3153–3158. https://doi.org/10.4161/cc.10.18.17435

Vaquero, A., Scher, M., Erdjument-Bromage, H., Tempst, P., Serrano, L., & Reinberg, D. (2007). SIRT1 regulates the histone methyl-transferase SUV39H1 during heterochromatin formation. *Nature*, *450*(7168), 440–444. https://doi.org/10.1038/nature06268

Vaquero, A., Scher, M., Lee, D., Erdjument-Bromage, H., Tempst, P., & Reinberg, D. (2004). Human SirT1 interacts with histone H1 and promotes formation of facultative heterochromatin. *Molecular cell*, *16*(1), 93–105. https://doi.org/10.1016/j.molcel.2004.08.031

Vaziri, H., Dessain, S. K., Ng Eaton, E., Imai, S. I., Frye, R. A., Pandita, T. K.,. . . Weinberg, R. A. (2001). hSIR2(SIRT1) functions as an NAD-dependent p53 deacetylase. *Cell*, *107*(2), 149–159.

Vazquez, B. N., Thackray, J. K., & Serrano, L. (2017). Sirtuins and DNA damage repair: SIRT7 comes to play. *Nucleus (Austin, Tex.)*, *8*(2), 107–115. https://doi.org/10.1080/19491034.2016.1264552

Vazquez, B. N., Thackray, J. K., Simonet, N. G., Kane-Goldsmith, N., Martinez-Redondo, P., Nguyen, T.,. . . Serrano, L. (2016). SIRT7 promotes genome integrity and modulates non-homologous end joining DNA repair. *The EMBO journal*, *35*(14), 1488–1503. https://doi.org/10.15252/embj.201593499

Vidal, A. E., Hickson, I. D., Boiteux, S., & Radicella, J. P. (2001). Mechanism of stimulation of the DNA glycosylase activity of hOGG1 by the major human AP endonuclease: Bypass of the AP lyase activity step. *Nucleic acids research*, *29*(6), 1285–1292.

Wang, J., & Lindahl, T. (2016). Maintenance of Genome Stability. *Genomics, proteomics & bioinformatics*, *14*(3), 119–121. https://doi.org/10.1016/j.gpb.2016.06.001

Wang, R.-H., Sengupta, K., Li, C., Kim, H.-S., Cao, L., Xiao, C.,. . . Deng, C.-X. (2008). Impaired DNA damage response, genome instability, and tumorigenesis in SIRT1 mutant mice. *Cancer cell*, *14*(4), 312–323. https://doi.org/10.1016/j.ccr.2008.09.001

Wei, H., & Yu, X. (2016). Functions of PARylation in DNA Damage Repair Pathways. *Genomics, proteomics & bioinformatics*, *14*(3), 131–139. https://doi.org/10.1016/j.gpb.2016.05.001

Wiederhold, L., Leppard, J. B., Kedar, P., Karimi-Busheri, F., Rasouli-Nia, A., Weinfeld, M.,. . . Hazra, T. K. (2004). AP endonuclease-independent DNA base excision repair in human cells. *Molecular cell*, *15*(2), 209–220. https://doi.org/10.1016/j.molcel.2004.06.003

Will, O., Gocke, E., Eckert, I., Schulz, I., Pflaum, M., Mahler, H. C., & Epe, B. (1999). Oxidative DNA damage and mutations induced by a polar photosensitizer, Ro19-8022. *Mutation research*, *435*(1), 89–101.

Yamamori, T., DeRicco, J., Naqvi, A., Hoffman, T. A., Mattagajasingh, I., Kasuno, K.,. . . Irani, K. (2010). SIRT1 deacetylates APE1 and regulates cellular base excision repair. *Nucleic acids research*, *38*(3), 832–845. https://doi.org/10.1093/nar/gkp1039

Yamamoto, H., Schoonjans, K., & Auwerx, J. (2007). Sirtuin functions in health and disease. *Molecular endocrinology (Baltimore, Md.)*, *21*(8), 1745–1755. https://doi.org/10.1210/me.2007-0079

Yuan, Z., Zhang, X., Sengupta, N., Lane, W. S., & Seto, E. (2007). SIRT1 regulates the function of the Nijmegen breakage syndrome protein. *Molecular cell*, *27*(1), 149–162. https://doi.org/10.1016/j.molcel.2007.05.029

Zhang, H., Head, P. E., & Yu, D. S. (2016). SIRT2 orchestrates the DNA damage response. *Cell cycle (Georgetown, Tex.)*, *15*(16), 2089–2090. https://doi.org/10.1080/15384101.2016.1184517

Zhou, L., Wang, F., Sun, R., Chen, X., Zhang, M., Xu, Q.,. . . Ye, D. (2016). SIRT5 promotes IDH2 desuccinylation and G6PD deglutarylation to enhance cellular antioxidant defense. *EMBO reports*, *17*(6), 811–822. https://doi.org/10.15252/embr.201541643

8   Curriculum Vitae

PERSONAL INFORMATION

Name:	Elena Robeska
Date of birth:	
Place of birth:	
Nationality:	
Email:	

12.2013-03.2018   **Research Associate (Wissenschaftliche Mitarbeiterin)**
Institute of Pharmacy and Biochemistry, JGU, Mainz, Germany

12.2013-03.2018   **PhD** in Pharmacy, Institute of Pharmacy and Biochemistry, JGU Mainz, Germany, Working group Pharmacology and Toxicology, supervised by Prof. Dr. B. Epe. International PhD Program, Institute of Molecular Biology (IMB) - Mainz
PhD Thesis: "Role of SIRT1 and SIRT6 of the preservation of genetic stability"

2011-2012   **MSc.** in Molecular Biology, Department of Biology and Ecology, Faculty of Sciences, University of Novi Sad, Serbia
Master Thesis: "Application of androgen anabolic steroids changed transcriptional profile of MAPK genes and transiently increased apoptosis of testicular Leydig cells", supervised by Prof. Dr. Silvana Andric

2007-2011   **BSc.** in Biology, Department of Biology and Ecology, Faculty of Sciences, University of Novi Sad, Serbia
Bachelor Thesis: "Androgenization of adult male rats initiates Leydig Cell apoptosis", supervised by Prof. Dr. Tatjana Kostic

2003-2007   Gymnasium "Mirce Acev", Prilep